

# Innovative Sensor Networks in Ghana

Operating and validating sensor networks for river discharge in Ghana during the wet season

Jolijn Hiemstra  
Luuk Streefkerk  
Jorrit Okkerman  
Annabel Rijsenbrij  
Jesse van Leeuwen  
Jonathan Linnebach

Delft University of Technology

# Innovative Sensor Networks in Ghana

Operating and validating sensor networks for river discharge in Ghana during the wet season

by

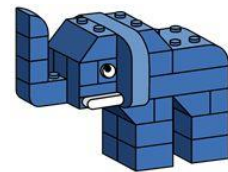
Jolijn Hiemstra  
Luuk Streefkerk  
Jorrit Okkerman  
Annabel Rijsenbrij  
Jesse van Leeuwen  
Jonathan Linnebach

| Student Name | Student Number |
|--------------|----------------|
| Hiemstra     | 4612736        |
| Rijsenbrij   | 4703081        |
| Linnebach    | 5843162        |
| van Leeuwen  | 5659760        |
| Streefkerk   | 4724593        |
| Okkerman     | 5375789        |

Supervisor: Prof. dr. ir. Nick van de Giesen  
Project Duration: September - November 2023  
Faculty: Faculty of Civil Engineering and Geosciences, Delft  
Course: Multidisciplinary Project (MDP) (CEGM3000)  
Cover: View of the Black Volta, at the location Chache, from boat



***TEMBO Africa:*** *The work leading to these results has received funding from the European Horizon Europe Programme (2021-2027) under grant agreement n° 101086209. The opinions expressed in the document are of the authors only and no way reflect the European Commission's opinions. The European Union is not liable for any use that may be made of the information.*



# Acknowledgement

We would like to express a special thanks to our supervisor Prof.dr.ir. Nick van de Giesen for enabling our research and especially for his guidance during this project.

Besides our supervisor, we want to express our gratitude to Frank Annor for his support during our project and for helping us getting to know and understand Ghana.

We want to express our gratitude to BPA and their employees for their support and guidance during our fieldwork, as well as their hospitality during our time in Bui. In particular, we want to thank Jakpa for assisting us with all our measurements and the associated practicalities at the Black Volta site. Also, a special thanks to Sulaiman and Jonathan (BPA Engineers) for their support with the fabrication of our measurement equipment.

Additionally, we are very thankful to the staff and students of the University of Development Studies (UDS) for accompanying us to various field sites and connecting us to local communities, as well as their readiness to support us wherever needed during our stay in Tamale, especially to; Prof. Gordana Kranjac-Berisavljevic, Dr Bizoola, Richard Dogbey and to the students who joined and helped us doing field measurements.

Another special thanks to Andreas Krietemeyer for his technical support and advice regarding the GNSS measurements and post-processing.

We also want to extend our appreciation to Richard from the Hydrological Services Department of the Northern Region for helping us with interpreting the water level gauge and sharing his experience on hydrological issues related to our work in the area and protecting measurement devices against theft.

Also we would like to thank Niels Hoogendoorn for providing us with his discharge model and bathymetry data, as well as answering our many questions.

We are grateful to Guus Wiersma from the African Water Corridor and Wesley van Beek for providing us with accommodation and practical support.

This project and our travel to Ghana would not have been possible without the financial support of TEMBO Africa, FAST Fund and Delft Global Initiative.

And finally, to the people who made our experience in Ghana a great and unforgettable one. We are especially thankful to our caretaker, Asibi, for all her hard work in and around the house which made our stay all the better and Kobi; our driver and our first friend in Ghana.

*Jolijn Hiemstra  
Luuk Streefkerk  
Jorrit Okkerman  
Annabel Rijsenbrij  
Jesse van Leeuwen  
Jonathan Linnebach  
Delft, December 2023*



# Summary

Long and continuous time series of hydrological data are scarce in Sub-Saharan Africa. However, this data is crucial for many engineering decisions from the planning to the management phase of a project. In 2013 the Bui power dam was constructed at the Black Volta in western Ghana. Uncertainties in the prediction of the reservoir inflow during flood events due to data scarcity and a short lead time in the prediction result in big challenges for the management team of the dam at the end of the wet season when the reservoir should be as filled as possible without risking an overflow. This situation led to two spillages of the dam within the last 10 years, which caused big damages to the downstream communities as well as large economic losses.

To mitigate this problem, this multidisciplinary project aimed to conduct new measurements at the Black Volta during the wet season to improve and further develop the models of two previous thesis projects and test newly developed measurement methods for remote areas within the TEMBO Africa project. The main objective is to provide proof of concept for various river parameter measurement devices and test them in the field. Furthermore a better understanding of the contribution of a floodplain to the river discharge was gained. This was done by performing field observations and thereby reducing uncertainties in the discharge measurements of the Black Volta to better predict the inflow in the Bui power reservoir and prevent future spillages.

The current rating curve at the measurement location in Chache fits well to measure flows in the dry season but has high uncertainties in the wet season when the water level exceeds the river banks. To investigate the contribution of the floodplains to the river discharge multiple field measurements were performed. Water level and discharge were measured using GNSS reflectometry and a camera-surface-velocity method to improve the rating curve with measurement points of the wet season. Furthermore, an existing hydraulic model was improved by observing the floodplain in the field and further specify the floodplain in the model based on the observations. With this model a full rating curve can be constructed.

The water level at the field site is measured using GNSS-reflectometry. During the course of the project the device required for this method was tested and validated at different locations and afterwards installed at the Black Volta to permanently measure the water level. This installation is a great success as it can automate and replace the manual measurements performed up till now.

To measure the discharge a camera is used to capture the surface movement of the river. From the video clips the surface velocity and discharge can be determined with the python package pyOpenRiver-Cam using the local bathymetry of the river. In the test phase the method could be used successfully on a small stream, while it failed on a river with a width receding 200 m. After testing, the measurement setup was installed at the final location at the Black Volta and discharge measurements of two days were taken. However, due to poor network connection and the lack of other discharge measurements for the calibration the device was not yet left in place permanently. In the future however, this measurement method will provide daily discharge measurements and can reduce the uncertainty of the rating curve when combined with the water level measurements.

To determine the contribution of the floodplain to the discharge system, field measurements have been done, both to manually measure the in-situ water velocity in the floodplains and to collect data that is required to determine the roughness coefficient of the floodplain, which is required for modelling the floodplain contribution. The floodplain has been divided into separate classes of which the roughness coefficient has been determined by using the Baptist equation. For this, vegetation data like stem density was collected.

Moreover, it was tried to automate the determination of the roughness coefficient by using the near-infrared vegetation index (NDVI), which is a remote sensing technique. However, it makes use of

---

Landsat, which has a resolution of 30x30 m and is not detailed enough to provide a proper classification.

The roughness coefficient values that were determined were implemented as rectangles parallel to the river into the existing Delft3D model. Two implementation scenarios were applied. Firstly, one roughness coefficient was determined per rectangle based on a standard Manning roughness coefficient look-up table by Forzieri et al. and in situ observations in the floodplain. Secondly, the roughness coefficient calculated by the Baptist equation was used. Since the height of the water column affects the calculated roughness coefficient, it has been done for different water heights. It was concluded that the results of the both scenarios are fairly similar and that scenario 1 is suitable for application in this situation, which requires much less labor and time than scenario 2. It was also concluded that the floodplains do contribute to the discharge of the river, since the water is not only stored, but also flows through them. The retrieved rating curve deviates from Kasteel's for higher discharges.

A point of discussion is the installation of the equipment towards the end of the rainy season, instead of at the beginning. Installation at the beginning would have provided a great amount of high discharge data, which could have been used to validate and improve the models.

Also the location of the equipment pole is a challenge. The building of a new bridge severely disrupts the natural flow of the Black Volta. This highly influences the data that is being collected and the bathymetry of the measured location, as the equipment pole is located just downstream of the bridge. However, once the bridge is finished, it could be of great advantage as it could simplify the data collection from above.

# Contents

|   |            |
|---|------------|
| <b>Acknowledgement</b>                                  | <b>ii</b>  |
| <b>Summary</b>  | <b>iii</b> |
| <b>1 Introduction</b>                                   | <b>1</b>   |
| 1.1 Background  | 1          |
| 1.2 Problem analysis                                    | 2          |
| 1.3 research questions                                  | 2          |
| 1.4 Structure   | 3          |
| <b>2 Project plan</b>                                   | <b>4</b>   |
| <b>3 Study area and existing data</b>                   | <b>5</b>   |
| 3.1 Study area  | 5          |
| 3.1.1 Field site Tamale (small stream)                  | 6          |
| 3.1.2 Field site Yapei (White Volta)                    | 7          |
| 3.1.3 Field site Chache (Black Volta)                   | 7          |
| 3.2 Data  | 9          |
| 3.2.1 Discharge data                                    | 9          |
| 3.2.2 Bathymetry data                                   | 9          |
| 3.2.3 Existing discharge model                          | 10         |
| 3.2.4 Rating curves                                     | 10         |
| <b>4 Water height</b>                                   | <b>12</b>  |
| 4.1 Methodology   | 12         |
| 4.1.1 Principle   | 12         |
| 4.1.2 GNSS-IR campaign Chache                           | 13         |
| 4.2 Results   | 13         |
| 4.3 Discussion  | 14         |
| <b>5 Bathymetry</b>                                     | <b>15</b>  |
| 5.1 Data collection                                     | 15         |
| 5.2 Results   | 16         |
| 5.3 Discussion and conclusion                           | 17         |
| <b>6 Surface velocity and discharge by OpenRiverCam</b> | <b>18</b>  |
| 6.1 Methodology   | 18         |
| 6.1.1 Tamale  | 18         |
| 6.1.2 Yapei   | 19         |
| 6.1.3 Chache  | 20         |
| 6.1.4 Control points                                    | 22         |
| 6.2 Results   | 22         |
| 6.2.1 Tamale  | 22         |
| 6.2.2 Yapei   | 24         |
| 6.2.3 Chache  | 26         |
| 6.2.4 Control points                                    | 29         |
| 6.3 Discussion  | 32         |
| <b>7 Floodplain contribution</b>                        | <b>34</b>  |
| 7.1 Theory roughness coefficient                        | 34         |
| 7.1.1 Manning roughness coefficient literature          | 34         |
| 7.1.2 Baptist equation                                  | 35         |
| 7.2 Remote sensing                                      | 36         |

|           |   |           |
|-----------|---|-----------|
| 7.2.1     | Available products for evaluating roughness . . . . .   | 36        |
| 7.2.2     | Quantifying vegetation at 30 m resolution with Landsat . . . . .                              | 37        |
| 7.3       | In situ observations . . . . .  | 38        |
| 7.3.1     | Vegetation surveys . . . . .  | 38        |
| 7.3.2     | Velocity measurements . . . . .   | 39        |
| 7.4       | Results . . . . .   | 39        |
| 7.4.1     | Vegetation surveys . . . . .  | 39        |
| 7.4.2     | Floodplain velocity . . . . .   | 40        |
| 7.4.3     | Roughness input for hydraulic model . . . . .   | 41        |
| 7.5       | Discussion . . . . .  | 42        |
| 7.5.1     | Field observations . . . . .  | 42        |
| 7.5.2     | Relating field observations to remote sensing data . . . . .                                  | 43        |
| <b>8</b>  | <b>Delft3D/Discharge model</b>  | <b>45</b> |
| 8.1       | Delft3D methodology . . . . .   | 45        |
| 8.1.1     | Roughness coefficient input . . . . .   | 45        |
| 8.1.2     | Boundary conditions . . . . .   | 47        |
| 8.2       | Results . . . . .   | 48        |
| 8.2.1     | Scenario 1, visual determination of roughness coefficient . . . . .                           | 48        |
| 8.2.2     | Scenario 2, Baptist determination of roughness coefficient . . . . .                          | 49        |
| 8.2.3     | Rating curve . . . . .  | 50        |
| 8.2.4     | Surface velocity comparison results: Delft3D, OpenRiverCam and in-situ measurements . . . . . | 51        |
| 8.3       | Discussion . . . . .  | 53        |
| 8.4       | Conclusion . . . . .  | 53        |
| <b>9</b>  | <b>Discussion and Conclusion</b>  | <b>55</b> |
| 9.1       | Planning and timing . . . . .   | 55        |
| 9.2       | Location . . . . .  | 56        |
| 9.3       | Validation of results . . . . .   | 57        |
| 9.3.1     | Bathymetry . . . . .  | 57        |
| 9.3.2     | Rating curve . . . . .  | 57        |
| 9.3.3     | Model calibration . . . . .   | 58        |
| <b>10</b> | <b>Recommendations</b>  | <b>59</b> |
|           | <b>References</b>   | <b>61</b> |
| <b>A</b>  | <b>Sensor and platform setup</b>  | <b>62</b> |
| <b>B</b>  | <b>Jupyter Notebook: Calculation of roughness coefficient by Baptist</b>                      | <b>64</b> |
| <b>C</b>  | <b>Roughness coefficient input Delft3D scenario 2</b>   | <b>67</b> |
| <b>D</b>  | <b>BASE station, offline test</b>   | <b>69</b> |
| <b>E</b>  | <b>Post processing GNSS reflectometry</b>   | <b>74</b> |
| <b>F</b>  | <b>Post processing kinematics</b>   | <b>76</b> |
| <b>G</b>  | <b>Photos of study site</b>   | <b>79</b> |
| <b>H</b>  | <b>Floodplain data collection</b>   | <b>80</b> |

# List of Figures

|      |  |    |
|------|--|----|
| 2.1  | Flow chart overview . . . . .  | 4  |
| 3.1  | a) Volta river basin in west Africa. b) Part of the Volta basin which is named the Black Volta Basin. c) Map of Ghana showing the elevation in the Black Volta Basin and the field sites relevant for this project. . . . .                          | 5  |
| 3.2  | Field site location in Tamale, a small creek. . . . .  | 6  |
| 3.3  | Field site location in Yapei at the White Volta River. Wide river main channel of about 200 m width with small floodplain extend on both sides (a). The Yapei bridge with a height of about 10 m spans across the river at the location (b). . . . . | 7  |
| 3.4  | Field site location in Chache at the Black Volta River. Wide river main channel of about 150 m width (a) with large floodplain extend up to 500 m on the Ghanaian side (b). . . . .  | 8  |
| 3.5  | Two existing structures in Chache to mount measurement equipment. (a) One pole recently constructed by BPA.(b) one scaffold already existing for the last two decades which was used to mount various sensors in the past. . . . .                   | 8  |
| 3.6  | Discharge of the Black Volta measured by BPA in Chache since 2000 and Lawra since 2010 [11] . . . . .  | 9  |
| 3.7  | Bathymetry of the main channel and floodplain of the Black Volta in Chache [10] . . . . .  | 9  |
| 3.8  | Delft3D FM suite model of N.Hoogendoorn showing the bed level and unstructured grid. . . . .   | 10 |
| 4.1  | GNSS-IR reflection-zone chache . . . . .   | 12 |
| 4.2  | GNSS-IR results Chache . . . . .   | 13 |
| 5.2  | Bathymetry at the Yapei bridge measured with a FishFinder sonar device and interpolated using a b-spline interpolation and bathymetry measured with a rope from the bridge (red box). . . . .  | 16 |
| 5.3  | Cross sections of bathymetry underneath the Yapei bridge measured with the Sonar-Chirp+ attached on a rope from the bridge (red) and attached to a boat and then interpolated over the full area (blue). . . . .                                     | 17 |
| 6.1  | Tamale camera views with different angles and number of control points. The red crosses show the control points. . . . .   | 19 |
| 6.2  | Yapei camera view with ground control points, shown as the red crosses . . . . .   | 20 |
| 6.3  | Solar charge controller with modem and battery (right), Camera setup diagram (left). Videos are sent remotely at intervals to the server or someone connected to wifi . . . . .  | 20 |
| 6.4  | Camera setup Chache . . . . .  | 21 |
| 6.5  | Chache camera view with four photoshopped boats and PPK antennae . . . . .   | 21 |
| 6.6  | PPK Base and Rover visualisation. By using both a base and a rover, precise coordinates of GCP's (small chessboards on the figure) can be captured by holding a rover still for some minutes . . . . .   | 22 |
| 6.7  | Tamale velocimetries without lens position higher camera view (left) and top view projection (right) . . . . .   | 23 |
| 6.8  | Tamale velocimetries with lens position and higher camera view (left) and top view projection (right) . . . . .  | 23 |
| 6.9  | Tamale velocimetries with small camera angle and little GCP's, with camera view (left) and projected topview (right) . . . . .   | 24 |
| 6.10 | Yapei area of interest corners (left) and aoi top view (right) . . . . .   | 24 |
| 6.11 | Velocities perpendicular to the transect with apple locations indicated in red . . . . .   | 25 |
| 6.12 | Yapei area of interest corners (left) and aoi top view (right) . . . . .   | 25 |

|      |  |    |
|------|--|----|
| 6.13 | Yapei area of interest with smaller indicated corners (left) the bigger indicated a.o.i. projected to an orthoprojected plane (right)  | 25 |
| 6.14 | Chache velocimetry means camera view (left) Chache velocimetry camera view (right)   | 26 |
| 6.15 | Chache velocimetry means top view with transect (bottom) and with google satellite (top)   | 26 |
| 6.16 | Manual speed test locations of object 1 (left, 1.3 m/s) and object 2 being closer to the fast flowing part of the main channel (right, 1.9 m/s)  | 27 |
| 6.17 | Velocities perpendicular to the transect with object locations indicated in red  | 27 |
| 6.18 | Tamale Control points statistics   | 30 |
| 6.19 | Yapei Control points statistics  | 30 |
| 6.20 | Chache (Ivory-coast side) Control points statistics  | 31 |
| 6.21 | Chache (Ghana side) Control points statistics  | 31 |
|      |  |    |
| 7.1  | Rough calculation of the flow through the main channel and floodplains at the Black Volta site. Each cell in the vertical direction represents a meter of water depth. Based on this calculation, which was based on observations from initial site visits and a rough idea of the shape of the river, a rough contribution of the floodplain to total flow was estimated at 10 percent.                   | 34 |
| 7.2  | Nine-class look-up table and relationship between land cover and Manning roughness coefficient [7]   | 35 |
| 7.3  | Schematization of the velocity profile in the vegetation model. A) partially submerged vegetation and B) Fully submerged vegetation. Figure by Nardin [12]   | 35 |
| 7.4  | a) Continuously varying NDVI values. b) Including visually identified distinct vegetation cover zones in the same image. c) Subdividing the NDVI values into discrete classes, each representing a range of possible values. d) Interpolated NDVI values.  | 38 |
| 7.5  | Measurement locations of our vegetation surveys to determine stem density and height in the floodplain at Chache   | 40 |
| 7.6  | Two velocity profiles that were obtained in the floodplain using a current meter. The height of the red part of the graph gives the measured velocity at the location along the bright-pink line in the direction of the river (black arrow). The white portion gives the highest velocity measured along the transect. This is 0.38 and 0.15 $m/s$ for the upstream and downstream transect respectively. | 41 |
| 7.7  | Roughness coefficient calculated by Baptist of different vegetation zones in the floodplain [1]  | 42 |
| 7.8  | The water level in the floodplain has receded by quite a bit, which is visible in the color of the vegetation. There is a clear line where the green-colored leaves end and where only brown vegetation features are found. This is the portion that was flooded previously this rainy season.   | 43 |
|      |  |    |
| 8.1  | Roughness coefficient implementation in discharge model scenario 1   | 46 |
| 8.2  | Roughness coefficient implementation in discharge model scenario 2   | 46 |
| 8.3  | Bed level [m] and water heights [m] for different downstream water level boundary conditions in Delft3D for a discharge of 2000 $m^3/s$  | 48 |
| 8.4  | Water height and velocity per discharge with visually determined roughness coefficients  | 49 |
| 8.5  | Water height and velocity per discharge with Baptist equation roughness coefficients   | 50 |
| 8.6  | Rating curves developed by the two scenarios in the discharge model compared to the previous developed rating curves by BPA and M. Kasteel   | 51 |
| 8.7  | Surface velocity comparison Delft3D model results and OpenRiverCam at the Chache site  | 52 |
|      |  |    |
| A.1  | Design of sensor setup on the pole in Chache.  | 62 |
| A.2  | Platform for sensor setup on the pole in Chache.   | 63 |
|      |  |    |
| E.1  | NR CAN selection   | 75 |
| E.2  | GNSS-IR web application screenshot   | 75 |
|      |  |    |
| F.1  | NR CAN selection   | 77 |
| F.2  | Screenshot RTKPOST main  | 77 |
| F.3  | Screenshot RTKPOST settings  | 77 |

---

|     |  |    |
|-----|--|----|
| F.4 | Screenshot RTKPOST output . . . . .  | 78 |
| F.5 | Screenshot RTKPOST position . . . . .  | 78 |
| G.1 | Photos of the construction of the bridge at the Chache site, taken on 04-10-2023 . . . . . | 79 |

# 1

## Introduction

### 1.1. Background

Rivers as a water resource have a large variety of influences on their environment and the people living along its banks. They contribute to the food stock through fishery and irrigation, are used for transportation and they can be a source of hydraulic energy. However, rivers can also be a threat to humans, as geo-hazards like floods can occur. In order to manage all applications and prevent geo-hazards the work of water management engineers is required. An example could be the measurement of flow parameters or the modelling of river discharge to build a flood early warning system. However, this generally requires expensive and temporary technologies, which makes proper water management not feasible for data scarce regions. TEMBO is a recent project offering solutions to these issues in Africa. Its objective is to set up cost effective and innovative sensor networks that can be financed and sustained by without the need of external financing, via climate services built on top of these networks. Examples of such climate applications are flood early warning systems and reservoir management systems.

A party that is interested in these developments is the Bui Power Authority (BPA), which manages a hydropower dam in the Black Volta river at the border between Ivory Coast and Ghana. The dam, which was constructed between 2009 and 2013 in the west of the country the Black Volta, covers 8.5% of the country's electricity generation. During the wet season the aim of BPA is to fill the reservoir to its maximum capacity. However, a chance exists of overfilling of the reservoir, which could lead to overtopping or even failure of the dam. To avoid this, the spillways of the dam can be used as an emergency solution, quickly discharging large volumes of water. This occurred in 2019 and 2023 and had disastrous consequences for the downstream area and its residents, as it causes not only the loss of potential electricity, but also flooding of the region.

Former research has been conducted on the discharge of the Black Volta and its catchment area. Hoogendoorn (2023) collected discharge measurements during the dry season at the river close to the village Chache. He used the software OpenRiverCam to map the surface water velocity, sonar and photogrammetry to obtain the bathymetry of the river section and estimated the friction coefficient of the river bed and the floodplains. He combined the data in Delft3D, which is a software that creates a hydraulic model. A rating curve from this model can be developed, which plots the water height in the river with the according discharge. The rating curve at this location predicts the discharge which flows into the reservoir up to two days in advance. Kasteel (2023) constructed a hydrological model of the whole Black Volta and its catchment area, which includes rainfall and evaporation data. This model can predict discharge into the reservoir up to fourteen days in advance. This rating curve is based on the water balance of the Bui dam reservoir, thus still overestimating the discharge for any water level measured upstream in Chache.

## 1.2. Problem analysis

This research will be focused on two different sections of the discharge modelling project: the validation of equipment, and the determination of the influence of the floodplains to the discharge, which includes their implementation into the hydraulic model that was made by N. Hoogendoorn. A main difference with former research is that this is conducted during the wet season, which leads to higher discharge rates and wider rivers including floodplains.

Since the research conducted by Hoogendoorn (2023), a new method has been developed to remotely measure the water height in the river, namely GNSS reflectometry. As a potential permanent solution, it will allow for continuous simple discharge predictions using the rating curve, as well as a source of data to update the rating curve for its location. One of the main goals of this research is to test the applicability of this new method. Also the Large-Scale Particle Image Velocimetry (LSPIV) method will be tested. This method has already been used by Hoogendoorn (2023), but only during the dry season by using a drone. During this research, the pertinence of the method on wide rivers with large water surface velocities will be investigated with a potentially permanently placed camera.

Furthermore, the influence of the floodplains on the river discharge needs investigation, as these are often neglected and depreciated as just storage. However, higher water levels could result in significant flow in the floodplains, which could influence the discharge of the river. The flow in the floodplains depends on the spatially varying roughness coefficient, which is induced by the local vegetation. Hoogendoorn (2023) used a global estimate for the whole floodplain in his hydraulic model, which is time-efficient, but not accurate. A method needs to be created to determine the roughness coefficient in the floodplain based on the spatial variation of the vegetation.

In order to better model the hydraulics of the Black Volta, it is important to consider the role of the floodplain in transporting and/or storing water during peak flow events. In comparison to the main channel, the floodplain hosts vegetation that hinders the flow of water. The friction caused by the roughness of the floodplain hence decreases the water velocity relative to the main channel. In the context of a rating curve, a more rough floodplain would lead to less flattening of the curve at high flows than a smooth floodplain, as lower velocities still need to convey the same discharge. Therefore, better understanding the hydraulic behaviour of the floodplain will lead to a better understanding of the processes that relate water level to discharge during peak flows. A better rating curve will allow BPA to optimize their production of green electricity as well as lower the risk of an emergency spillage.

One major objective of TEMBO is to enable data collection in remote regions. In the process of understanding the role of floodplains better, a remote sensing approach to estimate roughness serves this goal well. By estimating floodplain roughness with remote sensing data, one can easily get vegetation as an input for hydrodynamic models (like Delft3D) as a means to predict the hydraulic behaviour of any river or river section. Potentially, one could then install a water level measurement station and perform a couple of discharge measurements in any location to calibrate the model, which will then produce a neat rating curve for this area. Eventually one could consider modelling a larger stretch of a river hydro-dynamically to predict up- and downstream effects of any event that changes the water level and/or discharge in the river.

## 1.3. research questions

The research questions that will be answered in this report are subdivided into the three parts that have been discussed previously.

### 1. Equipment

- a. Can the GNSS reflectometry serve as a permanent in-situ water height data collector?
- b. Can the LSPIV method be applied at wide rivers with high flow velocities?

### 2. Floodplains

- a. How can the roughness coefficient be determined and implemented into the hydraulic model?

b. What is the contribution of the floodplains to the river discharge?

3. Rating curve

a. What is the influence of the wet season measurements on the rating curve?

## 1.4. Structure

Chapter 2 gives an overview of the project plan, which is followed by a description of the locations where measurements have been done and which existing data has been used. All different sections within the project have their own chapter, including methodology, results and discussion. Chapter 4 covers the water height methodology and results, which is followed by the bathymetry. In chapter 6 the use of OpenRiverCam has been explained in all locations. Chapter 7 discusses the contribution of the floodplains to the discharge by determining the roughness coefficient and chapter 8 covers the work regarding the software Delft3D. Lastly, an overall discussion and conclusion was written, followed by a list of recommendations.

# 2

## Project plan

The main goal of the project is to answer all research questions for the river section close to Chache, at the location of which N. Hoogendoorn has made his hydraulic model of the Black Volta. However, since this location is relatively isolated, the equipment has initially been tested on a small stream in Tamale and at the White Volta, where the river passes the village Yapei. The retrieved data is used to practice with the software. After the operation of the equipment has been assured, it was installed in Chache. During the installment, data has been collected that is required to answer the research questions regarding the floodplains.

Figure 2.1 shows a flow chart overview of the project stages and the collected data. Three software models are used to answer the research questions: RTKLIB, OpenRiverCam and Delft3D. The required input data for both models are water level and bathymetry. Additionally, RTKLIB uses satellite signals with which the water level is measured, OpenRiverCam uses water surface velocity and the RTKLIB water levels, and Delft3D uses the slope of the river and the roughness coefficient in the floodplains. With OpenRiverCam the river discharge for a specific measured water height is determined. Delft3D provides a rating curve, which is based on discharges and their corresponding artificial water heights, which are found by running the model. The retrieved results will be validated by plotting the river discharge from OpenRiverCam into the rating curve to determine if they match. OpenRiverCam can also provide surface velocity data for a specific water height, which will be compared with the surface velocity data that was collected for the OpenRiverCam model. By comparing the retrieved rating curve with formerly constructed rating curves that do not take into account the effect of the floodplains, the influence of the floodplains on the discharge can be determined. All results will lead to answers to the research questions and a better prediction of the discharge of the river for a specific water height.

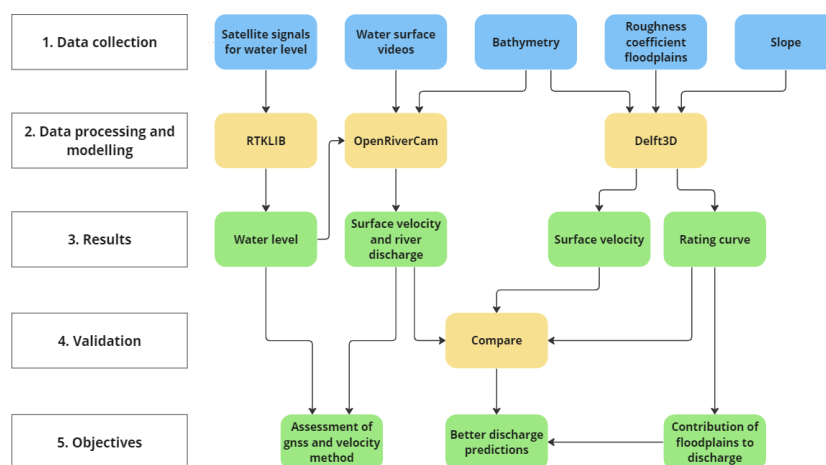


Figure 2.1: Flow chart overview

## Study area and existing data

This chapter firstly covers the area description of the entire Volta River Basin area regarding the climatic and geologic properties. Afterwards, the characteristics of the measurement locations are discussed in more detail. In the second section of this chapter, external data used for this project is discussed. This includes discharge data, bathymetry data as well as remote sensing data. Furthermore the existing hydraulic model, which this research aims to improve, is discussed.

### 3.1. Study area

The Volta River Basin is a river basin in western Africa with a size of about 405 000 km<sup>2</sup>. The river catchment covers parts of six countries and can be divided into three sub catchments (Figure 3.1):

- The Black Volta
- The White Volta
- The Oti river

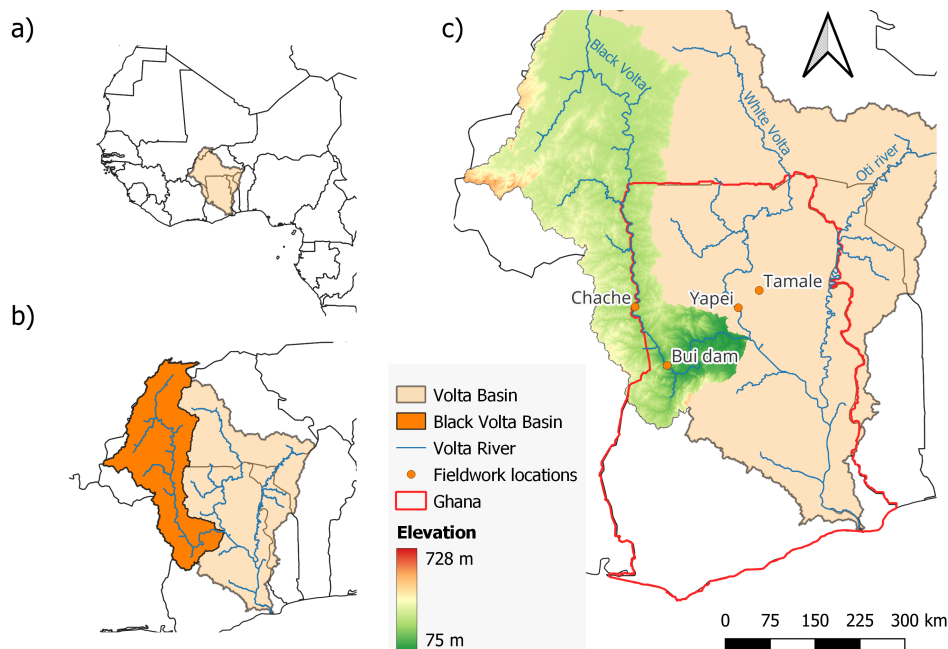


**Figure 3.1:** a) Volta river basin in west Africa. b) Part of the Volta basin which is named the Black Volta Basin. c) Map of Ghana showing the elevation in the Black Volta Basin and the field sites relevant for this project.

The main interest of this research lies on the Black Volta River. The subbasin of the Black Volta river can be seen in Figure 3.1. It covers parts of Mali, Burkina Faso, Ivory Coast and Ghana and has an area of 130,000 km<sup>2</sup>. The Köppen climate classification of the basin is predominantly tropical savanna (Aw), indicating the wet summer and dry winter. August until October are generally the months with the highest amount of rainfall, while November till March are the driest. This can also be recognized in the discharge of the Black Volta at the inflow of the Bui reservoir ranging from 0.7 m<sup>3</sup>/s in the dry season to 1800 m<sup>3</sup>/s in the wet season with an average inflow of about 150 m<sup>3</sup>/s for the years 2000 to 2022 [11]. The geology of the basin mainly consists of granitoids, which is a broad collective term for granitic igneous rocks that have encountered different levels of metamorphism. Towards the south, the basin geology shifts to extrusive volcanic rocks. Hydrogeological transport processes play a relatively small role in the catchment area with a groundwater recharge rate of 5 % to 12 % of annual precipitation [4].

During this project three field sites were used to test the equipment and perform measurements. The first location is a small stream in the city of Tamale in proximity to the accommodation used during the field trip. The second location is the Yapei Bridge at the White Volta, approximately 45 km away from Tamale. The third location is Chache at the Black Volta about 130 km upstream from the Bui reservoir. This is the most important location as it is the location of interest for BPA where a permanent measurement setup shall be installed in the future.

### 3.1.1. Field site Tamale (small stream)

The first field site is a small stream in the city of Tamale within the neighborhood Jekeryili at the coordinates with a latitude of 9°24'38.4"N and longitude of 0°48'40.3"W. The discharge of the stream mainly consists of rainwater runoff from the neighborhood and therefore varies a lot based on the local rainfall. This could also be recognized based on large amounts of trash lying along the stream and even high on the banks while no pathway or road is present there.

The location was chosen due to its proximity to the accommodation used in Tamale during the field trip and based on its size and the existence of a bridge and high banks (Figure 3.2). The stream is about 2.9 m wide at the narrow stretch that was used to take the measurements. Due to erosion during high rainfall events, relatively high banks have formed with a height of about 3 m at the highest point. Considering the width of the stream and the height of the banks and the proximity to the accommodation made it a great location to perform some first tests with the equipment.



**Figure 3.2:** Field site location in Tamale, a small creek.

### 3.1.2. Field site Yapei (White Volta)

The field site at the White Volta in Yapei ( $9^{\circ}08'29.8''\text{N}$ ,  $1^{\circ}09'36.0''\text{W}$ ) was chosen due to its strategic location regarding logistical matters. This includes the distance to Tamale of about 45 km, good access by public transport, good internet connection as well as the existence of the Yapei Bridge. The main channel in Yapei is approximately 200 m wide with an extensive floodplain of a view hundred meters depending on the exact location (Figure 3.3a). These dimensions are larger than at the other field sites tested before and therefore optimal to stress the limits of the measurement equipment before moving it to the permanent site. The existence of the bridge with a height of about 10 m (Figure 3.3b) also gives a few essential advantages. Most importantly it makes it possible to cross the river by foot whenever needed without being dependent on a boat. In addition, sensors can be installed high above the water surface without the construction of an extra structure.

Furthermore, due to previous projects of the University for Development Studies at the same location, the procedure of community entry was a straightforward act with the support of their employees. This step is essential in the rural areas of northern Ghana to gain permission to work on the ground of the local community. In addition, logistical support like a boat and guards to protect the equipment over night could be organized through the local community.



(a) White Volta



(b) Yapei Bridge

**Figure 3.3:** Field site location in Yapei at the White Volta River. Wide river main channel of about 200 m width with small floodplain extend on both sides (a). The Yapei bridge with a height of about 10 m spans across the river at the location (b).

### 3.1.3. Field site Chache (Black Volta)

The field site in Chache is the main focus location of this project. Chache is located on the Black Volta about 130 km upstream from the Bui reservoir ( $9^{\circ}09'26.4''\text{N}$ ,  $2^{\circ}43'59.8''\text{W}$ ). At this location, the river forms the border between Ghana and Ivory Coast which makes working on both sides of the river challenging. The location was chosen by BPA and water level and discharge measurements have been conducted there since the year 2000. Even though the location can only be reached after a three hour drive from the Bui reservoir it is still one of the best possible location given the fact that there are only a few locations upstream of the Bui reservoir where a road is present.

The main channel of the Black Volta in Chache is about 150 m wide (Figure 3.4a) with a wide floodplain extend on the Ghanaian side vegetated with large amounts of shrubs (Figure 3.4b). The only option to cross the river at this location is by a small ferry. However, currently a bridge is constructed to connect Ghana and Ivory coast at the site. Due to its remote location only patchy network connection from the Ghanaian GSM network is available while the 3G network from Ivory coast has a good connection.

The lack of a bridge at the location creates the need for other structures to place the measurement equipment on. Currently two structures are present at the location for this purpose. Due to sensors installed in the past an old scaffold structure is present on the river bank (Figure 3.5b). Some parts of the setup are still in place, however not operational anymore. The top of the scaffold is at about 9 m respective to the reference level of local water level measurement. This results in a height above water level of about 7.5 m in the dry season and 2.5 m in the wet season.

In addition to the old structure a new 6 m high concrete pole has been constructed about 50 m downstream from the old structure on the highest point of the river bank (Figure 3.4a). The top of the pole is at about 11 m respective to the local reference level which results in a height of 10 m above water level in the dry season and a minimum of 3 m above water level in the wet season. This pole was built for the purpose to allow for a more secure, permanent measurement setup with a larger height above the water level and good field of view on the river.



(a) View on the main channel in Chache



(b) Floodplain in Chache

**Figure 3.4:** Field site location in Chache at the Black Volta River. Wide river main channel of about 150 m width (a) with large floodplain extend up to 500 m on the Ghanaian side (b).



(a) Newly constructed pole for measurement platform



(b) Old measurement structure

**Figure 3.5:** Two existing structures in Chache to mount measurement equipment. (a) One pole recently constructed by BPA. (b) one scaffold already existing for the last two decades which was used to mount various sensors in the past.

## 3.2. Data

Due to previous studies at the same location like the master thesis of N. Hoogendoorn [10] and M. Kasteel [11] a variety of data is already available and can be used for future research. Furthermore, data from measurements of the hydrological service department (HSD) and BPA can be used for modelling and validation purposes. The existing data includes discharge data, bathymetry data and an existing hydraulic model for the location in Chache.

### 3.2.1. Discharge data

The discharge of the Black Volta is measured in two locations. In Chache measurements started in 2000 and in Lawra in 2010. In both locations the discharge is not measured directly but calculated from measured water height through a rating curve. In Figure 3.6 the measured time series can be observed. Even though no large tributaries exist along the 200 km stretch of river between the two measurement locations the measured discharge in Chache reaches values up to five times as high as the ones in Lawra during the wet season. This led to the conclusion by M. Kasteel that the discharge data for Chache should only be used after transformation with a new rating curve [11].

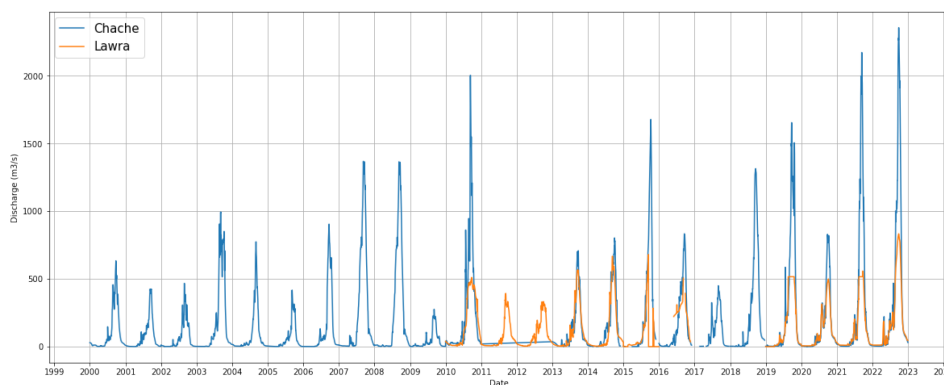


**Figure 3.6:** Discharge of the Black Volta measured by BPA in Chache since 2000 and Lawra since 2010 [11]

### 3.2.2. Bathymetry data

The bathymetry in Chache was measured by N. Hoogendoorn during the dry season 2023. The results of these measurements are displayed in Figure 3.7. The wet bathymetry of the main channel was measured with a fishfinder which uses sonar technology while the dry bathymetry was captured by a UAV-drone up to a distance of 200 m from the main channel.

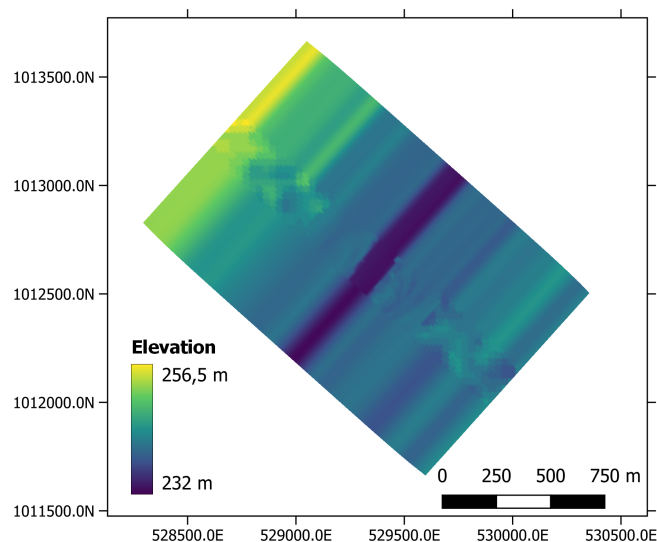


**Figure 3.7:** Bathymetry of the main channel and floodplain of the Black Volta in Chache [10]

The complete bathymetry was then obtained by performing an interpolation which gives neighboring points in direction parallel to the channel a higher weight than neighboring points in direction perpendicular to the channel. Through this step the natural shape of the channel is better represented after the interpolation. However, while this 2D bathymetry is available for the location in Chache, no detailed single measurement of the exact cross-section was taken.

### 3.2.3. Existing discharge model

This study expands on the 3D discharge model in Delft3D FM suite developed by N. Hoogendoorn at the Chache site [10]. Delft3D relates the flow velocity to the hydraulic radius, the hydraulic slope and the roughness coefficient to model river flow. All input of the discharge model of N. Hoogendoorn is used, except for the friction coefficient in the floodplains which is altered to determine the influence of the floodplains on the river flow.

The input of the 3D discharge model in Delft3D FM suite is listed in this following paragraph. Firstly, the model includes the bathymetry data mentioned in section 3.2.2, which is assigned to an unstructured grid. The grid has a dimension of 6 kilometres in length and 1.7 kilometres in width, with every grid cell having an equal layer distribution of ten layers to transform the model to 3D. The bathymetry and the grid have a coordinate system of WGS 72 / UTM zone 30N. Secondly, the hydraulic slope is used of 0.0003. The slope was estimated using the photogrammetry point cloud and also using SRTM DEM [10]. Two boundary conditions need to be defined; an upper discharge boundary condition and a lower water height condition. These boundary conditions were chosen to be at a great distance from each other to ensure that the boundary conditions have a negligible influence on the results. In the study of N. Hoogendoorn a Manning's friction coefficient of  $0.045 \text{ s/m}^{1/3}$  was determined in the river channel by fitting it to the rating-curve from M. Kasteel [11]. Lastly, an initial water level condition is set so that the steady state in the modelled river is reached faster, which reduces the required running time of Delft3D. All other model settings are kept on default. Figure 3.8 shows the model of N. Hoogendoorn, including the bed level and the unstructured grid. The eyes and the cross-sectional lines represent observation points, which are placed to observe the water level, flow velocities and cross-sectional discharges.

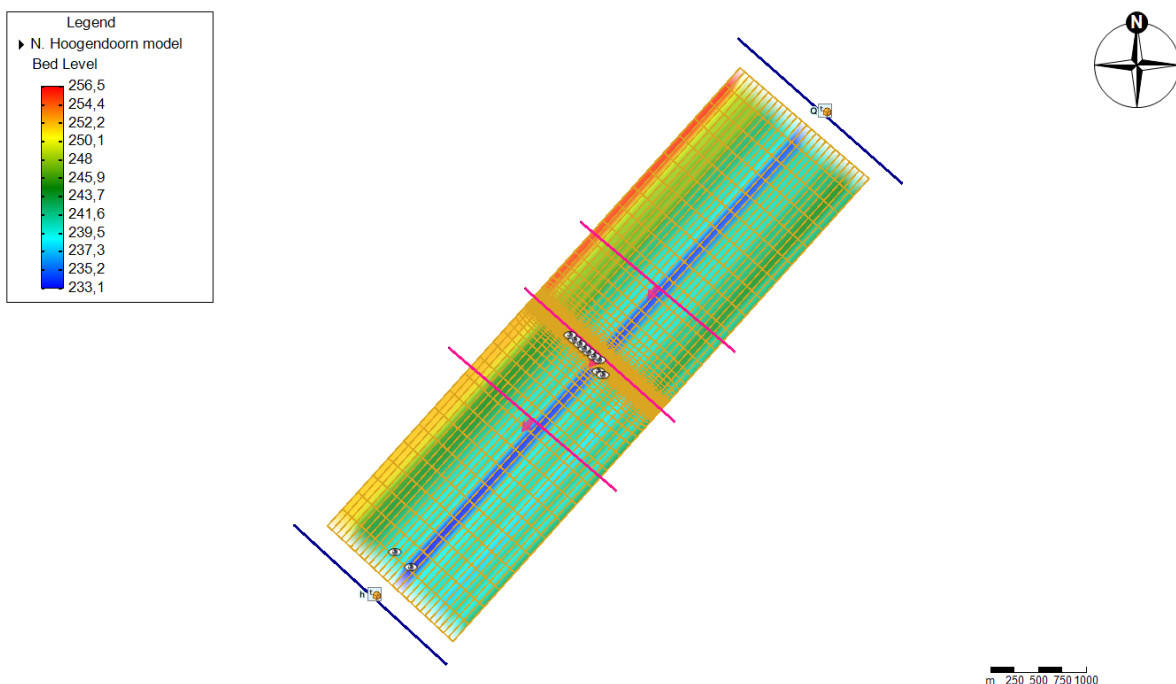


**Figure 3.8:** Delft3D FM suite model of N.Hoogendoorn showing the bed level and unstructured grid.

### 3.2.4. Rating curves

Currently, the inflow into the reservoir at the Bui dam is estimated by a rating curve shown in Equation 3.1. This water level  $[m]$  - discharge relation  $[m^3/s]$  was developed by BPA during the dam's feasibility

study prior to 2013 using an Acoustic Doppler Current Profiler (ADCP) [10]. This rating curve was established based on water levels below 4.6 m, when the river flow is within the river banks and no floodplain was taking into consideration [11].

$$Q = 21.5(H - 0.55)^{2.4} \quad (3.1)$$

In the study of M. Kasteel a new rating curve was established based on the reservoir water balance, taken into consideration daily water height measurements, evaporation rates, local precipitation and reservoir volume curve [11]. The rating curve relationship is shown in the equation 3.2 below.

$$Q = 20(H - 0.32)^{2.27} \quad (3.2)$$

# 4

## Water height

### 4.1. Methodology

First the core principles of GNSS-IR are described. After that, the findings are discussed and a thorough account of the measurement effort is given, including its outcomes. In this study, the choice of GNSS-IR for gathering water height data was made without first investigating alternative comparable measurement methods for practical reasons related to the project.

#### 4.1.1. Principle

By measuring the Water height and the DEM of a river, the river's cross-sectional area can be estimated. By indicating the river's cross-sectional area together with the measuring of the speed of the water in the river, an estimate can be made for the river's discharge rate.

GNSS reflectometry is a suitable remote sensing option to obtain the water height for several reasons. First, due to the diagonal direction of the multipath signals it is possible to install the receiving antenna far from the river (with the appropriate height). Second, GNSS reflectometry offers a broader coverage area, allowing for measurements over larger sections of the river compared to localized sensors on bridges. Third, GNSS reflectometry can provide continuous and real-time data collection, offering a more dynamic and responsive monitoring system compared to manual periodic measurements of river level gauges.

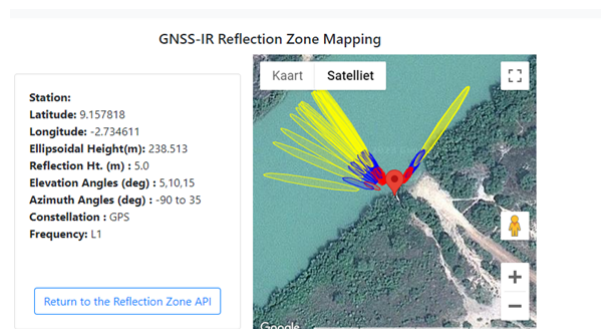


Figure 4.1: GNSS-IR reflection-zone cache

Signals from the GNSS are picked up by an antenna that is positioned next to the river. It concurrently catches signals from the satellites directly, as well as signals from the satellites that first are reflected by the water before reaching the antenna. The distance between the direct and reflected signals changes as the satellites travel through their orbits. As a result, the antenna receives these signals intermittently in phase or out of phase, which causes changes in the SNR. Christine Larson [3] showed that the SNR can be defined as a function of the satellite's elevation angle and the height in each case when a GNSS

satellite aligns with the water surface, causing the antenna to receive reflected signals. The equation which is used in Christine's Larsons software can be viewed in equation 4.1 [14],

$$SNR(e) = A(e) \cdot \sin\left(\frac{4\pi H_r}{\lambda} \cdot \sin(e) + \sigma\right) \quad (4.1)$$

where  $e$  is the GNSS satellite elevation angle with respect to the horizon,  $\lambda$  is the GNSS wavelength,  $\sigma$  is a phase constant,  $H_r$  is the vertical distance between the GNSS antenna phase center and the horizontal reflecting surface, and  $A(e)$  represents the amplitude of the SNR data. To be clear, this representation of SNR data is time dependent because  $e$  is a function of time.

#### 4.1.2. GNSS-IR campaign Chache

Prior to beginning the Chache measurement project, it was made sure that the location was suitable for GNSS reflectometry. Therefore, an online application known as the Christine Larson Reflection Zones tool was used. At the GNSS reflection measurement station, the observations are depicted in Figure 4.1. During the measurement day, the GNSS antenna was positioned as close as possible to the target object, maintaining a static stance at the predetermined location identified by the Reflection Zones web application. It was crucial to ensure an elevated height compared to the water whenever possible. It was also made sure that the antenna remained stationary in the location recommended by the Reflection Zones web app. A U-blox F9P was used as GNSS measuring on a sample frequency of 0.07 Hz, to receive the satellite signals. Connected to this receiver was the ArduSimple 'budget antenna'. The collected data was prepared for analysis after the measurement day was over. For further information, see Appendix E. This section of the paper details the procedures that were used to clean up and get the data ready to obtain the river height.

## 4.2. Results

The measurement campaign resulted in five river height epochs with a total measurement time of ten hours. This means a GNSS-IR sample frequency of approximately one measurement per two hours. The result can be seen in figure 4.2. It is not useful to statistically analyze these results due to the combination of a low number of epochs and the lack of control data. However, with PPK the coordinate of the water line was obtained one time and this seemed to match the GNSS-IR water height in tenths of centimeters.

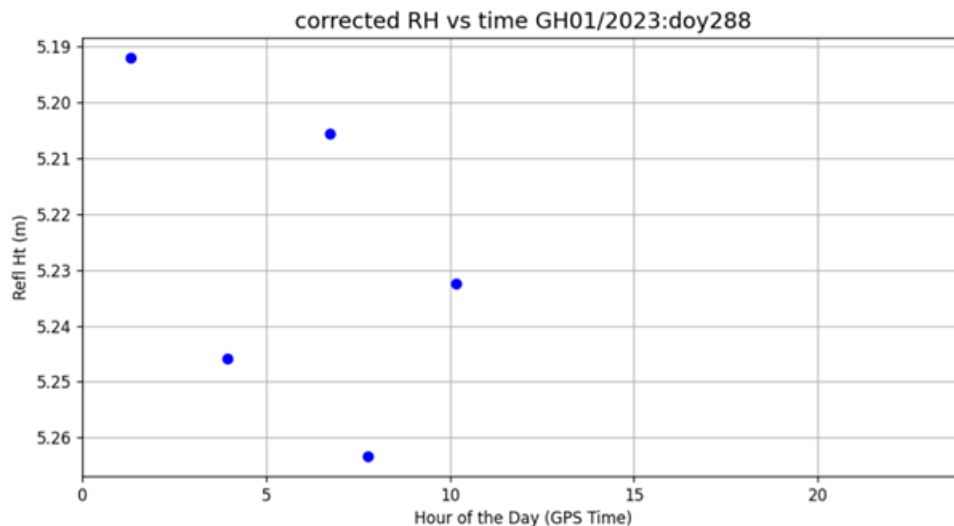


**Figure 4.2:** GNSS-IR results Chache

The exploration of the sub-research query, "Can GNSS reflectometry act as a continuous in-situ water level recorder?" is supported by findings from the Chache measurement campaign. The results affirm that GNSS-IR is capable of serving as an enduring in-situ water level data collector.

### 4.3. Discussion

Five river height epochs were obtained from the measuring campaign; each was sampled roughly every two hours. The findings, which are shown in Figure 4.2, suggest that river height may gradually drop during the campaign. However, statistical analysis remains ambiguous because of the small number of epochs and lack of control data. Before implementation of this workflow, it should be verified with control data, to create a measurement and pre-process workflow.

Reducing the amount of data that is shared between the GNSS- IR modules and the central server is critical in Africa, where communication infrastructures are scarce. In order to reach this goal, internal GNSS-IR processing software could be developed. While developing this software one should balance the need for accurate river heights with the constraint of limited onboard computational resources of the measurement unit.

# 5

## Bathymetry

Multiple methods used in this project require a the bathymetry of the measurement location as basic input. For the field site in Chache this data was already available (Section 3.2.2). However, to test the discharge measurement method with OpenRiverCam on the other field sites as well, the bathymetry had to be measured first. Due to the small size of the stream at the field site in Tamale the depths in the cross section could be measured with a tape measure. In contrast, obtaining the bathymetry for the field site in Yapei was a complex process.

### 5.1. Data collection

At the field site Yapei the wet bathymetry of the river bed was measured using a similar methodology applied by N. Hoogendoorn at the field site in Chache [10]. Multiple cross sections of the bathymetry were measured by attaching a floating device to a canoe which then crossed the river multiple times at different locations (Figure 5.1a and 5.1b). The floating device has a sonar device attached at his bottom; the Deeper Sonar Chirp+. This cost-effective device measures the depth of the water surface to the river bed and its location, using the GPS data from a smartphone which is connected to the device through a Wi-Fi connection. It can measure up to 100 meters depth and send out a signal with  $7^\circ$ ,  $20^\circ$  and  $47^\circ$ , where the smallest angle gives the most exact results. The higher the turbidity, the larger the required angle to get a result [5].



(a) Canoe with floating device at the left side.



(b) Set-up of Deeper Sonar Chirp+ device on floaters.

The captured points are then used to perform a b-spline interpolation to obtain a 2D bathymetry for the field site in Yapei. This interpolation method gives a good result for the average cross section at the site. However, details in the bathymetry at a specific cross section get lost in the interpolation process.

To account for this issue, another method was applied as well to capture one detailed cross section. The sonar device was attached to a rope and lowered from the bridge present at the location. Water depth measurements were taken in a cross-section by walking up and down the bridge. To prevent the sonar device from getting influenced by the different river flow velocities the rope has to be stretched at all times which can be archived with a heavy weight at the bottom.

## 5.2. Results

The results of both methods applied to obtain the bathymetry can be observed in Figure 5.2. As can be seen in the figure the depth in the main channel varies between 8 and 12 m. At the side of the main channel the steep, but at this season submerged, riverbanks can still be recognized. Along the travel routes of the boat and underneath the bridge much higher detail can be observed compared to the interpolated sections of the channel. This leads to the situation that some features of the bathymetry might not be captured in the interpolated product. An example is the deep area on the right side of the channel just before the bridge. This spot with a depth of about 14 m was only captured with one line of the boat observations. Due to the fact that the boat didn't pass by again in the proximity of this area it is just shown as a deep spot in the interpolated bathymetry.

To validate the bathymetry which was obtained from observations with the boat and then interpolated over the whole river section, a second cross section was measured below the bridge. In Figure 5.3 the cross section of the bathymetry below the bridge, measured with the two different methods can be observed. When comparing the two cross sections it can be seen that they match well at the right side of the main channel while there is a difference of up to two meters in the center of the channel. However, on the right side of the channel there are less features along the cross section while in the center of the channel the measured depth varies by up to 3 m within an distance of 15 m. Therefore the difference could also be due to errors in the measurements from the bridge.

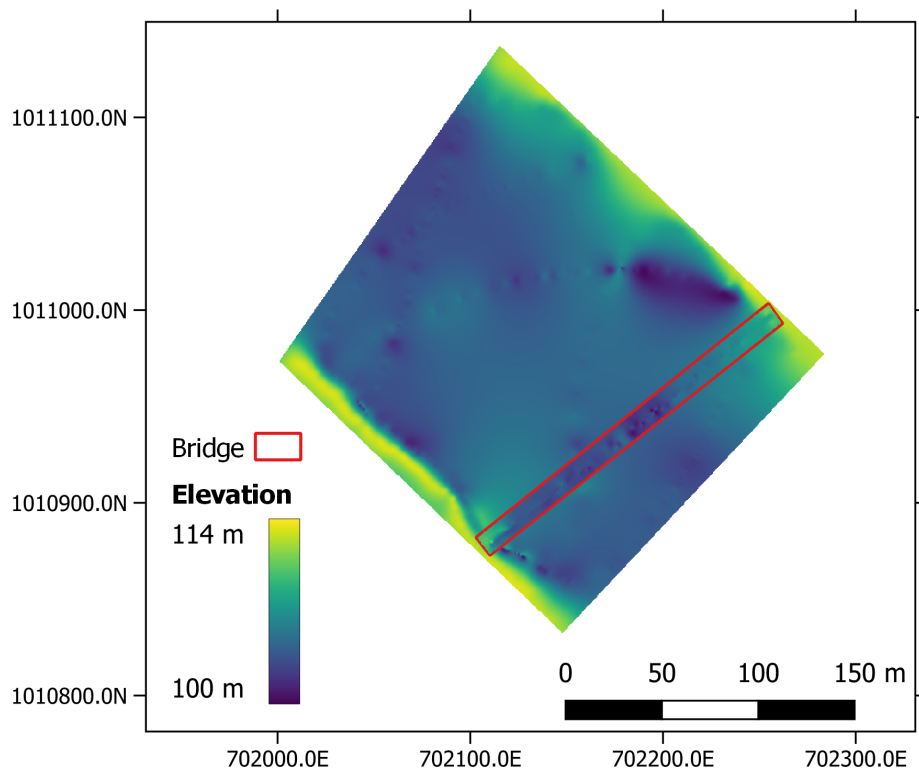


**Figure 5.2:** Bathymetry at the Yapei bridge measured with a FishFinder sonar device and interpolated using a b-spline interpolation and bathymetry measured with a rope from the bridge (red box).

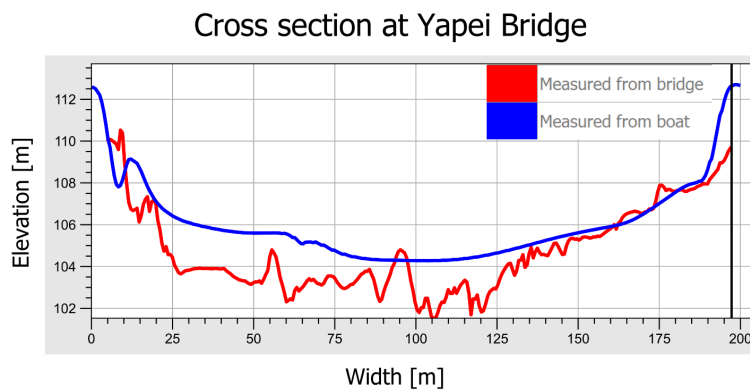


**Figure 5.3:** Cross sections of bathymetry underneath the Yapei bridge measured with the SonarChirp+ attached on a rope from the bridge (red) and attached to a boat and then interpolated over the full area (blue).

### 5.3. Discussion and conclusion

The measurement and post processing methodology could be improved in many steps to reduce uncertainties and produce more accurate bathymetry data. A first step would be to use a more accurate measurement device. Even though the used SonarChirp+ can measure the water depth with sufficient accuracy, the uncertainty of the measured point is still high due to the poor quality of the GNSS antenna of the connected smartphone. A solution to improve this issue would be to connect an external RTK-GNSS to the smartphone to get more accurate point measurements in real time. This technology, however, could not be achieved in time.

Another method was tested to still gain more precise point measurements even though the right equipment was not available. As can be seen in Figure 5.1b, a GNSS antenna connected to a GNSS-IR module was attached to the floater on top of the Deeper Sonar Chirp+. This GNSS device was the same, which was used to capture the control points described in section 6.1.4. However, due to its low measurement frequency of 0.067 Hz to 1 Hz, the device is not suitable to capture locations while moving. In addition the needed post processing steps made the matching of the measured depth and location more difficult. Therefore, this method was not usable and the smartphone antenna still gave the best results.

However, the quality of the interpolated bathymetry is not only dependent on the accuracy, but also on the density of acquired data points as well as the chosen post processing steps. Due to the strong current of the White Volta during the wet season and the only available boats being canoes without engine, the crossing of the river was a challenging task for the local fishermen. They were not willing to cross the river more than a few times due to safety reasons and therefore only limited cross sections could be measured. This issue led to limited information about special features in the bathymetry and big challenges for the interpolation of the whole grid in the post processing.

To get a first idea of the bathymetry the b-spline interpolation was performed with the available cross sections measured from the boat. However, it is clearly visible in Figure 5.2 that details in the bathymetry are only available along the travel routes of the boat while an average depth without special features is calculated for the rest of the area. When comparing the interpolated bathymetry with the measurements from the bridge it can also be concluded that the obtained bathymetry is not sufficient for further usage in hydraulic models. Further steps to improve the interpolation would be to give neighboring points in direction of the flow a higher weight than neighboring points along the width of the river as described by N. Hoogendoorn [10]. By assuring that every cross section area along the river is equal the quality of the bathymetry could even be improved further. Due to the issues encountered with OpenRiverCam at the Yapei Bridge which are described in section 6.2.2 an accurate bathymetry at the site does not add significant value to the goal of the project. It was therefore decided to not spend large amounts of time to perform further steps to improve the bathymetry which is based on limited data points with poor quality. Using the cross section of the bathymetry measured from the bridge would be recommended if possible for the application.

# 6

## Surface velocity and discharge by OpenRiverCam

One of the three things needed to calculate discharge of the main channel is velocity. This chapter explains the methodology, results and discussion of how water velocity was retrieved by processing videos with the software OpenRiverCam and how one of its inputs so-called ground control points were captured with the RTK GNSS method.

### 6.1. Methodology

The Python software pyOpenRiverCam (pyorc) is used to determine the surface velocity and the discharge of the river using small videos that are taken of the river. Pyorc uses Large-Scale Particle Image Velocimetry (LSPIV) to retrieve surface velocities from a video. Inputs of OpenRiverCam are the water height, bathymetry and accurate coordinates of ground control points (GCP's). The methodology of measuring the water height and the bathymetry is explained in Chapter 4 and Chapter 5, respectively. The locations of the ground control points are captured with a gnss rover according to Post Processed Kinematic (PPK), a position measurement technique (further elaborated in Section 6.1.4), these control points should be located at a distance from each other whilst within camera view. Another thing to take into consideration are the lens characteristics of the camera, which are calibrated by OpenRiverCam.

With its recent release in 2021 OpenRiverCam has yet to be tested on wide rivers [17]. Wide rivers have multiple complications, such as a small camera angle, loss of visual information at pixel size at the far side of the river, inaccurate control point selection and difficulties in solving the orthoprojection. To research and mitigate this, two additional sites were used to test the method before installing the camera at the Chache site.

#### 6.1.1. Tamale

The first test site is a small stream in a close by neighborhood in Tamale, where both good angles and good ground control points (Figure 6.1a) were tested against bad angles and bad ground control points (Figure 6.1b) in order to test the limits of OpenRiverCam. Here, GCP's are considered bad when they don't cover much space together while having a minimum amount of GCP's (six), so only two GCP's were put close to each other at the other side of the stream. A relatively uniform part of the stream was selected and a phone was taped onto a tripod. Plastic bottles lying around the area were used as reference points. The location of the colorful caps of the bottles were measured in with a PPK rover and marked in the video frame in pyorc. The value of the z-coordinate was afterwards subtracted by the 1.5 meter length of the PPS pole, which was held level with an air bubble. Furthermore, a rough bathymetry was measured by writing down the depths in 50 cm intervals. Lastly, a rough velocity profile was retrieved by measuring the water velocity with current meters in intervals of 50 cm to validate the velocity results of OpenRiverCam. The videos were then processed with pyorc. The settings in OpenRiverCam influence the results, but were left standard for this stream.



**Figure 6.1:** Tamale camera views with different angles and number of control points. The red crosses show the control points.

### 6.1.2. Yapei

The second test site at Yapei is similar to Chache and therefore a good location to test the equipment to get ready for Chache. Yapei differed from Chache in mainly two ways; the river in Yapei is wider (being +200m) and in Yapei there was a lack of a tall pole available to install the camera on. Instead of a pole, the camera was installed next to the bridge at the side of the river, being +- 14m above water level, as can be seen in Figure 6.2.

Six control point locations were chosen spread across the camera view. After getting community access, a boat was made available to install and measure in the locations of the control points, along with the bathymetry. Towels were spray painted with a cross to serve as reference points and hung at stable branches.

For the PPK, the site was visited before the measurement day to install the PPP base station (see chapter 6.1.4), which was guarded overnight by a local. The rate of measuring was set at standard Chache settings being once every 15 seconds. That is why every coordinate capture was done for a minimum of five minutes.



**Figure 6.2:** Yapei camera view with ground control points, shown as the red crosses

### 6.1.3. Chache

#### Ideal final setup

A platform will be mounted to the concrete pole built by BPA, to which all the equipment can be attached for final installation of the equipment. This platform must have space for both the OpenRiverCam setup and the equipment from SEBA, who have their own camera and software to measure surface velocity. This includes the reflectometry antennae, two base modules, two cameras, a pole for the GSM antennae and four solar panels. To be more theft proof, the solar panels can be slid in and were locked with padlocks. For pictures of the design and more details see Appendix A.2.

As this is the final site, the equipment was added to make the system automatic, continuous and remotely controllable. The theoretical overview is as follows:

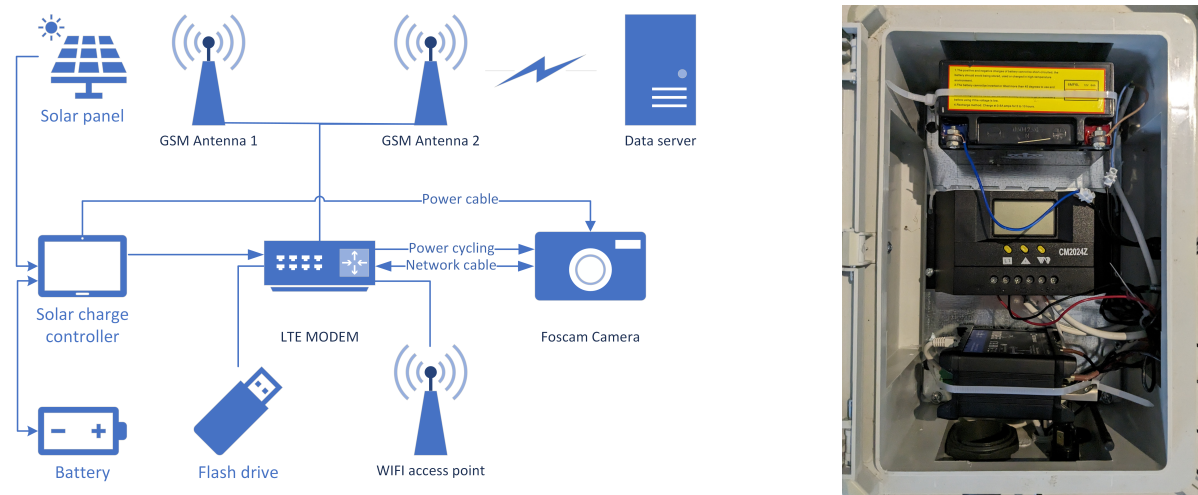


**Figure 6.3:** Solar charge controller with modem and battery (right), Camera setup diagram (left). Videos are sent remotely at intervals to the server or someone connected to wifi

The camera stores its videos on the 128GB flash drive in the LTE modem. The solar powered modem, in turn powering the camera, is connected to two antennae for 3G internet connection and sends the videos to a server. The videos are then retrieved and processed with OpenRiverCam. Power cycling was introduced by setting the LTE modem to make videos of approximately six seconds long. This setup can provide continuous and automated measurements and upload or live stream them, making the

method very suitable for remote regions. To be fully automatic, however, it needs internet connection. Even though 3G roaming was found meaning an internet connection from Ivory coast could be possible, retrieving a sim card from Ivory Coast was at that time too difficult to arrange for BPA and too difficult to get ourselves since single entry visas were booked. Therefore, only a couple of video's during the days of fieldwork were made. A 2G network from Ghana was found for the reflectometry and the connection was made using the sim module and a Ghanaian sim card.

#### Data collection

Since the water level was too high and the ground too muddy for a large period of our stay, it was deemed impossible to build a scaffolding to mount the platform. Therefore, an old scaffolding structure (used for water level measurements and satellite internet connection) was used to install a temporary setup on top. The camera was mounted on a pole for extra height and a better camera angle, next to the reflectometry sensor, see Figure 6.4a. Still, the platform was used and secured on top of the structure, including padlocks. The solar panels were in turn locked to the platform.

For this site, ten GCPs were measured in. This is four more points than the minimum, this was done to be more accurate and to be more certain of success since the coordinate captures were occasionally off by multiple meters. Selecting and capturing GCP's in Chache had been a challenge from the start, since there is no riverbank at the camera side and the other side was a country we had no visa or contacts for. As can be seen in Figure 6.4b, the camera barely sees the other side and just a few branches at the bottom. The boat was used for multiple control points. This was done with relative precision and the four positions of the boat can be seen in Figure 6.5. GCPs have also been placed at the riverbank of Ivory coast by quickly crossing the river.

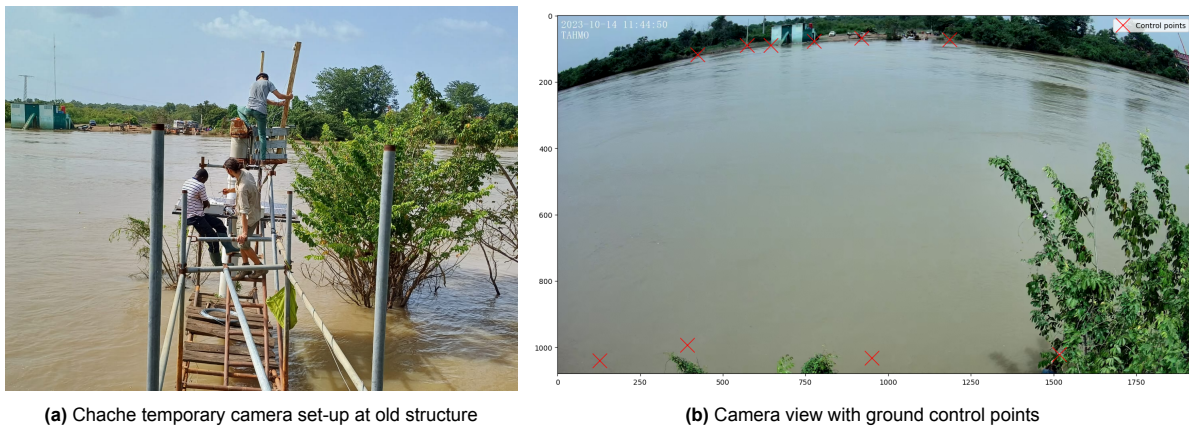


**Figure 6.4:** Camera setup Chache



**Figure 6.5:** Chache camera view with four photoshopped boats and PPK antennae

Finally, a validation check for OpenRiverCam has been done by manually performing a speed test. Floatable objects, apples and oranges, were thrown into the water and after measuring the required time to travel a certain distance, the local velocity could be calculated and compared to the velocities retrieved from OpenRiverCam. In addition, a range of settings were tested to check and improve performance.

#### 6.1.4. Control points

To obtain large numbers of control points in a relatively short time for OpenRiverCam, the choice has been made for GNSS PPK. This position measurement technique was carried out with two of the GNSS-IR measurement devices. Since the GNSS-IR measurement devices already were obtaining position data together with the elevation data.

For the PPK principle two GNSS instruments need to be measuring at the same time at a different position. One Base (static GNSS) and one Rover (GNSS which will measure all the point required). For the OpenRiverCam use case this operation is visualised in figure 6.6. One can see the Base which is kept on one place during the whole campaign, and the rover which moves to a new position after five minutes of measuring.

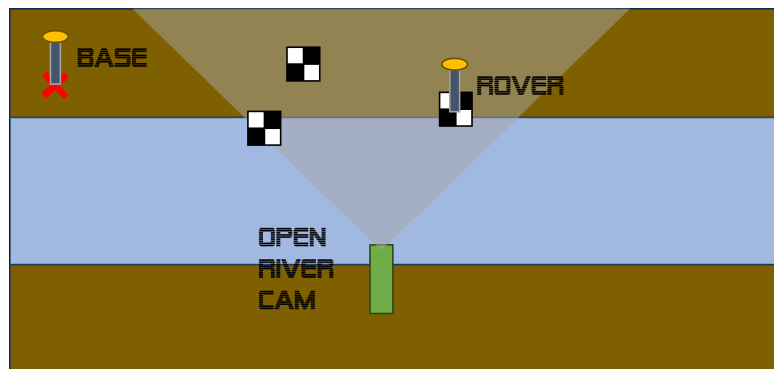


**Figure 6.6:** PPK Base and Rover visualisation. By using both a base and a rover, precise coordinates of GCP's (small chessboards on the figure) can be captured by holding a rover still for some minutes

After the measurement campaign the GNSS data of the rover and base are combined to cancel out the GNSS orbit error, clock errors, and the atmospheric errors. Another advance of 'Relative GNSS positioning' is that carrier-phase ambiguities become integers, and so, the estimation of the carrier-phase ambiguities is possible. This also greatly contributes to a better precision, due to the fact that it adds another relatively precise measurement. With this we are able to obtain benchmarks with a precision of < 5cm in < 15 minutes (measuring at 1 Hz with 2 U-blox F9P receivers). For a guide on the post processing consult appendix F.

## 6.2. Results

### 6.2.1. Tamale

OpenRiverCam managed to produce velocimetry as can be seen in Figure 6.7(left). A transect can be seen with median velocity arrows ranging from 0 to 2 m/s, at the location where the bathymetry was measured (figure 6.7). When inserting lens position, the projection deforms and median velocities become lower, ranging from 0 to 1.5 m/s (figure 6.8).



Figure 6.7: Tamale velocimetry without lens position higher camera view (left) and top view projection (right)



Figure 6.8: Tamale velocimetry with lens position and higher camera view (left) and top view projection (right)

Pyorc also managed to process the worst camera angle with the worst reference points 6.9. However, velocities were not captured everywhere, like near the banks and the whole left half of the stream. Velocities that were captured range from 0 to 1.7 m/s. This is without lens position. To see more differences the scale is set to a maximum of 2 instead of 2.5.

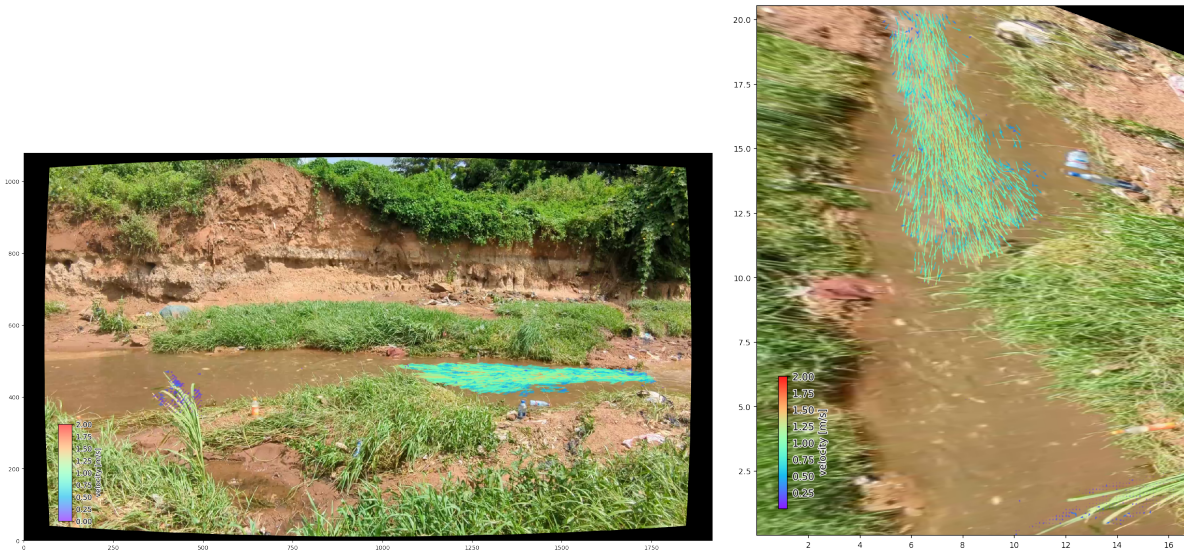


Figure 6.9: Tamale velocimetries with small camera angle and little GCP's, with camera view (left) and projected topview (right)

The current meter measurements were on the low side, ranging from 0.3 to 1.1  $m/s$  with an average of 0.50  $m/s$ . Values are summarized in table 6.1.

Table 6.1: Summary of measurements in tamale (velocity in m/s, discharge in m3/s)

| (camera) position | option lens position | mean efficient velocity median | max. efficient velocity median | discharge median | discharge range quantiles 1 till 5 |
|-------------------|----------------------|--------------------------------|--------------------------------|------------------|------------------------------------|
| high              | without              | 0.72                           | 1.52                           | 0.55             | 0.93                               |
| high              | with                 | 1.01                           | 1.80                           | 0.77             | 1.15-0.44                          |
| low               | without              | X                              | 1.7                            | X                | X                                  |
| current meter     | -                    | 0.5                            | 1.1                            | 0.26             | -                                  |

### 6.2.2. Yapei

Pyorc did not manage to calculate velocimetries for Yapei, mainly because it was not able to correctly perform orthorectification. Indicating different corners of the area of interest (a.o.i.) had effect on what seemed pyorc's geometrical solution of matching the a.o.i. to where it is in reality. In figure 6.10 the indicated a.o.i. can be seen in blue on the left and the top view on the right. Afterwards, however, the computed area of interest fails in camera view. As shown in 6.11, area of interests go all over the place.

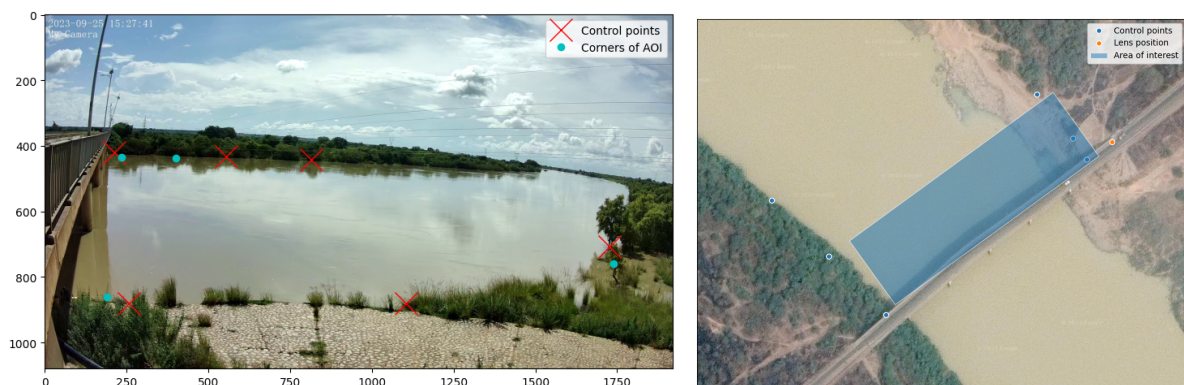


Figure 6.10: Yapei area of interest corners (left) and aoi top view (right)

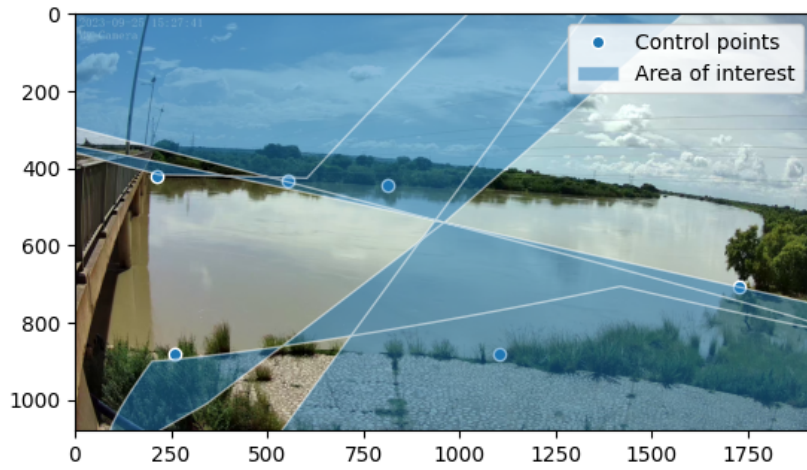


Figure 6.11: Velocities perpendicular to the transect with apple locations indicated in red

Indicating a smaller a.o.i. proved help for Chache, so this was given a try 6.12. Even though less lines and planes can be seen 6.13 (left), pyorc would not solve a correct area of interest. This influences orthorectification as can be seen in 6.13, where the sky and the opposite side are upside down.

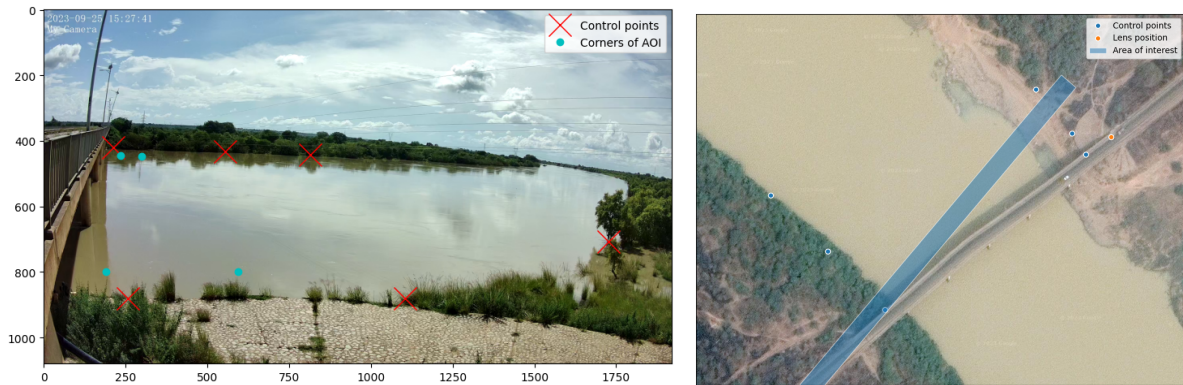


Figure 6.12: Yapei area of interest corners (left) and aoi top view (right)

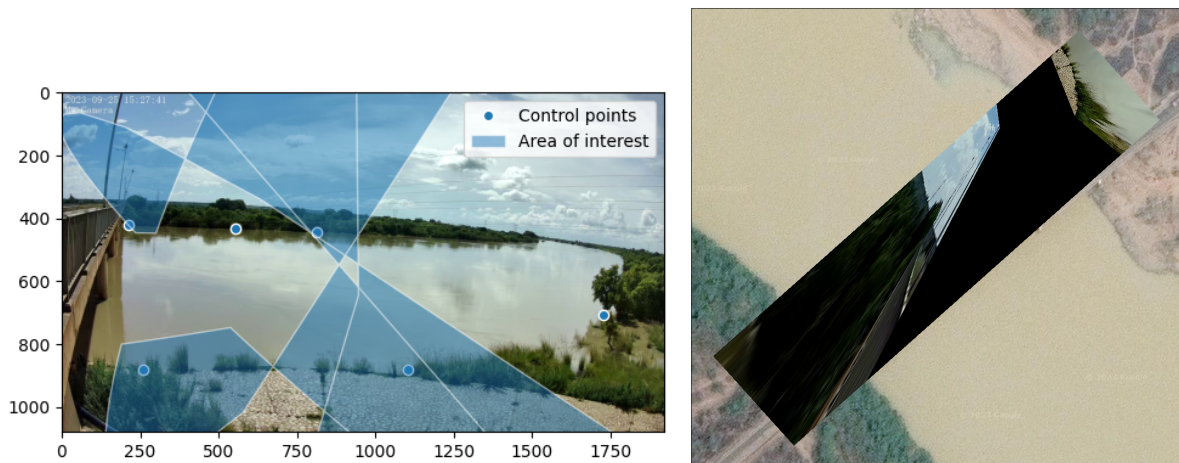


Figure 6.13: Yapei area of interest with smaller indicated corners (left) the bigger indicated a.o.i. projected to an orthorectified plane (right)

### 6.2.3. Chache

Pyorc managed to perform velocimetry at the temporary location, although barely. The final results with chosen settings are shown in camera view in fig 6.14 and in top view in figure 6.15. The transect arrows represent the median of velocities over time, the other arrows represent mean velocities.



**Figure 6.14:** Chache velocimetry means camera view (left) Chache velocimetry camera view (right)

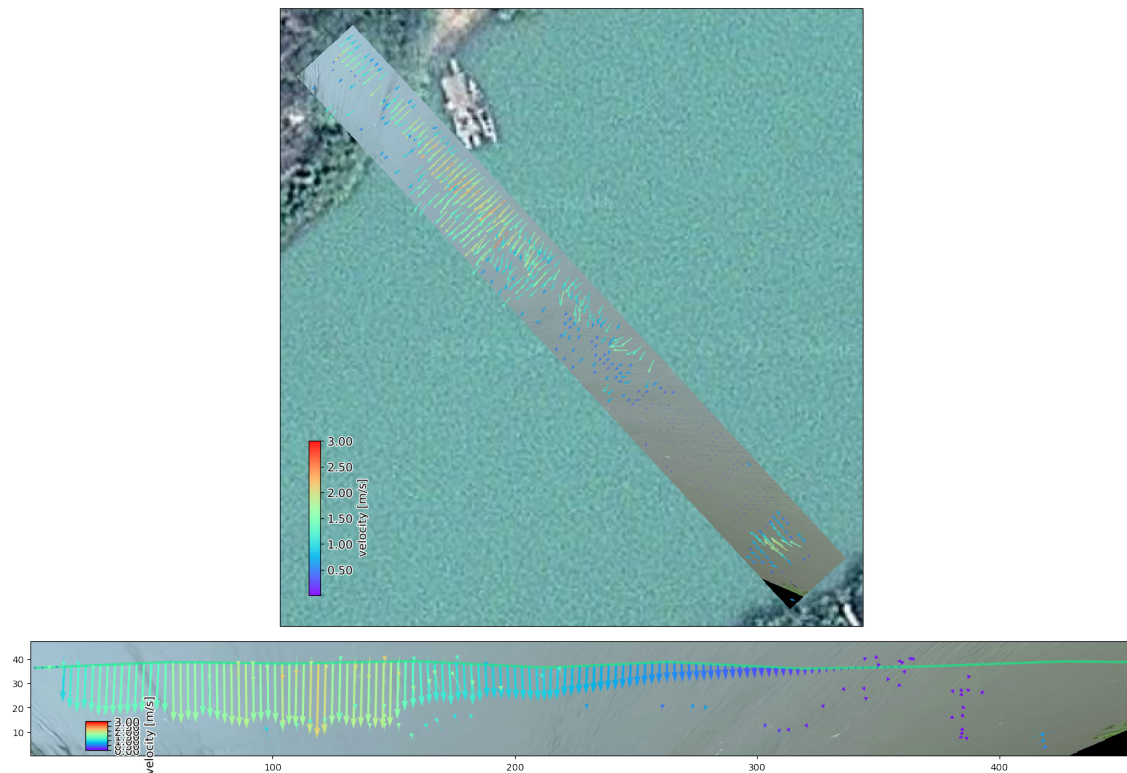


**Figure 6.15:** Chache velocimetry means top view with transect (bottom) and with google satellite (top)

Velocities range from 0 to around 2.5 m/s but the maximum velocity median with the final pyorc settings is around 2.0 m/s. This means taking the highest median of all local medians of the transect, of which a median is the most occurring value over time. The highest maximum velocity is around 3.8 m/s, always located at a turbulent spot close to the camera. As can be seen the river is thought wider than it is on google maps. Therefore the velocities in the camera view can correspond better with their real position in the river than in the top views. The discharge with final settings, explained hereafter, is around 840 m<sup>3</sup>/s. A surface-to-average velocity correction factor of 0.85 was used, a standard ratio from literature [13],[9].

### Manual speed test

The speed test resulted in two velocity measurements. Figure 6.16 shows where the floatable objects (apples) landed and where they are after tracking their flow path. Figure 6.17 shows where these are estimated to be in the velocity transect with red lines. For object 1 a speed of 1.2 m/s was measured, object 2 near the fast flowing part of the river had a speed of 1.8 m/s. At the location where object 1 was, pyorc's velocity median is around 1.3 m/s, for object 2 this is around 1.9 m/s. In the main channel, speeds go up to 2.5 m/s locally and for the median roughly between 1.5 m/s and 2.05 m/s.



**Figure 6.16:** Manual speed test locations of object 1 (left, 1.3 m/s) and object 2 being closer to the fast flowing part of the main channel (right, 1.9 m/s)

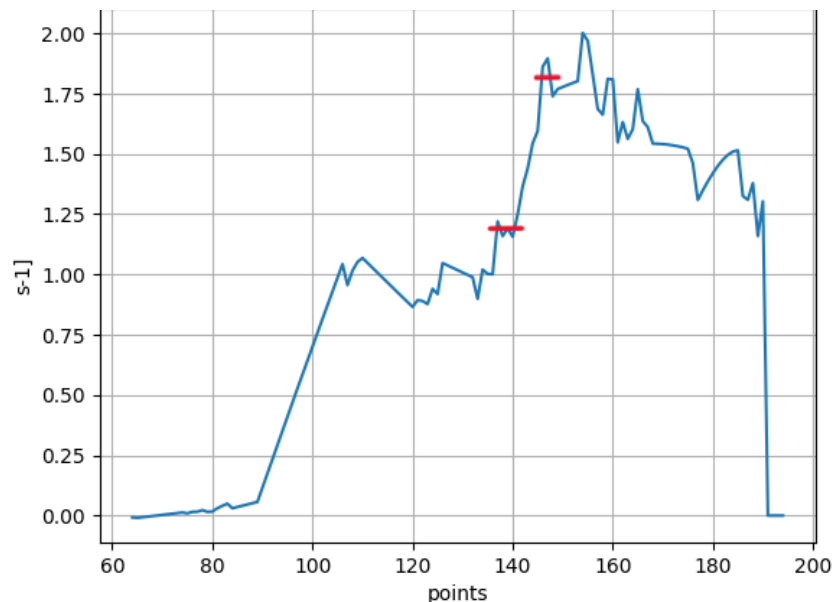


**Figure 6.17:** Velocities perpendicular to the transect with object locations indicated in red

For specific settings, pyorc's (co)creator was about to help but did not react in time, so multiple settings were tried out and put together in table 6.2. Finally, settings were chosen being the last row of the table. Choosing perfect settings are ambiguous and was not a priority of this project, but might still be interesting. The most sensitive parameters were resolution (in short, window pixel size) and window size (amount of pixels to perform velocimetry on).

A resolution of 0.30 is chosen as most representable outcome. This is where pyorc showed a lot of successful velocity measurement points in the cross section without having to auto-fill. Rerunning the same code results in different outputs. The post velocimetry processing mask option "wdw"(window used to determine relevant neighbours), showed small variations between 700 m<sup>3</sup>/s and 740 m<sup>3</sup>/s. The final window size chosen was 25 since values of discharge tend to go down when going both sides from here.

**Table 6.2:** Pyorc results with different settings.

| resolution<br>- | window<br>size | wdw<br>- | end<br>frame | mean eff. m/s<br>velocity Q50 | max. eff.<br>velocity Q50 | disch.<br>median | disch. m3/s<br>Q05-Q95 |
|-----------------|----------------|----------|--------------|-------------------------------|---------------------------|------------------|------------------------|
| 0.25            | 25             | 9        | 125          | 0.87                          | 1.47                      | 699              | -74-1570               |
| 0.25            | 25             | 2        | 125          | 0.89                          | 1.43                      | 674              | 72-1470                |
| 0.25            | 25             | 4        | 125          | 0.91                          | 1.47                      | 740              | 68-1766                |
| 0.25            | 25             | 6        | 125          | 0.89                          | 1.47                      | 740              | 61-780                 |
| 0.25            | 25             | 8        | 125          | 0.86                          | 1.47                      | 689              | -158-1532              |
| 0.25            | 25             | 4tol=0.7 | 125          | 0.89                          | 1.47                      | 734              | 62-1737                |
| 0.25            | 25             | 4        | 161          | 0.85                          | 1.76                      | 746              | -47-1754               |
| 0.25            | 20             | 4        | 161          | 0.74                          | 1.68                      | 609              | -247-1030              |
| 0.25            | 15             | 4        | 161          | 0.66                          | 1.20                      | 598              | -326-2178              |
| 0.25            | 30             | 4        | 161          | 0.89                          | 1.83                      | 700              | 37-1513                |
| 0.20            | 25             | 4        | 161          | 0.66                          | 1.59                      | 522              | -158-1289              |
| 0.15            | 25             | 4        | 161          | 0.43                          | 0.86                      | 374              | -256-2061              |
| 0.10            | 25             | 4        | 161          | nan                           | nan                       | X                | X                      |
| 0.30            | 25             | 4        | 161          | 0.97                          | 2.05                      | 744              | -61-1695               |
| 0.30            | 25             | 4        | 161          | 1.06                          | 1.94                      | 921              | 79-1933                |
| 0.30            | 25             | 4        | 161          | 1.06                          | 1.93                      | 896              | 104-1863               |
| 0.30            | 25             | 4        | 161          | 0.94                          | 2.00                      | 834              | 30-1930                |
| 0.30            | 25             | 4        | 161          | 1.00                          | 2.07                      | 796              | 41-1928                |
| 0.30            | 25             | 4        | 161          | 1.04                          | 1.97                      | 852              | 101-1842               |
| 0.40            | 25             | 4        | 161          | 0.97                          | 2.17                      | 765              | 52-1640                |
| 0.10            | 40             | 4        | 161          | nan                           | nan                       | X                | X                      |
| 0.50            | 25             | 4        | 161          | 0.75                          | 1.20                      | 688              | -15-1832               |
| 0.25            | 25             | 4        | 161          | 0.87                          | 1.92                      | 657              | -148-1832              |
| 0.25            | 25             | 4        | 161          | 0.88                          | 1.77                      | 674              | -184-1946              |

#### 6.2.4. Control points

This paragraph about the control points will further elaborate on the quality to be expected of the control points which are used by the OpenRiverCam in order to geo-reference its view. General measurement information together with measurement statistics of the measured and post processed control points are visualised in Figure 6.18 to 6.21. In the section below the concerned figures will be explained.

All four the graphs are built of the same format. The first upper sub-graph contains the standard deviation of the computed position estimates by RTKLIB regarding the north-south, east-west, and up-down direction.

The second sub-graph contains the average number of satellites which the antenna could receive during the measurement. In the measurements an atypical behaviour is observed regarding the number of satellites and the amount of standard deviation from the first graph. Namely, the average amount of satellites that are received does not negative linearly influence the standard deviation of the measurement.

The third sub-graph indicates the average status of the post processed ambiguity algorithm. When this value equals 1, the the ambiguity was solved for all the measurements, when it is higher than 1, this indicates that the ambiguity was not always solved for all the measurements. When the ambiguity is solved the carrier-phase counting measurements can be included to estimate the position. This greatly increases the precision. This behaviour can be seen in the regression of a low ambiguity value with an low standard deviation value. [15].

The fourth sub-graph indicates the total time of the measurements in seconds.

The last sub-graph indicates the baseline length in meters between the rover and the base.

During the campaign the real position of the antenna of the GNSS was observed by the measurement-technicians. Out of this some PPK position estimates seemed off around 1 meter. This discovery has been made due to the fact that the OpenRiverCam software could not run its algorithm when the faulty control points where included. Specifically these point where p3 and p5 in figure 6.20. Unfortunately, the average ambiguity of p3 and p5 are still above 1.95, which would indicate that the estimate would lay in decimeter distance from the real position.

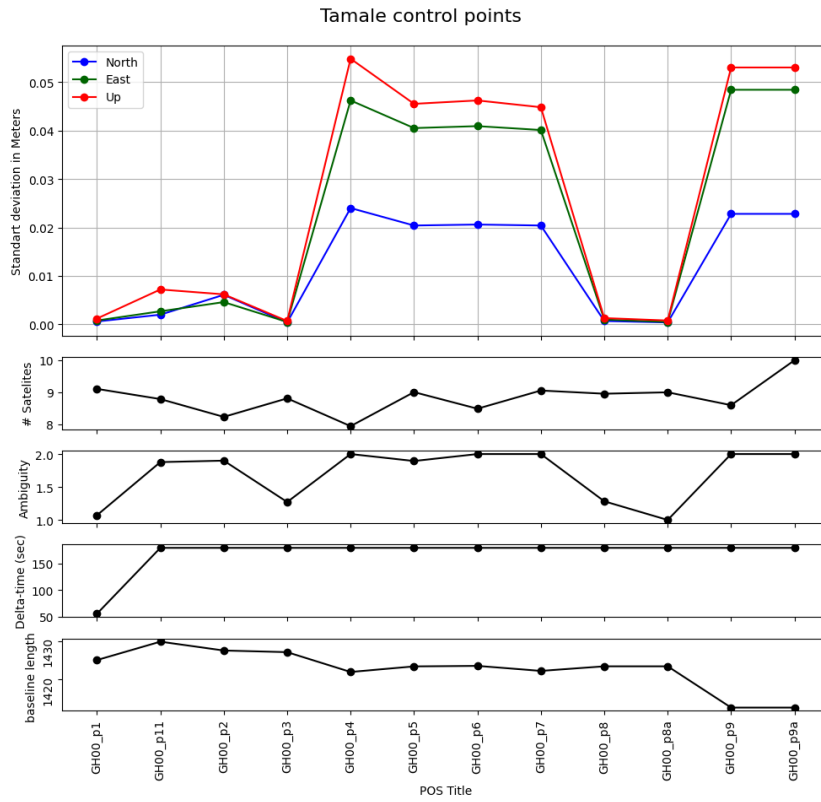


Figure 6.18: Tamale Control points statistics

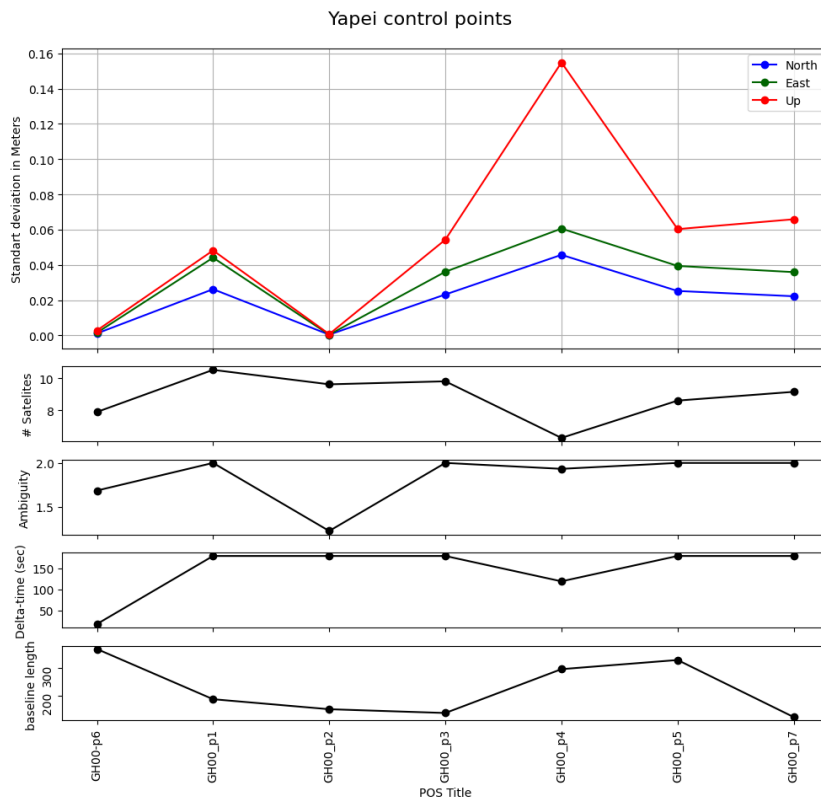


Figure 6.19: Yapei Control points statistics

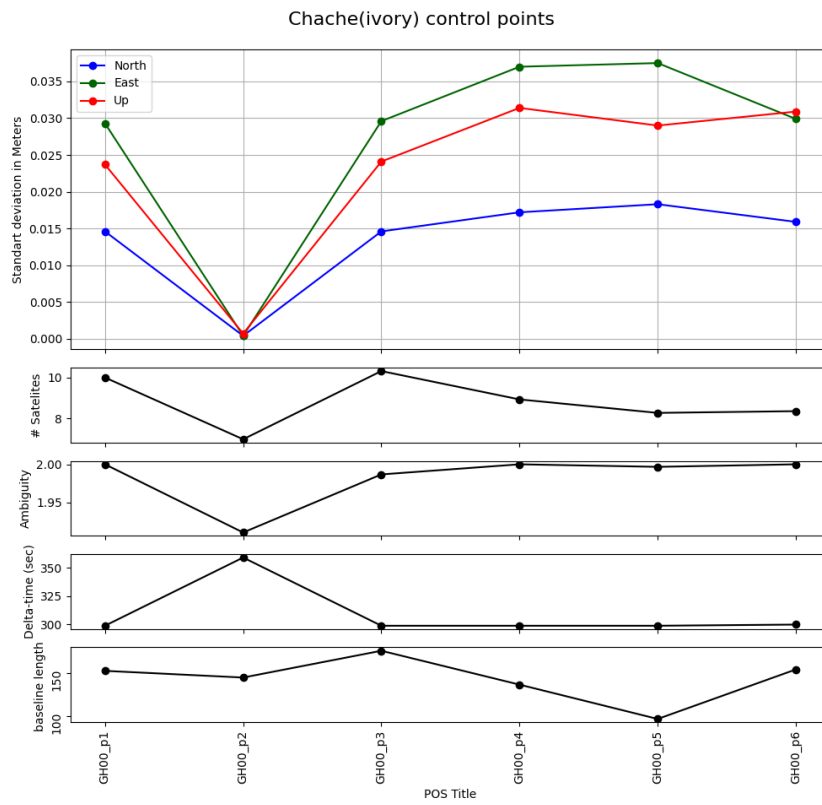


Figure 6.20: Cache (Ivory-coast side) Control points statistics

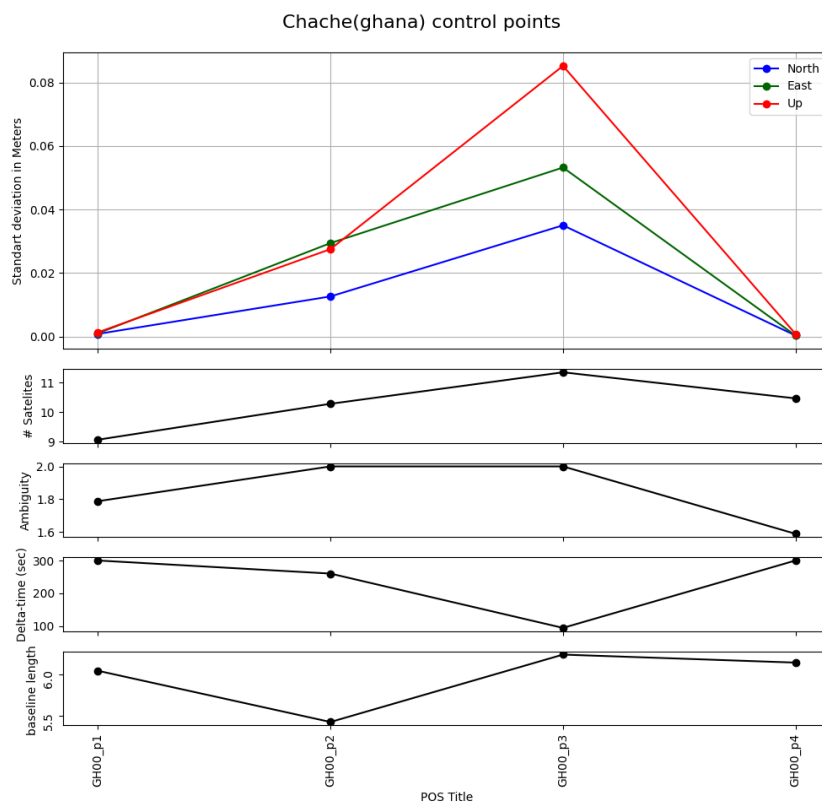


Figure 6.21: Cache (Ghana side) Control points statistics

## 6.3. Discussion

Overall, it can be seen that OpenRiverCam is made for small to medium streams. For example, despite bad angle and imperfect reference points, results were obtained for the low camera position in Tamale's small stream, although it is missing velocimetry arrows (figure 6.9). Similarly, when looking at Yapei's large river, the reference points were nicely spread out in the camera view but still did not yield results.

It is interesting how indicating different area of interests corners results in a wrong and chaotic area of interest (figure 6.13), as if the program must go to infinity to solve an equation or simply has no clue what is where. Indicating area of interest is also important for the orthorectification step. Two options can be thought of why the software cannot compute this projected area correctly.

The first is that the modelled 3D space is incorrectly solved and does not match reality. When points are selected which are modelled to be far off than in reality, the program would space out trying to make a rectangle out of something that is not. Wrong coordinate captures would help explain this, but they seem fine. It is also possible that OpenRiverCam is not used to extreme wide views, that are additionally tilted to the right, as can be seen with the far right GCP in figure 6.2. This in combination with automatic calibration of lens characteristics could result in errors and a wrongly solved 3D space. Possibly, the camera angle needs to be straight towards the middle, perpendicular to the river.

The second option is that the software is simply not programmed to handle corner points very far across wide rivers to make very long and small area of interests.

In any case, reasons for Yapei's failure are not entirely certain, and future research is needed including software expertise to resolve the matter. Although results were not successful for OpenRiverCam, the fieldwork fulfilled its preparation purpose and the methods proved to work, like hanging towels on branches with the boat for GCP's.

Then finally, Chache did yield results. Although the area of interested needed to be played with and is still solved imperfectly, complete velocimetry transects were made. The velocities even seem realistic and match the results from the manual speed test fairly well. Therefore, the research question *Can the LSPIV method be applied at wide rivers with high flow velocities?* can be answered as follows:

Yes, the Black volta at Chache seemed to be just inside the limit of pyorc's capabilities. However, the results still need to be calibrated and validated with proper discharge measurements like ADCP. Only then can be told how well LSPIV performs at wide rivers. The software could probably be improved to handle even wider rivers. For now, the performance can only be speculatively evaluated.

Firstly, results varied with multiple settings. Even with the same settings, running the code gave significantly different outputs every time (table 6.2). This is unknown territory and requires expertise in the software package. Other variations are induced by different reflections at different times of the day, which changed significantly. Reflections could also have misleading information. Inserting lens position also mattered, research is needed why this seemed to decrease performance (from Q50 0.72 m/s to Q50 1.1 m/s) when compared with the current meter measurements (0.5 m/s).

All these fluctuations might on average not matter after calibration. This does mean, however, that multiple ADCP measurements are recommended at different times for proper calibration and validation.

Furthermore, for this location at Chache, the culvert present near the bridge influences the surface velocities and their validity. Both unnatural turbulences and still areas make a location 50m downstream or upstream of the bridge more desirable. Although this location is imperfect, installation and measurements was conducted smoothly despite many challenges faced.

If OpenRiverCam is wanted to be used for wider rivers, more validation needs to be done and probably improvements in the software too. That said, pyorc did produce results in the right order of magnitude and has potential. When in the future doing large rivers, it is recommended to pick reference points that are large enough to see from the camera view. Our towels used were big but ended up being only a few pixels for Yapei. Taking a drone proves handy to validate, specifically for angle comparison too.

Further research can also include the accuracy of velocities far away, which pyorc has to compute

from a small amount of pixels. Depending on this sensitivity and the width of the river, high poles are desirable for better angle. A drone would be handy to identify this bad angle influence and validate in general.

The control points occasionally exhibited a discrepancy of several meters from their actual positions (commented by the measurement technicians). The measurement technicians spotted this discrepancy on point 3 and 5 of the Chache(Ghana) campaign (see figure 6.20). This is most likely due to the precision degradation when the RTKLIB positioning software encounters unresolved ambiguities. In this case the phase measurements cannot be regarded in the RTKLIB positioning software. Different environmental variables impact the resolution of these ambiguities. Enhancing the algorithm's capacity to resolve these ambiguities can be achieved by for example: prolonging the duration of measurements per control point, minimizing the baseline length, and reducing the presence of objects that potentially reflect GNSS signals in the vicinity of the GNSS antenna could further improve the RTKLIB positioning software's capability for solving the ambiguity.



**Figure 7.2:** Nine-class look-up table and relationship between land cover and Manning roughness coefficient [7]

| Class type       | Class number | Hydraulic class   | Hydraulic roughness (Manning $n$ ) |       |       |
|------------------|--------------|---|------------------------------------|-------|-------|
|                  |              |   | Min                                | Norm  | Max   |
| Trees            | 1            | Heavy stand of timber, few down trees, without undergrowth, flow below branches       | 0.03                               | 0.055 | 0.08  |
|                  | 2            | Heavy stand of timber, few down trees, little undergrowth, flow below branches        | 0.08                               | 0.1   | 0.12  |
|                  | 3            | Heavy stand of timber, few down trees, little undergrowth, flow into branches/willows | 0.1                                | 0.15  | 0.2   |
| Bushes           | 4            | Bushes  | 0.04                               | 0.1   | 0.16  |
| Cultivated areas | 5            | Mature row crop and mature field crop, pasture no brush (short and high grass)        | 0.03                               | 0.04  | 0.05  |
| Bare soil        | 6            | Earth, rock, gravel, cultivated areas (no crop)                                       | 0.02                               | 0.03  | 0.04  |
| Urban            | 7            | Asphalt   | 0.013                              | 0.015 | 0.016 |
|                  | 8            | Concrete  | 0.01                               | 0.015 | 0.02  |
| Water            | 9            |   | 0.023                              | 0.023 | 0.023 |

### 7.1.2. Baptist equation

The relationship of the vegetation and the flow resistance can also be modelled using the equation proposed by Baptist [2]. This equation takes into account different types of vegetation properties and water depths. Two cases are considered: submerged and non-submerged vegetation, the velocity profile of both cases is shown in figure 7.3 below. As seen in the figure 7.3B, the velocity profile for fully submerged vegetation is divided into two zones. The zone inside the vegetated part assumes a constant flow velocity,  $u_v$  [m/s], and the zone above the vegetation assumes a logarithmic velocity profile,  $u_u$  [m/s].

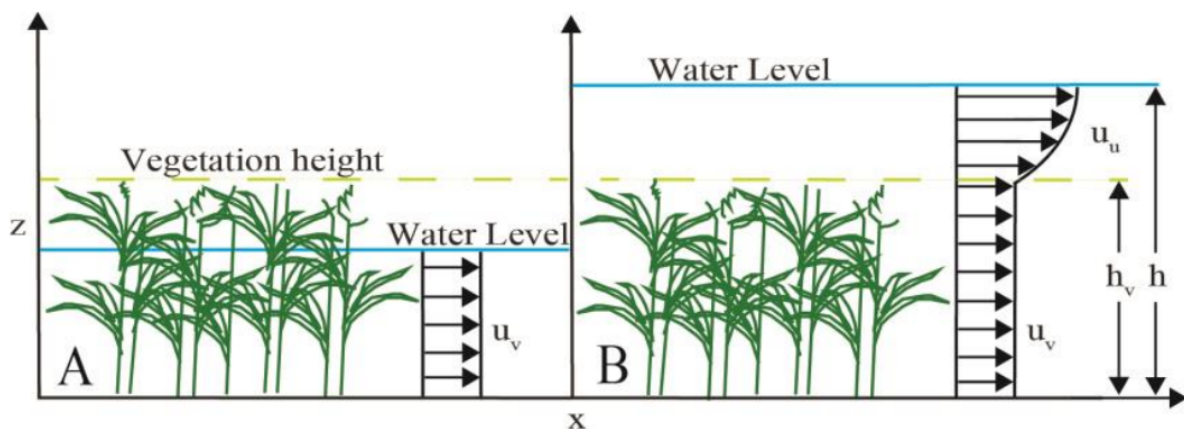


**Figure 7.3:** Schematization of the velocity profile in the vegetation model. A) partially submerged vegetation and B) Fully submerged vegetation. Figure by Nardin [12]

The equations 7.2 and 7.1 below show the developed equations for vegetation resistance by Baptist et. al. [1].

For non-submerged vegetation

$$C = \frac{1}{\sqrt{\frac{1}{C_b^2} + \frac{C_D n h}{2g}}} \quad (7.1)$$

In the case of submerged vegetation

$$C = \frac{1}{\sqrt{\frac{1}{C_b^2} + \frac{C_D n h}{2g}}} + \frac{\sqrt{g}}{\kappa} \ln\left(\frac{h}{h_v}\right) \quad (7.2)$$

Both equations require the following parameters as input: the bed roughness according to Chézy  $C_b^2$  [ $m^{1/2}/s$ ], the vegetation density  $n$  [1/m], the drag coefficient of the vegetation structure  $C_D$  (equal to 1.65) [-], the Von Karman constant taken as 0.4  $\kappa$  [-], the vegetation height  $h_v$  [m] and  $h$  represents the water height [m]. The vegetation density is defined by  $n = mD$ . Where  $m$  is the number of cylinders per unit area [ $m^{-2}$ ] and  $D$  is the diameter of cylinders [m].

## 7.2. Remote sensing

### 7.2.1. Available products for evaluating roughness

To estimate the roughness of the floodplain, a broad range of remote sensing options can be considered. By characterising the vegetation in the floodplain, one can estimate the friction that results from it [7]. Making use of known relationships between different structural and hydrodynamic properties of vegetation, it then becomes possible to link that which is measurable from a large distance to other relevant properties of the vegetation [16]. For example, a tree with a larger crown height will likely also have a larger stem width. While the latter characteristic is not observed, one can assume that it is there. Later, it will also be explained how field observations help us to make this link.

The three-dimensional structure of the landscape can be found with airborne measurements. Light Detection and Ranging, or LiDAR in short, has long been used to measure vegetation structure and shows to be a promising approach to evaluate floodplain roughness [8]. Unfortunately there is currently no such data available for this study site. Furthermore, because of the high costs it is unfeasible to expect this data being available in the near future. Because of this, high resolution orthophotography is also ruled out as a source of data. For this study, as well as future efforts of TEMBO in similar places, it is therefore necessary to make use of satellite products as a source of remote sensing data.

Among satellite products available to evaluate vegetation, several options exist with different spatial, temporal and spectral resolutions. Here spatial refers to the pixel size of the data, temporal refers to the interval at which a satellite collects data in the same location and the pixel is updated, and spectral refers to the number of different radiation frequencies that can accurately be recorded. Differences in radiative properties between materials can be used to identify them with sensors. At the highest spectral scales, it is even possible to use the spectral fingerprint of different plant species to differentiate between species.

An important consideration here is the trade-off between the different resolutions. For example weather satellites have a high spectral and temporal resolution but a low spatial resolution, allowing different types of land cover to be classified but at a pixel size too large to see differences relevant on the scale of floodplains. At the other extreme, high-resolution images provide information at very fine spatial scales but the amount of information that can be derived from these pixels is limited. Because of this, high resolution RGB imagery is mainly used in combination with visual assessment or classifications based on shapes consisting of multiple pixels [8]. Despite these trade-offs, technological development of sensors allows us to measure at an ever increasing spectral resolution without compromising on spatial resolution.

For the purpose of this study a fine temporal resolution has no added value. On the other hand, a high spectral resolution will allow the characterisation of the landscape with minimal human effort or error. Landsat has 7 different bands at a 30 meter resolution, showing intermediate spatial and spectral resolutions. This data will therefore be considered. High resolution RGB images will also be used to

identify different landscape components visually. For this, data from GeoEye has been requested but could unfortunately not be obtained in time for processing. While satellite products already exist that combine both a high spatial and spectral resolution, such as IKONOS and Quickbird, the costs of these datasets hinder usage for a student project.

### 7.2.2. Quantifying vegetation at 30 m resolution with Landsat

One way of using remote sensing to assess the hydraulic behavior of the floodplain is by evaluating vegetation-induced roughness based on the 'greenness' of the landscape. This is done by calculating the near-infrared vegetation index (NDVI) from different bands of the Landsat imagery. What follows is a map that has a value between -1 and 1 for every pixel, where values around 0.1 would represent bare soil and higher values represent the presence of more vegetation. What follows is two simple approaches to assess roughness: either to (1) relate the NDVI value of each cell directly in a monotonic manner, or to (2) use the NDVI to create discrete classes of vegetation cover that can later be linked to predetermined roughness coefficients. The second approach does not necessarily consider a monotonic relationship between NDVI and roughness, as a greener surface does not have to mean a more rough surface.

Figure 7.4 displays the NDVI for a part of the floodplain. Visually comparing satellite imagery with NDVI shows that the latter roughly represents the former. Especially the most densely vegetated areas around the river are well captured, having a high NDVI. Nevertheless, there is a mismatch, in on the one hand, the spatial extent of vegetation features and zones of similar cover types emerging from it and, on the other hand, the pixel size of the NDVI. One way to address this is by interpolating the NDVI raster to create pixels to create a more fine raster. Figure 7.4 shows how this looks like by using bilinear interpolation from the GRASS tool 'r.resamp.interp' in QGIS. The obvious limitation of interpolating data to reduce its coarseness is considered, but does not pose a problem when it is only used for a rough assessment of floodplain vegetation distribution. Furthermore, since small features in the landscape are already overlooked with the NDVI, interpolating does not introduce any significant bias that was not already there. Visual comparison shows that the interpolated NDVI succeeds in capturing gradual changes in land cover type, but indeed does no better job at identifying polygons of a specific vegetation class such as patches of forest or side channels. Nevertheless it can help to assign more realistic shapes vegetation cover classes already identifiable at the 30 m scale. In the discussion of this chapter, the usability of the NDVI for this project will be discussed.

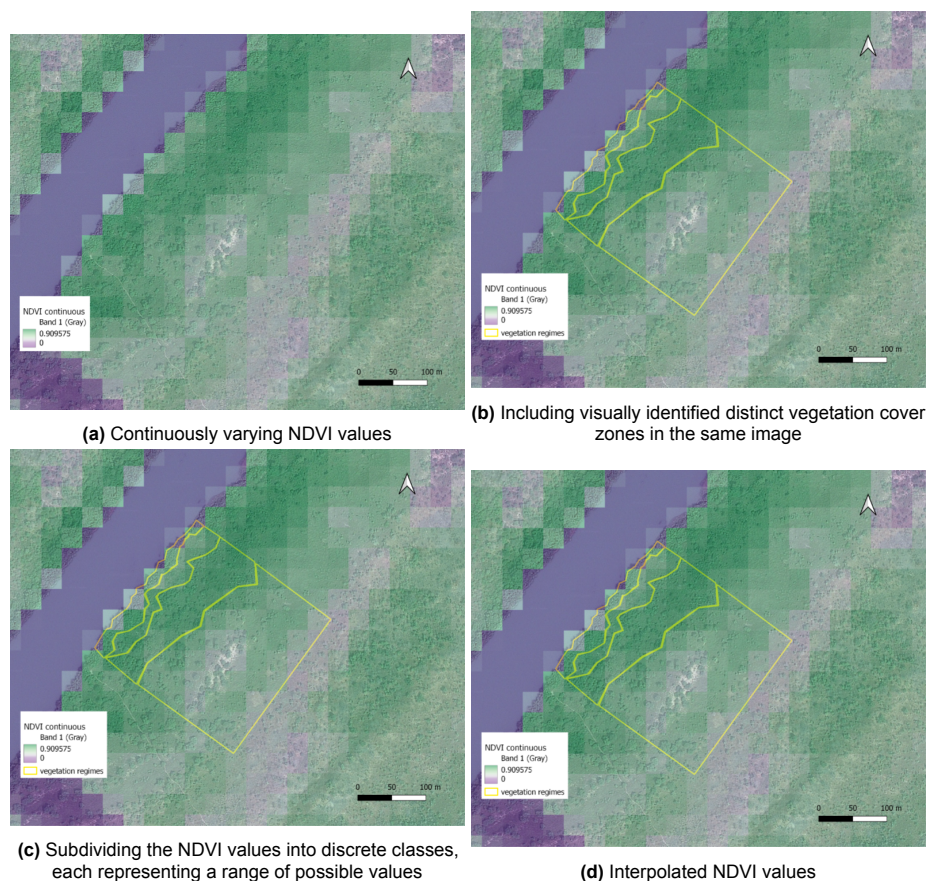


**Figure 7.4:** a) Continuously varying NDVI values. b) Including visually identified distinct vegetation cover zones in the same image. c) Subdividing the NDVI values into discrete classes, each representing a range of possible values. d) Interpolated NDVI values.

## 7.3. In situ observations

In addition to remote sensing data, it is important to assess the situation on the ground visually and manually. In-situ observations allow to both confirm any inferences made using remote sensing data and evaluate any hydrodynamic properties of the floodplain that cannot be observed from a large distance. For the purpose of this study, to guide decisions made in modeling the hydraulics of the floodplain, data on the vegetation cover and flow velocities in the floodplains of our study site was collected. This was done in a qualitative manner, without the aim of concluding significant relationships between the data.

### 7.3.1. Vegetation surveys

By measuring vegetation in the floodplain, records of vegetation cover to link remote sensing observations to actual vegetation cover are obtained. This vegetation cover can then be used to either compute the roughness analytically with baptist or with a lookup table. By linking vegetation cover patches identified from satellite data to hydrodynamic vegetation properties, each area can attain its own roughness coefficient. Furthermore, it is possible to link quantifiable features from remote sensing data to quantifiable hydrodynamic properties. For example, crown width can be linked to stem thickness. (In the field it was decided to focus on the former, empirical lookup tables are probably most reliable in linking cover types to roughness).

To check NDVI the vegetation was measured in plots sufficiently large to represent a whole pixel. This was done with the goal to quickly check if the NDVI indeed differentiates between different levels of vegetation cover. Visual estimation already shows that dense vegetation can be identified. Nevertheless, based on the required accuracy of the model, more delicate differences in vegetation cover the floodplain also need to be identified. Each plant was located on a plot sketch and structural properties such as stem thickness and height, which are necessary to derive roughness analytically.

To check satellite-identified patches the quantity and dimensions of plants occurring in 6 by 2 meter plots were measured and chosen to be of equal length as the canoe that was used to reach the plots. The locations were chosen beforehand, to make sure that data would be collected for every distinguishable vegetation cover class. To speed up the process, observed plants were clustered in groups with average values for stem thickness and height. This determination was done in the field.

### 7.3.2. Velocity measurements

By measuring the flow velocities in the floodplain, a ground truth is obtained about the hydraulics. This allows for a benchmark to be established; to see if the modeled roughness profile of the floodplain indeed results in the flow velocities measured in the floodplain. Furthermore, it can help to distinguish between zones of vegetation with significant differences in the effect on flow velocities. Lastly, it helps to evaluate whether modeling the floodplains is of any use at all, or if flow is negligibly small.

In the field, a canoe was used to travel in a straight line perpendicular to the main channel into the floodplain, taking a velocity measurement every 5 meters just below the water surface. For this, a simple current meter was used. If the velocity was too low for the propeller to spin and register a value above zero (which happens when the flow is below 0.1 m/s), the velocity was visually estimated by timing how long it takes particles on the water surface to travel one meter. Velocity profiles were collected both upstream and downstream of the construction site and were done until dry land was reached.

## 7.4. Results

### 7.4.1. Vegetation surveys

Two plots in close proximity of each other with a hydro dynamically significant difference in vegetation cover were surveyed to check NDVI values for these locations. During the survey, plot 1 was inundated and plot 2 was not. In plot 2, the vegetation density was three times higher than in plot 1. Due to the water depth, low vegetation such as young shrubs and grasses may have not been observed in plot 1, resulting in a lower vegetation cover. Despite the difference in observed vegetation cover, the NDVI was very similar in plot 1 and 2. This prevented the use of the NDVI as a proxy for vegetation density outside of the densely vegetated river banks.

Figure 7.5 shows the measurement locations in which vegetation was surveyed (see AppendixH for more detailed results). By evaluating the amount of plants and their stem thickness for each plot a mean stem density was derived, which is given in Table 7.1. Together with the observed vegetation height, these values are the input for the baptist equation later. Combining visual interpretation of both satellite imagery and observations on the ground of the same locations, it was concluded that the most reliable classification of the floodplain vegetation is in three categories. Table 7.1 gives the mean stem density for three distinct vegetation zones; densely vegetated banks, open patches, and moderate vegetation. This is less than our initial classification which differentiated between shrub and tree dominated vegetation cover. The simplification was done because expected differences between these cover types that were based on satellite imagery were not observed in the field.

**Table 7.1:** Vegetation density classes derived from field observations

| Class                            | Plots included | Stem density [ $m/m^2$ ] |
|----------------------------------|----------------|--------------------------|
| 1. Densely vegetated bank        | 1, 2           | 0.27                     |
| 2. Open patch                    | 3, 4           | 0.08                     |
| 3. Intermediate vegetation cover | 5, 6, 7, 8     | 0.14                     |



**Figure 7.5:** Measurement locations of our vegetation surveys to determine stem density and height in the floodplain at Chache

#### 7.4.2. Floodplain velocity

Velocity was measured in three lines, of which two at 300 and 400 m upstream and one 300 m downstream of the bridge construction site. The flow velocities upstream varied between 0 and 0.4 m/s and coincided with the density of the vegetation in the same location. Downstream of the construction site, velocity was mainly zero and sometimes values below 0.1 m/s, which could only be estimated visually. Figure 7.6 visualises the upstream velocity profiles in the locations where they were measured. At the time of taking measurements, the water level was at 6.12 m. As can be seen, high velocities are measured at the outer edge of the floodplain, where the dense vegetation comes into contact with the high flow velocity of the main channel. Going outward, the velocity then dips in the dense vegetation and increases again in the relatively open area. Finally, it decreases to zero towards the dry bank. In the lower transect, this bank was located right after the dense vegetation, within 20 m of the main channel. Based on expert knowledge, it was concluded that this is due to the height of the bank, which is higher close to the construction site. Behind the bank water was visible, but this was storage emptying into the main channel and therefore not actively conveying river discharge. At the upper transect, the first bank was below the water table, and the floodplain stretched 70 m away from the main channel.



**Figure 7.6:** Two velocity profiles that were obtained in the floodplain using a current meter. The height of the red part of the graph gives the measured velocity at the location along the bright-pink line in the direction of the river (black arrow). The white portion gives the highest velocity measured along the transect. This is 0.38 and 0.15  $m/s$  for the upstream and downstream transect respectively.

### 7.4.3. Roughness input for hydraulic model

To translate the observations in the field into a usable roughness input for the discharge model, multiple steps have to be conducted. Using the three vegetation cover classes defined above, zones around the river are created in QGIS. For these zones field observations of vegetation and velocity are used, as these seem to be the most reliable source of data. For each of these zones a roughness coefficient is then calculated and used as spatial input for the discharge model.

By using the vegetation density of each vegetation class, the roughness coefficient can be determined with the Baptist equation (Equation 7.1 and 7.2). Due to the input of this equation, the roughness coefficient of the floodplain is dependent on the water level and the height of the vegetation. In Figure 7.7 the Manning roughness coefficient of the different vegetation zones is displayed for changing water levels. As can be seen in the figure, the roughness coefficient increases with increasing water level until the mean height of the vegetation in the defined vegetation zone is reached. Afterwards the roughness due to vegetation decreases again as the influence of the vegetation on the total roughness decreases. These calculated roughness coefficients can then be used in the adaptive modelling process with different coefficients for different water levels. The calculation of the parameters can be studied in detail in Annex B.

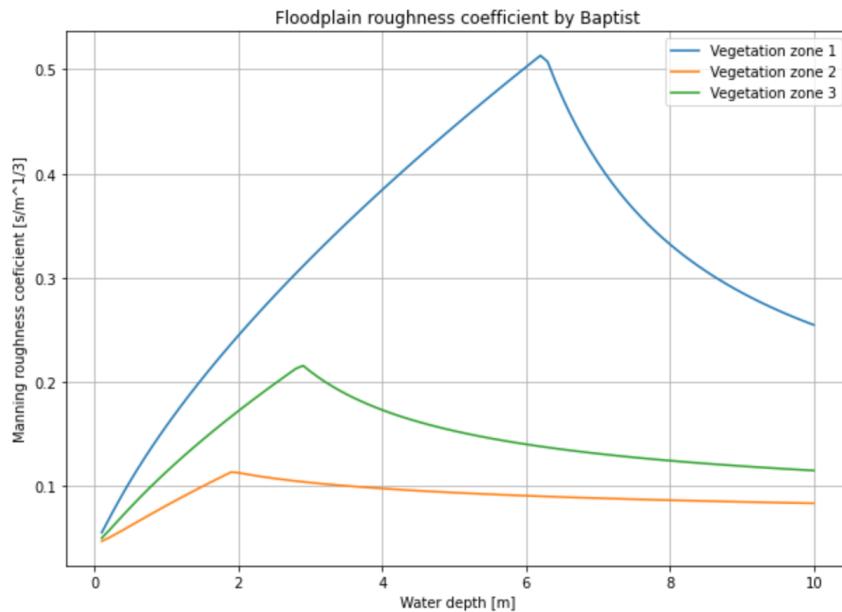


Figure 7.7: Roughness coefficient calculated by Baptist of different vegetation zones in the floodplain [1]

## 7.5. Discussion

### 7.5.1. Field observations

The main goals of our field observations of vegetation in the floodplain was to better understand how plants are distributed around the river, how this affects flow velocities, and how it relates to available remote sensing products. While the vegetation surveys were quantitative, they merely serve to roughly characterise the floodplain and test ideas, and not to conclude any significant relationships. In this section, first the observations done within this project are reflected on, then this is related to remote sensing products and finally recommendations for modelling the roughness of the floodplain will be provided.

Velocity measurements up- and downstream of the bridge showed different results, as no velocity was measured 300 m downstream of the bridge. On the other hand, flow velocities of up to  $0.4 \text{ m/s}$  were measured at 300 and 400 m upstream of the bridge. As can be seen in 7.6, the velocity varies roughly in correspondence to the vegetation cover type right upstream of the line: a dip in the densely vegetated banks, relatively high flow in the part with little vegetation cover, and varying flow in the part with intermediate vegetation cover. The amount of velocity measurements is too little to conclude any significant relationships. Nevertheless, these measurements, in combination with observations in different parts of the floodplains, do show that the well-researched relationship between vegetation and hydraulic roughness [1] may be observed from satellite imagery.

A limitation of our field measurement lies in the way the hydraulic roughness changes with the water level. As described in [1], the roughness of a vegetated river section increases with water level, as shrubs and trees branch out and the density of stems and leaves that apply friction to the water increases. As shown in 7.8, at the time of measuring, the water level had already receded by more than a meter, and therefore does not capture the hydraulic behaviour of the floodplain during the highest peak flows. This affects the ability of the velocity measurements at one point in time to determine the changing roughness at different water levels. Therefore, in order to determine this, one can either make simplifications or model the vegetation analytically based on field observations, which is discussed later. To validate both options, velocity measurements should be performed at different water levels, especially during the relatively poorly documented peak flow events.



**Figure 7.8:** The water level in the floodplain has receded by quite a bit, which is visible in the color of the vegetation. There is a clear line where the green-colored leaves end and where only brown vegetation features are found. This is the portion that was flooded previously this rainy season.

Vegetation measurements ended up being the most important source of data to determine the roughness of the floodplain. Solely by inspecting the characteristic vegetation cover at different locations, it is possible to determine the cover type. By directly relating the vegetation cover type to predefined roughness coefficients, one can make use of more in depth research to determine the floodplain hydraulics. The use of the observed stem density in these zones was used to compute the Baptist equation, leading to different roughness values for different water heights. Obviously, a larger sample size would have improved the accuracy of the Baptist roughness that is computed from it. Based on the added value of measuring

### 7.5.2. Relating field observations to remote sensing data

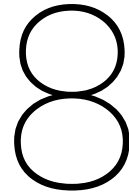
Our vegetation surveys used to evaluate the accuracy of the NDVI as a proxy for floodplain vegetation cover differences were inconclusive. The most obvious limitation of using the NDVI in the context of modeling floodplain roughness, however, is the coarseness of the data. Interpolation of the data may help to define the most rough classes, but visual evaluation has pointed out that it does not lead to a better representation of the floodplain. Moreover, field observations showed that the NDVI does not differentiate well between relatively similar cover types. It can therefore be concluded that NDVI by itself does make a meaningful contribution to modelling the hydraulics of the floodplains of the Black Volta.

Using openly accessible satellite imagery from Google Maps, on the other hand, did turn out to match conditions on the ground better. It worked especially well in defining the first two zones (dense vegetation and open patch). Nevertheless, it was difficult for the human eye to identify discrete land cover classes beyond these two from this remote sensing data. While big trees were clearly identifiable, smaller trees and shrubs were not, and initial expectations about the density of these were therefore not matched in the field. This uncertainty led to the generalization of all land beyond the open patches into a third zone of intermediate vegetation cover. Another limitation is the lack of automation in the approach used in this project. The three zones were manually drawn based on visual inspection of remote sensing and field data. Supervised classification in GIS can help to overcome this, as it performs the classification of a larger area based on the manual classification of a smaller area.

Further research into remote sensing of floodplains should therefore focus on the classification of land cover types. This can, as explained in 7.2, be done in different ways. From low to high costs, this would

---

range from using high resolution RGB imagery (GeoEye), to high resolution multi-spectral (Quickbird), to combined approaches using information from both, as well as airborne collected data. For the last method, the use of a UAV-drone may be considered as the area is relatively small. As explained previously, it needs to be evaluated whether taking the floodplain into account in the hydraulic modelling of the Black Volta river is important enough to invest time and money in obtaining and processing additional remote sensing data sources.



# Delft3D/Discharge model

## 8.1. Delft3D methodology

Delft3D D-Flow Flexible Mesh is a software released by Deltares in which a 3D discharge model is made using the module D-Flow FM [6]. D-Flow FM is a multidimensional hydrodynamic simulation program which calculates non-steady flow and transport phenomena on a structured and unstructured, boundary fitted grid. In this study river flow simulations are done to get different water heights for different discharges in the river. Delft3D FM solves nonlinear equation for shallow water flow including friction. The discharge model is run to produce a rating curve at the Chache site. As mentioned before, the model of N. Hoogendoorn is used with the same friction coefficient in the main channel of  $0.045 \text{ s/m}^{1/3}$  [10]. Our aim of the study is to determine the influence of the roughness coefficient in the floodplain on the discharge. This is done by defining the roughness coefficient in the floodplain. The study of N. Hoogendoorn uses an uniform roughness coefficient of  $0.15 \text{ s/m}^{1/3}$  in the floodplain. In this study different values of roughness coefficients in the floodplain are analysed.

### 8.1.1. Roughness coefficient input

There are different methods to implement roughness coefficients in Delft3D. This can be achieved by assigning specific values to different grid cells using spatial operations or by employing a built-in function to calculate the roughness coefficient.

Delft3D Flow FM has a built-in function to define the flow resistance on each sub-grid, called Trachytopes. This function makes use of the Baptist equation (see *Chapter 7*). This would be the ideal option to take into consideration the vegetation in the floodplain, including the varying friction coefficient per depth. However, due to this function still being in development, the function does not work in Delft3D FM Suite. This is why this study opted for assigning roughness coefficients using spatial operations. The roughness coefficient has been implemented manually by adding a layer 'Roughness' to the model. This feature can be found in 'Spatial Operations'.

#### Scenario 1

The roughness coefficients in the floodplain are determined by the in situ observations and the Manning roughness coefficient look-up table by Forzieri et. al. [7], explained in chapter 7. In Delft3D polygons are created parallel to the river (*Figure 8.1a*). These polygons overwrite the roughness input defined in the section physical parameters. From the river outward, the roughness coefficients in the floodplain are 0.2, 0.07 and  $0.12 \text{ s/m}^{1/3}$  (*Figure 8.1b*). Since it was not possible to visit the other side of the river, as this is located in Ivory Coast, it was decided to mirror the input data from the Ghana side floodplain to the Ivory coast floodplain.

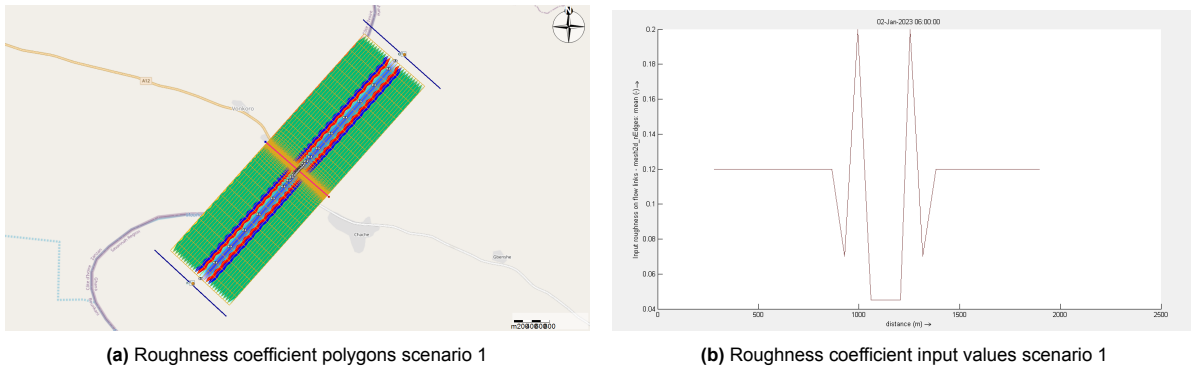


Figure 8.1: Roughness coefficient implementation in discharge model scenario 1

Scenario 2

In the second scenario the roughness coefficient in the floodplain is determined using the Baptist equation and the in-situ observations, also explained in chapter 7. Since the built-in function of Delft3D FM Suite of the Baptist equation did not work, the by hand calculated roughness coefficients using the Baptist equation are used.

Similar to scenario 1, polygons parallel to the river are used to define a certain roughness coefficient. However, this time each grid column next to the river has a specified roughness coefficient, seen in Figure 8.2a. The color of the polygons correspond to their roughness coefficient, resulting in some polygons having the same color. The first step in determining the roughness coefficient per grid cell is to define the vegetation zone to them. The vegetation zones of all the grid numbers in Delft3D are determined depending on their location, since the Manning roughness coefficients are calculated in Chapter 7.4.3, dependent on their vegetation zone. Secondly, the water levels in the different grids for different discharges are calculated using the water level results from scenario 1, as it is assumed that they will not substantially deviate when implementing the Manning roughness coefficients. The calculated Manning roughness coefficient is then defined using the results of Figure 7.7, dependent on the water level and the vegetation zone of that certain grid. Table 8.1 below shows an example of these determined values for a discharge of  $2500 \text{ m}^3/\text{s}$ . The input roughness coefficients for the other discharges are shown in Appendix C.

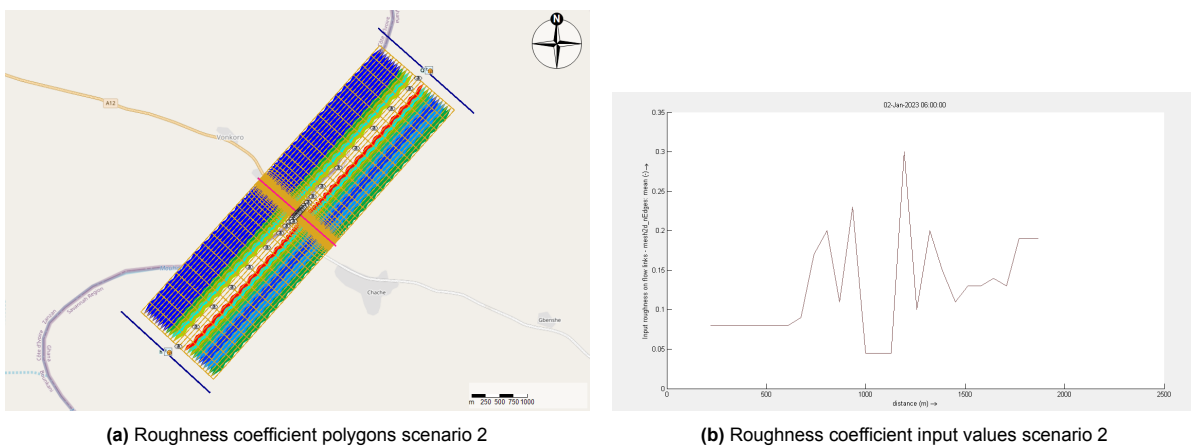


Figure 8.2: Roughness coefficient implementation in discharge model scenario 2

**Table 8.1:** Manning roughness coefficient with according water level at certain grid cell for a discharge of  $2500 \text{ m}^3/\text{s}$ 

| Vegetation zone | Grid number | Water level (m) | Roughness coefficient ( $s/m^{1/3}$ ) |
|-----------------|-------------|-----------------|---------------------------------------|
| 3               | 1           | 0.6             | 0.08                                  |
| 3               | 2           | 0.6             | 0.08                                  |
| 3               | 3           | 0.7             | 0.09                                  |
| 3               | 4           | 1.9             | 0.17                                  |
| 3               | 5           | 2.7             | 0.20                                  |
| 2               | 6           | 2.7             | 0.11                                  |
| 1               | 7           | 1.9             | 0.23                                  |
| Main channel    | 8           | -               | -                                     |
| Main channel    | 9           | -               | -                                     |
| Main channel    | 10          | -               | -                                     |
| 1               | 11          | 2.8             | 0.30                                  |
| 2               | 12          | 2.8             | 0.10                                  |
| 3               | 13          | 2.7             | 0.20                                  |
| 3               | 14          | 1.7             | 0.15                                  |
| 3               | 15          | 0.7             | 0.11                                  |
| 3               | 16          | 1.0             | 0.13                                  |
| 3               | 17          | 1.3             | 0.13                                  |
| 3               | 18          | 1.3             | 0.14                                  |
| 3               | 19          | 1.4             | 0.13                                  |
| 3               | 20          | 1.3             | 0.19                                  |
| 3               | 21          | 2.3             | 0.19                                  |

### 8.1.2. Boundary conditions

The upstream boundary condition is defined by discharge and the downstream boundary condition is defined by its corresponding water height. These boundary conditions are determined for different simulations, with the discharges ranging from  $0.7$  to  $2500 \text{ m}^3/\text{s}$ . The water level heights are determined by iteration to fit the according discharge until there was no backwater curve in our area of interest of more than  $5 \cdot 10^{-5}$ . In other words, the goal of this iterative process is to obtain a constant water depth in our model with a very small tolerance. The model with a certain discharge and an initial guess of water height is run in Delft3D, where multiple observation points are placed in a line parallel to the river. The water heights at these observation points are obtained from the model, including the distances between these points. From these points the water height slope is calculated. The river bed slope is known to be equal to  $0.0003$  and the goal is for these slopes to be the same to obtain a constant water depth in our model. The model is run again with different water heights until this constant water depth along the river is achieved. *Figure 8.3* shows a simulation of the water heights for different downstream water height boundary conditions for a discharge of  $2000 \text{ m}^3/\text{s}$ . The figure shows that the water heights of the boundary condition of a water height of  $249$  meter matches the bed slope the best and is chosen as downstream boundary condition to run the model with. The figure also shows that a backwater curve can still be observed at the end of the river, which continues outside of our model area. However, since this is not located in our area of interest this is assumed to be negligible.

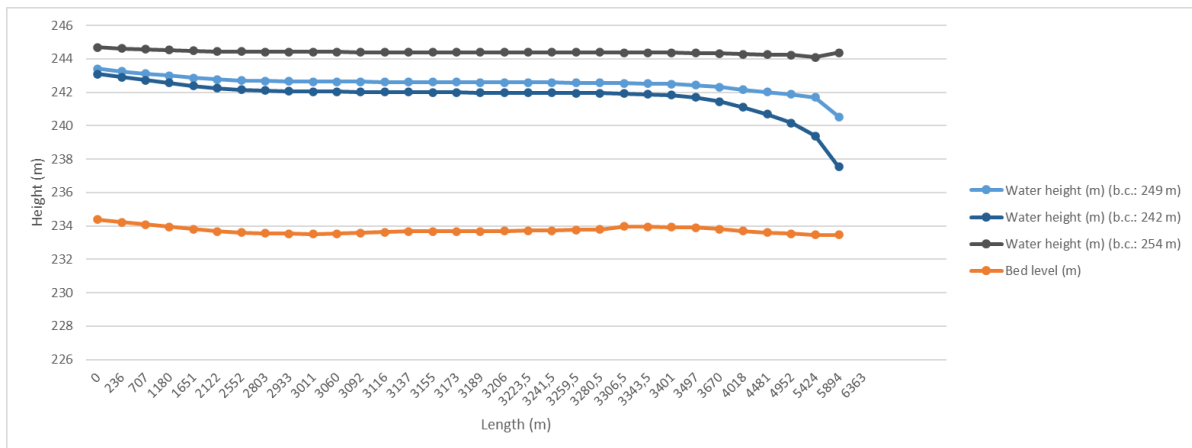


**Figure 8.3:** Bed level [m] and water heights [m] for different downstream water level boundary conditions in Delft3D for a discharge of  $2000 \text{ m}^3/\text{s}$

These simulations are done for every  $500 \text{ m}^3/\text{s}$  until  $2500 \text{ m}^3/\text{s}$ , starting from  $500 \text{ m}^3/\text{s}$ . Up and until a discharge of  $500 \text{ m}^3/\text{s}$  the water level does not exceed the river bank, so it does not reach the floodplain. This means that for discharges below that, the model is not different from the model by N. Hoogendoorn with a uniform main channel roughness coefficient of  $0.045 \text{ s}/\text{m}^{1/3}$ .

## 8.2. Results

### 8.2.1. Scenario 1, visual determination of roughness coefficient

The discharge model has been run with the newly visually established roughness coefficients for the ascending discharges. For each discharge, a corresponding water height and velocity were calculated by the model (*Figure 8.4*). It can be noticed that the water height is not constant through the whole cross-section of the river, but depends on velocity, friction and bathymetry. The modelled velocity in the floodplain corresponds with the velocities that were manually measured (*section 7.4.2*): very low at the sides of the main channel, after 30m floodplain inwards an increase to  $0.5$  and  $1.0 \text{ m}/\text{s}$  for  $20 \text{ m}$ , after which the velocity decreases again to negligible values.

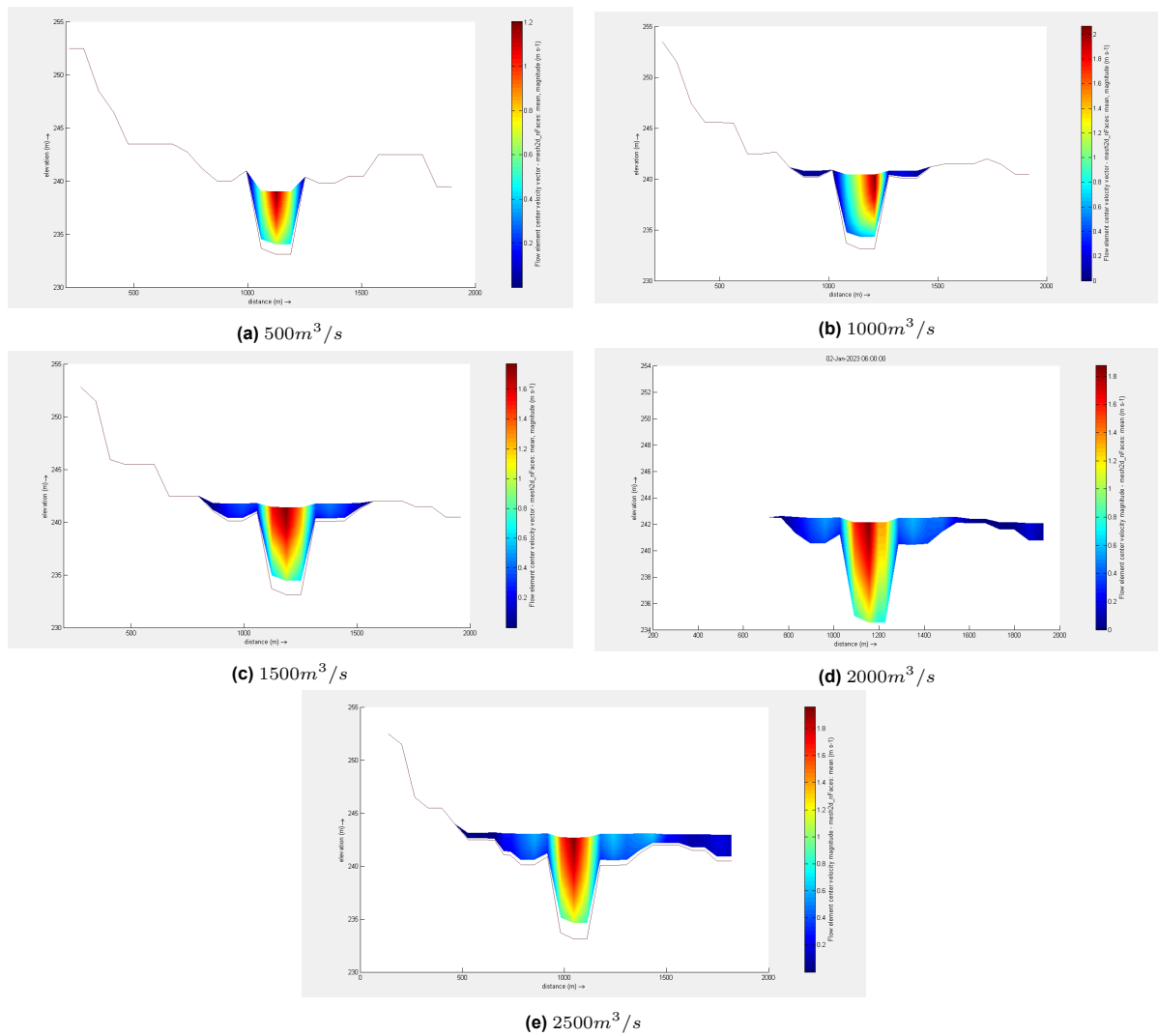


**Figure 8.4:** Water height and velocity per discharge with visually determined roughness coefficients

### 8.2.2. Scenario 2, Baptist determination of roughness coefficient

The velocity cross-sections of the river that were obtained, after implementing roughness coefficient using the Baptist equation, can be seen in *Figure 8.5*. In these results the higher velocities in the side channel are less clear than in the results with the visually determined roughness coefficient (scenario 1). This could be caused by the more fine implementation of the Baptist values, since this is done by using polygons that are as wide as one grid cell, subdividing the floodplains in 11 sections. The floodplain in the model with the visually determined roughness coefficient has been subdivided in only 3 sections, making the result more rough.

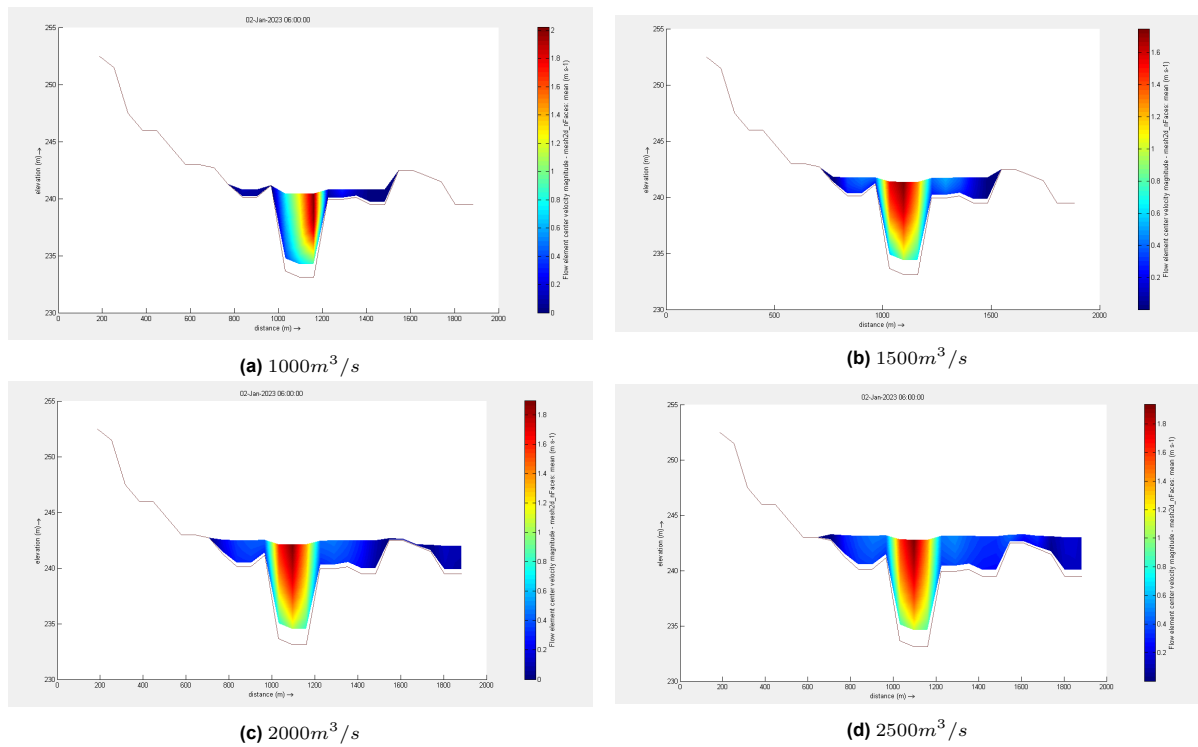


**Figure 8.5:** Water height and velocity per discharge with Baptist equation roughness coefficients

### 8.2.3. Rating curve

The developed discharge model with the two scenarios of roughness coefficient input is run for several different discharges, as mentioned before. For these different discharges the water height at a specific location in the main channel is obtained from the discharge model. This water height and discharge relationship, for both scenarios, is shown in the rating curves in Figure 8.6. This figure also shows the water height - discharge relationship previously developed by M. Kasteel and BPA for comparison.

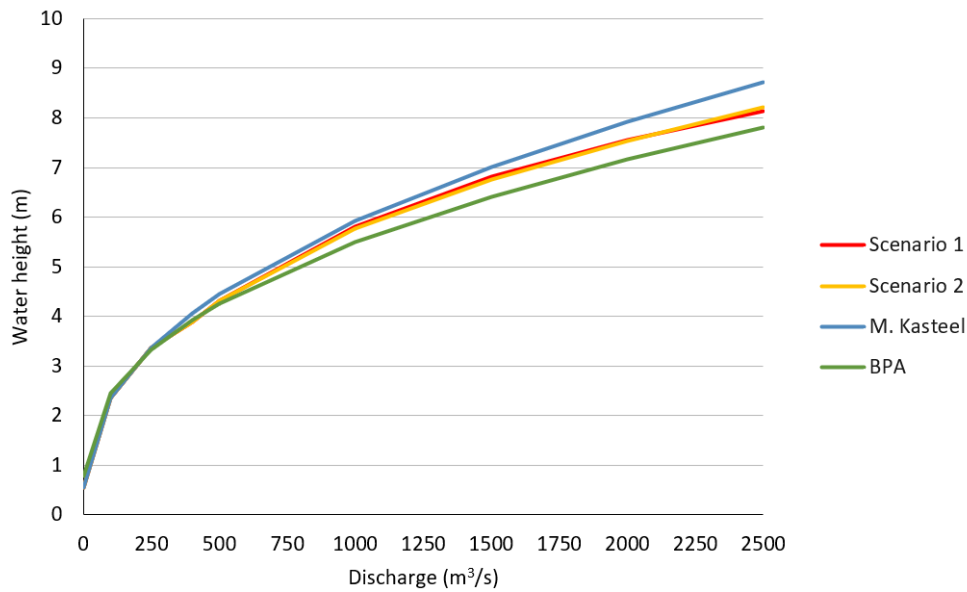


**Figure 8.6:** Rating curves developed by the two scenarios in the discharge model compared to the previous developed rating curves by BPA and M. Kasteel

From the figure it can be observed that the rating curve of scenario one and two are almost similar. There is an average difference 0.04 m between both scenarios. The figure also shows that the newly established rating curve, for both scenarios, returns lower discharges for a specific water height compared to the rating curve by BPA. Compared to the updated rating curve by M. Kasteel, both scenarios of the new established rating curve show a higher discharge for a specific water height. Up and until a water height of 4.5 m, all rating curves are similar. This is the depth of the river channel, meaning that the floodplain roughness coefficient does not influence the models simulated water height in the channel.

#### 8.2.4. Surface velocity comparison results: Delft3D, OpenRiverCam and in-situ measurements

The initial goal was to compare the surface velocities modelled in Delft3D to the results of the surface velocities determined by OpenRiverCam at the Chache site (Section 6.2.3) to validate the discharge model. However, in practice there were some unexpected challenges that occurred; the discharge during the surface velocity measurements is unknown and therefore is needed to be estimated using visual estimation. On the staff gauge at the river site Chache a water height of 5.60 m was read off, using the developed rating curve this corresponds to a discharge of about  $1000 m^3/s$ . Additionally, the visit to the floodplain showed that the water came up to the second river bank with a water depth of about 1 meter (Appendix H), which corresponds to an average discharge of  $1000 m^3/s$  in the discharge model. The surface velocity modelled at this discharge of  $1000 m^3/s$  in Delft3D is therefore used to compare the OpenRiverCam and the in-situ measurement results to.

### Surface velocity comparison main channel

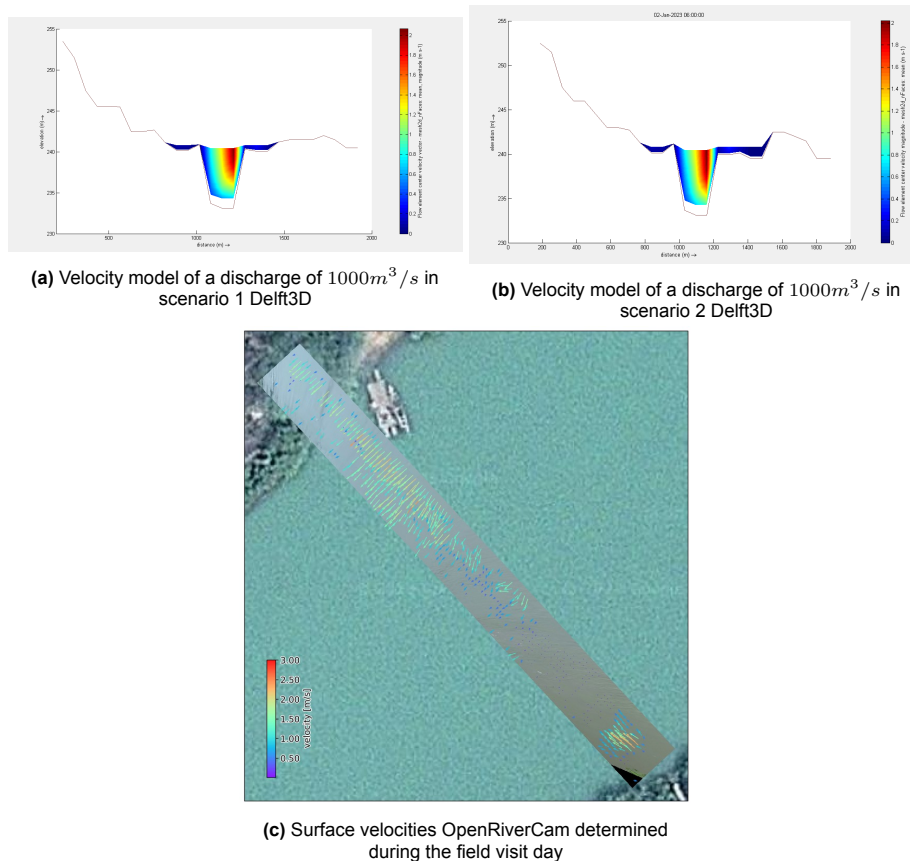


**Figure 8.7:** Surface velocity comparison Delft3D model results and OpenRiverCam at the Chache site

Figure 8.7 shows a comparison of the modelled surface velocities. The figures 8.7b and 8.7a show that the discharge model models a surface velocity of between  $0.8 - 2.0\text{ m/s}$  in the main channel. The results from Figure 8.7c give a range of  $0$  to  $2.5\text{ m/s}$  in the main channel. However considering the discussion points of the results of OpenRiverCam at the Chache location (see section 6.3) a velocity of  $1.0\text{ m/s}$  to  $2.1\text{ m/s}$  is considered to compare the discharge model velocity results to. Additionally, a speed test was done with apples to get an estimate of the river surface velocity, explained in Section 6.2.3. This test gave the results of a surface velocity of  $1.3\text{ m/s}$  in one part of the main channel and  $1.9\text{ m/s}$  in a faster flowing part of the main channel. The surface velocities in the main channel of the river of the discharge model compared to the measured OpenRiverCam and the speed test match, with a small error of about  $0.2\text{ m/s}$ .

#### Surface velocity comparison floodplain

The results of the in-situ velocity propeller measurements of the floodplain, given in Section 7.5.1, show a surface velocity varying between  $0.0$  and  $0.4\text{ m/s}$ . Where the highest velocity of  $0.4\text{ m/s}$  was measured at about  $50$  metres from the main channel. The surface velocities modelled in Delft3D agree with these measurements; given values between  $0$  and  $0.4\text{ m/s}$  as well.

To summarize, the results of surface velocities are shown in Table 8.2 below.

**Table 8.2:** Comparison of surface velocities modelled and measured at the Chache river site in the main channel and in the floodplain

| Location     | Delft3D                | OpenRiverCam           | Apple speed test       | Propeller              |
|--------------|------------------------|------------------------|------------------------|------------------------|
| Main channel | $0.8-2.0\text{ [m/s]}$ | $1.0-2.1\text{ [m/s]}$ | $1.3-1.9\text{ [m/s]}$ | -                      |
| Floodplain   | $0.0-0.4\text{ [m/s]}$ | -                      | -                      | $0.0-0.4\text{ [m/s]}$ |

## 8.3. Discussion

*Figure 8.4d* and *Figure 8.4e* show clearly that the high and low roughness coefficients closest to the river have a significant impact on the water velocity, as the flow decreases and then increases again when moving perpendicular to the channel. The modelled water velocities correspond to the velocities that were measured manually in the floodplain on the Ghana side of the river. Since it was not possible to investigate the floodplain that is situated in Ivory Coast, the roughness coefficient has been modelled equally on both sides of the river. The vegetation on both sides of the river has been compared by using satellite images in order to back-up this decision, however it is still a rough estimate.

As can be seen in *Figure 8.4* and *8.5* the height of the floodplain rapidly increases on the Ivory Coast side, causing the floodplain basin to be small. This results in a low contribution of the Ivory Coast floodplain, which decreases the effect of the estimated roughness coefficients on that side of the river. Another inconsistency of the model is the extent of the floodplain on the Ghana side of the river. Local inhabitants have shown the maximum distance from the river that the water can reach during the wet season, which was approximately 500 meters away from the main channel. The model is 2000 meters wide, which should be enough to cover the whole floodplain. However, it can be seen in *Figure 8.4* and *Figure 8.5* that the floodplain continues after the ending of the model. This indicates that probably the bathymetry of the model is not entirely correct, as it should have a greater slope angle to ensure the ending of the floodplain.

Unfortunately it was not possible to do a complete validation of the discharge model. So, no conclusion can be made to say if the newly developed rating curve is more reliable than the previously developed ones. However, when comparing the surface velocities of Delft3D to the results of OpenRiverCam and the in-situ measurements a good match is shown. It needs however to be considered how reliable these results are, besides it being a good estimation. Since, the discharge at these moments of measurements are estimated. Also, the locations of measurements and the discharge model are different. The discharge model is modelled upstream of the newly build bridge and the OpenRiverCam is measured downstream of the bridge. These locations are about 150 meters apart from each other. At these locations the bathymetry might differ, mainly due to the presence of a bridge in between them and processes of sedimentation due to the construction of the bridge. The different bathymetry might influence the result of Delft3D to a great extent.

## 8.4. Conclusion

This chapter gives an answer to the two research questions regarding the floodplains and the modelling of it.

### *2a. How can the roughness coefficient be determined and implemented into the hydraulic model?*

Delft3D already contains the function to use the Baptist equation to calculate the Manning roughness coefficient per depth. However, this has not yet been implemented properly in the software, and therefore could not yet be used. Because of this, the roughness coefficient was now modelled by averaging it for a specific water height over the whole depth. By taking into account the water height per discharge for each polygon (so also depending on the bathymetry) the roughness coefficient has been modelled more precisely. However, the plug-in itself will give even more accurate results, as it takes into account varying roughness coefficients over depth, using vegetation heights, which influences the velocity over depth. Moreover, being able to use the plug-in will greatly decrease the required amount of manual labour. However, as the results of both scenarios are very similar, it would not be necessary in similar floodplains to perform the entire implementation of the Baptist method. This will decrease the required time to characterise the floodplain from approximately three to half a day, as it will not be necessary to measure the dimensions of each tree.

### *2b. What is the contribution of the floodplains to the river discharge?*

The rating curve in *Figure 8.6* indicates that the implementation of the floodplain in the hydraulic model does have an influence on the discharge of the river. The graph shows that compared to Kasteel's rating curve, the discharge rate is higher for a specific water height in the river when implementing the floodplains. This implies that there is discharge through the floodplains as well. It can also be stated

---

that the contribution of the floodplains increases for higher water levels, as the graph deviates more from Kasteel's graph for higher water levels. This makes sense since the average roughness coefficient decreases when the water column height increases, which leads to higher flow velocities.

# 9

## Discussion and Conclusion

In addition to method specific issues some general challenges and problems were encountered during the project and have to be discussed. This includes problems due to the planning and timing of the project as well as challenges faced due to the fixed measurement location. Further challenges include the difficulty in the validation of measurements and models. In this chapter all these issues are discussed and remaining research questions are answered.

### 9.1. Planning and timing

The major problems encountered during the project were already given by the timing of the field visit and other planning mistakes before. The goal being to measure the flows and observing the floodplain during the rainy season arriving only at the end of August was not ideal. While the pole (on which the equipment was planned to be installed) was constructed before the start of the rainy season, with water levels not yet exceeding the inner banks, the measuring equipment was planned to be installed early October, in the middle of the rainy season. As late as 14 October, the pole was still inaccessible for installation as the high water around it did not allow the construction of a scaffold. As a result, all equipment was installed on the existing scaffold structure about 50 m upstream of the concrete pole. This led to the disadvantages of; a lower height of the camera, a lower filming angle, more interference from the construction site, a distorted surface velocity profile and easier accessibility to make the equipment more vulnerable for theft.

An improvement would have been if the construction and installation works had already been performed in the weeks before the rainy season, when the conditions for these tasks are ideal. During the end of the dry season the equipment could then still be tested since data of the wet season is wanted to be measured. During this time, it could be made sure that everything works perfectly when the rain comes, and discharges start increasing. Another advantage of a visit before the start of the wet season would be that vegetation surveys are easier to perform on dry land when all the vegetation is visible.

Due to the late arrival in the middle of the rainy season, the largest peak flow in the river already happened in the first weeks of the project when the equipment was not yet ready for installation. Therefore, it was not possible to measure the most extreme flow conditions, of which the data is most scarce. Furthermore, due to the installation towards the end of the wet season, no time series of high flows could be collected for a longer period of time. This led to single point measurements all at roughly the same discharge and water level which made it impossible to improve the current rating curve by adding new wet season observations.

Another problem was that against the original plan the visit and installation of SEBA did not match with the time frame of the project. Therefore, it was not possible to perform a high-accuracy discharge measurement of the Black Volta using an ADCP which could only be organized for the purpose of the installation of the discharge keeper system of SEBA. Furthermore, no continuous discharge measurements of the discharge keeper system could be used, other than expected before. This time series

would have been really important to update the existing rating curve with data points of high water level as the obtained data from the Discharge Keeper system is more reliable than OpenRiverCam.

In addition, some more equipment like a drone or a RTK-GNSS base and rover and could not be acquired in time which resulted in major difficulties during the project in the field. Before leaving for the field work, a drone was considered as one of the most important pieces of equipment for the floodplain characterization as well as the validation of the discharge measurements by camera mounted on the pole using OpenRiverCam. However, due to some unexpected problems with the battery of the drone, it could not be used.

The same counts for the RTK-GNSS base station and rover. A kit was ordered too close to the departure date and didn't arrive in time which led to the usage of the PPK-GNSS method. Even though PPK-GNSS has some advantages like being more accurate it comes with multiple disadvantages when working in the field. The most important being the fact that there is no live feedback if a measurement was successful or not. Especially when working in remote areas where one day in the field requires large logistical efforts missing values of specific reference points can mean that the whole day of measurements has to be repeated. Furthermore, the data collection of the bathymetry could have been improved significantly if the RTK-rover would be connected to the FishFinder sonar device to replace the smartphone GNSS antenna.

Finally, it was expected that SimCards with sufficient signal strength could be organized in the field without preparation. Within the first week of the project it was concluded that SimCards from Ivory Coast might be needed to successfully set up a working telemetry. However, the SimCards could not be acquired in time and therefore the telemetry of the measurement setup could not send continuous measurement points to the server. This prevented a time series with a length of more than 24 hours from being collected.

## 9.2. Location

Another challenge for the project was the predefined measurement location in Chache. While the measurement location for flow has some obvious advantages, such as accessibility and a relatively large amount of historical hydrological data. There were a number of limitations to be found for collecting data in the future. Firstly, during and after the construction of the bridge in Chache, the natural flow of the Black Volta is severely disrupted. The pillars that are already constructed, as well as sediment deposits on the river bed have a large influence on the observed flow velocities. This makes new observation difficult to compare with historical data. Since obtaining discharge from measured flow velocities depends on the bathymetry of the river, any measurement will also require a recent river profile to be measured.

Furthermore, the backwater effect changes the relationship between discharge and water level upstream of the bridge. Additionally, a culvert of about 8 meters wide was observed under the road that leads to the bridge on the Ghanaian side, about 100 meters away from the main channel. This culvert conveys flow from the floodplain as well as part of the flow from the main channel, which seemed to be diverted using a broad crested weir. As a result, the flow coming out of this culvert on the downstream end flows back into the main channel over a distance of about 100 meters. This flow from the side created a zone in the main channel stretching some 10s of meters where there was hardly any flow visible at the water surface. Likely, the reduced flow downstream of the bridge in the main channel pulls the water back in. Because of this, any river flow measurements made within 100s of meters downstream of the bridge will be affected by the bridge. (See Appendix G for photos of the bridge and influence on the flow).

In the future however, once the construction of the bridge is completed, its existence will be a great advantage for discharge observations in Chache. The new bridge will not only create the opportunity to cross the river at any given time but also give new possibilities to conduct measurements from the bridge which are not possible from the side of the river. Furthermore, disadvantages caused by the construction, like the strong changes of the bathymetry in short amount of time, will not longer exist. If

the discharge through the culvert would be measured as well the existence of the bridge could even be beneficial for this specific due to the fact that uncertainties due to unknown flow in the floodplain could be reduced.

Another challenge at the location is to get a strong enough network connection for the telemetry to send the observed data to server. A GSM connection of the Ghanaian Vodafone network is available is available at the location which is sufficient for the telemetry of the reflectometry measurement. The strength of the signal however depends on the specific spot. Unfortunately the signal was not tested before the construction of the pole and could also not be tested during the field visit at the location. On top of the old scaffold however the connection was not strong enough to establish a reliable connection. To solve this issue to options are possible. During the field visit it could be observed that the 3G network of Ivory Coast seems to give a strong network connection. However, due to the lack of a Ivory Coast simcard the connection could not be tested, Another option would be to use satellite telemetry. The first options requires larger logistical efforts to maintain sufficient credit on the simcard while the second option would result in higher costs.

### 9.3. Validation of results

Due to the circumstances mentioned above, less data was collected as initially expected. Furthermore, data and results of N. Hoogendorn [10] and M. Kasteel [11] were used under the assumption that these are correct. This results in the situation that only single point measurements are available for some parameters. Therefore the validity of the results has to be discussed.

#### 9.3.1. Bathymetry

The bathymetry used in this research project was taken from the study done by N. Hoogendoorn. This bathymetry was measured in March 2023, during the construction of the bridge located just downstream of the measurement location. The bathymetry data showed some inconsistencies, which influenced the results of the discharge model and OpenRiverCam, for which the bathymetry is used as an input. The bathymetry outside of the measurement location upstream and downstream the river was extrapolated using a slope of 0.0003. However, at some point in the river, inside the measured bathymetry location, the bed level instantly highers by about half a meter when going downstream in the main channel. This rise of bed level is most likely explained by the construction of the bridge at that exact location. This measurement was taken during the construction of the bridge when there was some sand deposited at this location to construct poles in the water. Therefore as mentioned above, it is recommended in future research to do bathymetry measurements at the same moment of conducting the other measurements; such as surface velocities and discharge. Due to sedimentation, the deposits at the construction of the bridge changes the bathymetry of the river with time.

#### 9.3.2. Rating curve

The third research question of this project was: 'What is the influence of the wet season measurements on the rating curve?' The data that was collected during this project was insufficient to confidently update the existing rating curve or establish a new rating curve. As explained above, the main cause of this lies in the timing of our operations. Nevertheless, the experience gained while doing discharge measurements in the rainy season in this specific location form a basis for further development. For BPA our works may help to in getting good discharge measurements in the near future. Within the TEMBO framework, our experience translates into a set of instructions that can ensure the proper installation in different locations. In the 'Recommendations' chapter, this will be elaborated further. If the prepared equipment will be moved to the final measurement location to measure the discharge and water height continuously during the next wet season this goal can be achieved without extensive efforts.

Besides a rating curve based on empirical data from discharge and water level measurements, it was attempted to model a three dimensional section of the Black Volta using Delft3D. Comparing the rating curve that was created by simulating flow through this river section, which was modeled using field observations, to the rating curve from M. Kasteel [11], based on the reservoir balance, shows a mismatch. For the same water level, especially at high flows, the water balance rating curve gives a

lower discharge than the rating curve from Delft3D. By using the inflow at the reservoir, roughly 200 km downstream of the measurement location at Chache, the rating curve for the upstream location should overestimate the discharge in the rainy season. A closer look at the reservoir balance method led to the assumption that it should give robust predictions of the reservoir inflow. It is therefore very unlikely that the rating curve simulated with Delft3D gives a better representation of reality. It should therefore not be considered as a replacement of the existing rating curve.

The reason of this discrepancy likely results from the way in which the floodplains were modeled. A more smooth channel bed results in less friction and higher flow velocities. In this situation, the same amount of discharge will flow at a lower water level than the situation where the channel bed is more rough. The difference between the channel bed used in this project and that of N. Hoogendorn [10] is that the floodplains were assigned different roughness values. The most simple explanation for the Delft3D simulations giving a higher discharge values for the same water level is therefore that the roughness was too low. A complementary explanation lies in the way in which the roughness was structured in the simulation. By creating straight zones parallel to the main channel, relatively fast-flowing side channels were effectively created. In reality, the different vegetation zones were more spatially heterogeneous. If this were modeled correctly, the average roughness may have been the same while the effective roughness is higher. This argues in favor of the approach used by N. Hoogendorn, as the effective roughness was calibrated in his research. Modeling the heterogeneity in vegetation zones would, on the other hand, be unnecessarily costly. An alternative explanation may lie in the process of mirroring the roughness for the other side of the river. On satellite imagery it can be observed that there is more vegetation on the other side and roughness is therefore likely higher. Modeling this difference correctly would have also led to lower discharge predictions. As these explanations argue in favor of using a calibrated effective roughness coefficient, they point towards the necessity of obtaining high-accuracy discharge measurements, as is done using ADCP.

### 9.3.3. Model calibration

The python package OpenRiverCam as well as the hydraulic model Delft3D require a calibration to obtain correct results. Because no ADCP measurement could be performed to obtain precise discharge values some other methods were used to test the validity of the OpenRiverCam measurements as described before. However, these methods are not backed up by any previous studies but improvised in the field. Even though the results were promising they should be taken carefully because they only test the surface velocity. The translation from surface velocity to discharge require a precise bathymetry and a calibrated parameter to account for the bottom friction. A rough calibration for the discharge could therefore only be performed by using the reservoir balance developed by M. Kasteel [11]. The required data to do this was not available at the time of data analysis. However, it might be possible in the future in case the measurements should be recalibrated.

A similar challenge was the calibration of the Delft3D model. Due to the fact that no time series but only one data point was available, the model could not be calibrated for multiple water levels. The results from the model therefore follow the assumption that the calibration parameters at this water level are valid for all water levels. However, this is usually not the case. With changing water levels parameters like the bottom friction might change as well due to the influence of the river banks. Therefore, multiple measurements of a larger variety of water levels are needed to calibrate the model and reduce the uncertainties for modeled discharged with a large difference to the measurements used for the calibration. However, once the ADCP measurement and the installation of the Discharge Keeper system are done, this data can be used to recalibrate the model to obtain a more valid model for all water levels.

# 10

## Recommendations

Based on our experience and findings a list of recommendations has been compiled. These recommendations are aimed at achieving better discharge predictions in the near future.

To ensure a smooth installation process and obtain the right data it is important to get the timing right. It is therefore advised to install the equipment used for measuring the water level and the discharge in the dry season, so that the banks can be reached properly and without unnecessary risks. Furthermore, by installing equipment before the start of the rainy season, it can be made sure that data is collected for a wide range of relatively high flows, which is especially important to update the rating curve.

It is recommended to use an RTK-GNSS instead of a PPK setup for precise positioning of reference points to speed up the process of data collection. Furthermore, the RTK gives a direct indication of whether the measurement was a success, which prevents the situation where collected data is not usable.

Another recommendation is to use reflectometry to measure the water level remotely. The setup, which is an affordable way of collecting continuous and accurate discharge measurements. For further validation of the system, it should be considered to first combine the reflectometry setup with manual gauge readings as is currently done after which it may operate autonomously.

It is recommended to redo the bathymetry measurements, as the obstruction of the channel by the bridge and the addition and transport of sediments to the river at this location significantly changes the shape of the riverbed. This has a big effect when the river discharge is determined with the surface velocity and cross-sectional area of the river flow. Furthermore, slope measurements along the direction of the river should be included in the study because they have a big influence on discharge model accuracy.

The discharge measurement installation using Openrivercam is recommended as an affordable way to measure discharge in the Black Volta and other rivers in remote locations. The angle at which the camera was pointing at the river was much lower than the recommended angle, but the velocities that were measured still roughly matched other velocity measurements. In chapter 6, potential pitfalls in setting up and using the equipment have been identified and avenues for further validation of this system for large rivers provided.

Despite the potential for using Openrivercam, the location of this setup should be reconsidered as the culvert at the bridge interferes with the surface velocity. Placing the equipment a few hundred metres upstream or downstream of the bridge should solve this issue. Alternatively cameras could be installed at the openings under the bridge and the culvert, where water flows in a more predictable way and cameras could be positioned above the channel. This will, however, be a more costly approach as more time and money is needed to install multiple instances of the camera setup.

---

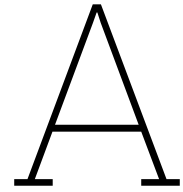
Ensuring adequate connectivity is vital. Organizing Ivory-Coast/Ghana SIM cards and conducting network tests are necessary to assess whether local networks suffice for data transmission. If necessary, considering satellite telemetry could enhance connectivity and data transmission reliability.

To account for the flow through the floodplain, several approaches are feasible. The most simple approach is to use a rough percentage to add to the measured flow in the main channel. Measuring the flow through the floodplains is also possible, but requires extensive effort at various water levels in the rainy season, as the relative contribution of the floodplains changes with water height. This can be used to obtain an effective roughness coefficient for the floodplain for different water levels, which is likely the most robust approach to achieve accurate measurements. Based on the added value for precise discharge measurements to predict reservoir inflow, it may be decided to put in the effort. An intermediate way of determining the roughness in terms of costs that can still be explored is to use a UAV drone that can measure the structure of vegetation more precisely and at a larger scale than with surveying.

The use of Delft3D is recommended to analyse river systems, as it is a versatile tool to obtain an accurate rating curve. Delft3D has a lot of options and can be used for a large variety of methods to analyse discharge in rivers. If the software is further developed it would be recommended to use the build-in Baptist equation option of determining the the roughness coefficient with the presence of vegetation. This function is expected to give very accurate results, as well as an roughness coefficient in the z-direction. Our results of the two different methods of implementing the roughness coefficient in the floodplain did not give significant difference in the discharge of the river. Therefore, a simpler method, such as a table of roughness coefficient per type of vegetation, to analyse the roughness coefficient in the floodplain is sufficient.

# References

- [1] M.J Baptist et al. "On inducing equations for vegetation resistance". In: *Journal of Hydraulic Research* 45.04 (2007).
- [2] M.J. Baptist. "Modelling floodplain biogeomorphology Ph. D. thesis". In: *Technische Universiteit Delft* (2005).
- [3] Andria Bilich and Kristine M Larson. "Correction published 29 March 2008: Mapping the GPS multipath environment using the signal-to-noise ratio (SNR)". In: *Radio Science* 42.06 (2007), pp. 1–16.
- [4] A. Consult. "Diagnostic study of the black volta basin in ghana. Final Report." In: (2012).
- [5] Deeper Sonar Chirp+. *Deeper Sonar Chirp+*. Accessed September 20, 2023. [https://deepersonar.com/nl/nl\\_nl/producten/smart-sonar-chirp-plus-2](https://deepersonar.com/nl/nl_nl/producten/smart-sonar-chirp-plus-2). n.d.
- [6] Deltares. "User Manual Delft3D D-Flow Flexible Mesh". In: (2023).
- [7] Giovanni Forzieri, Fabio Castelli, and Federico Preti. "Advances in remote sensing of hydraulic roughness". In: *International Journal of Remote Sensing* 33.2 (Oct. 2011), pp. 630–654. DOI: 10.1080/01431161.2010.531788. URL: <https://doi.org/10.1080/01431161.2010.531788>.
- [8] F. Richard Hauer, Mark S. Lorang, and Tom Gonser. "Remote Sensing to Characterize River Floodplain Structure and Function". In: *Remote Sensing* 14.5 (Feb. 2022), p. 1132. DOI: 10.3390/rs14051132. URL: <https://doi.org/10.3390/rs14051132>.
- [9] Alexandre Hauet, Thomas Morlot, and Léa Daubagnan. "Velocity profile and depth-averaged to surface velocity in natural streams: A review over a large sample of rivers". In: *E3s web of conferences*. Vol. 40. 2018, p. 06015.
- [10] N. Hoogendoorn. "3D River Discharge Modelling using UAV photogrammetry". In: *Master Thesis* (2023).
- [11] M. Kasteel. "An Assessment of Predictive Models for Operational Management of a Reservoir in a Data-Scarce Basin: A Case Study of the Black Volta Basin." In: *Master Thesis* (2023).
- [12] W. Nardwin, D.A. Edmonds, and S. Fagherazzi. "Freshwater vegetation influence on sediment spatial distribution in river delta during flood". In: (2015). DOI: 10.13140/RG.2.1.3678.0968.
- [13] Saul Edward Rantz. "Measurement and computation of streamflow". In: *Water Supply Paper* 1.2175 (1982).
- [14] Carolyn Roesler and Kristine M Larson. "Software tools for GNSS interferometric reflectometry (GNSS-IR)". In: *GPS solutions* 22.3 (2018), p. 80.
- [15] Peter JG Teunissen. "GNSS ambiguity bootstrapping: theory and application". In: *Proceedings of international symposium on kinematic systems in Geodesy, geomatics and navigation*. 2001, pp. 246–254.
- [16] Susan L. Ustin and John A. Gamon. "Remote sensing of plant functional types". In: *New Phytologist* 186.4 (May 2010), pp. 795–816. DOI: 10.1111/j.1469-8137.2010.03284.x. URL: <https://doi.org/10.1111/j.1469-8137.2010.03284.x>.
- [17] Hessel Winsemius et al. "OpenRiverCam, open-source operational discharge monitoring with low-cost cameras". In: *EGU General Assembly Conference Abstracts*. 2021, EGU21–5880.



## Sensor and platform setup

### Platform design

To allow for a safe and durable setup of the sensors on the pole on Chache a platform was designed to carry all needed equipment. The design accounts for the following equipment to be carried by the platform:

- GNSS module + budget antenna (For reflectometrie)
- OpenRiverCam camera and telemetry setup
- DischargeKeeper camera and telemetry setup
- 3 x 55 W solar panel (For OpenRiverCam and DischargeKeeper)
- 35 W solar panel for GNSS module
- Batteries for both camera setups

A sketch of the design can be observed in Figure A.1:

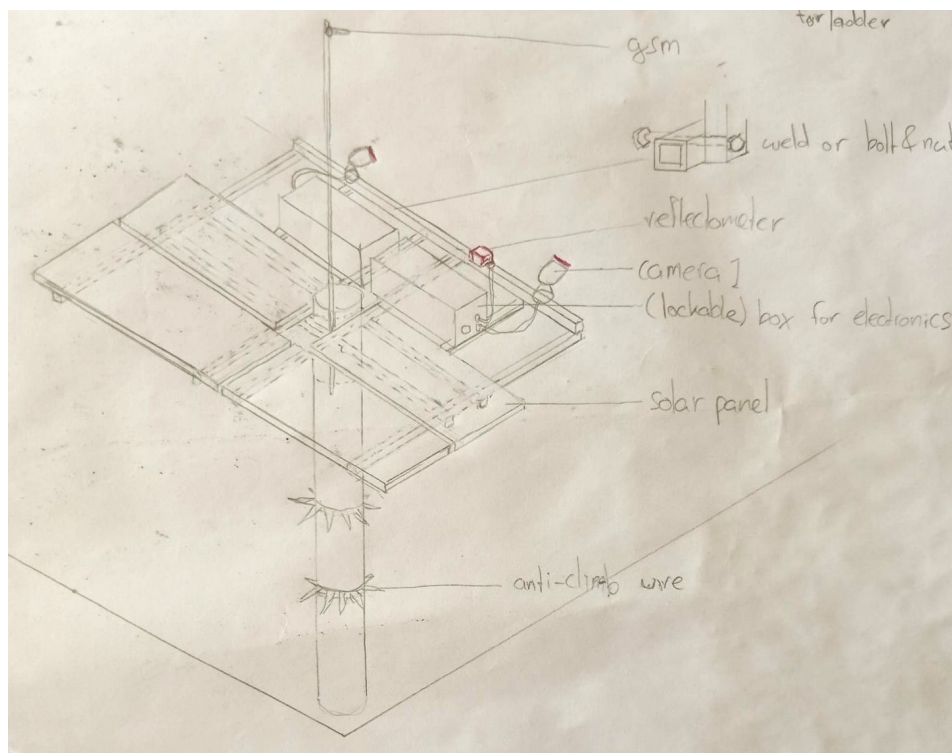


**Figure A.1:** Design of sensor setup on the pole in Chache.



**Figure A.2:** Platform for sensor setup on the pole in Chache.

To make the platform stable, it will lie on an edge of the pole and it can be tightened with two thick bolts. Its weight is evenly distributed and can potentially be supported with metal strips or pipes. During installing, the platform can be carried on top of the pole with a ladder. That is why heavy square metal profiles lying around BPA's quarters were exchanged to a local business man for lightweight square profiles. These were just about thick enough to weld.

In the process of fabrication some minor changes were made to the design due to practical reasons. The camera of the DischargeKeeper setup from SEBA was already delivered with a mounting kit for the 6-inch pole. Therefore, it was decided to mount the two cameras not on the platform but directly on the pole in the highest possible position. This led to the decision to mount the platform not on top of the pole but about one meter below the top where it can rest on the next section with a larger diameter. The platform which can be observed in Figure A.2 does therefore only carry the data loggers, telemetry and power supply including batteries and solar panels. The platform is fabricated in a way that solar panels and other equipment can't be removed without special tools.

# B

## Jupyter Notebook: Calculation of roughness coefficient by Baptist

```
In [1]: 1 import numpy as np
        2 import pandas as pd
        3 import matplotlib.pyplot as plt
```

### Load data

```
In [2]: 1 #Load data
        2 df = pd.read_csv('vegetation_data.csv', sep=';')
        3 df['height_sum'] = df['tot height'] * df['totqty']
        4 df.head()
```

```
Out[2]:
```

|   | plot | type  | thickness | bunch of | qty | totqty | m/m2 stem | height | depth | tot height | height_sum |
|---|------|-------|-----------|----------|-----|--------|-----------|--------|-------|------------|------------|
| 0 | 1    | shrub | 0.025     | 1        | 40  | 40     | 0.166667  | 2.0    | 4.5   | 6.5        | 260.0      |
| 1 | 1    | tree  | 0.200     | 1        | 2   | 2      | 0.066667  | 3.0    | 4.5   | 7.5        | 15.0       |
| 2 | 2    | shrub | 0.015     | 1        | 25  | 25     | 0.062500  | 2.0    | 3.5   | 5.5        | 137.5      |
| 3 | 2    | tree  | 0.050     | 1        | 14  | 14     | 0.116667  | 3.0    | 3.5   | 6.5        | 91.0       |
| 4 | 2    | tree  | 0.100     | 1        | 3   | 3      | 0.050000  | 3.5    | 3.5   | 7.0        | 21.0       |

### Restructure data

```
In [3]: 1 #Order data per plot
        2 df_per_ID = pd.DataFrame()
        3 df_per_ID['ID'] = [1, 2, 3, 4, 5, 6, 7, 8]
        4
        5 df_per_ID['Quantity'] = df.groupby('plot')['totqty'].sum().values
        6 df_per_ID['veg_density'] = df.groupby('plot')['m/m2 stem'].sum().values
        7 df_per_ID['avg_height'] = df.groupby('plot')['height_sum'].sum().values / df_per_ID['Quantity']
        8 df_per_ID['veg_zone'] = [1, 1, 2, 3, 3, 3, 3, 3]
        9 df_per_ID['height_sum'] = df_per_ID['Quantity'] * df_per_ID['avg_height']
        10 df_per_ID
```

```
Out[3]:
```

|   | ID | Quantity | veg_density | avg_height | veg_zone | height_sum |
|---|----|----------|-------------|------------|----------|------------|
| 0 | 1  | 42       | 0.233333    | 6.547619   | 1        | 275.0      |
| 1 | 2  | 43       | 0.312500    | 5.965116   | 1        | 256.5      |
| 2 | 3  | 36       | 0.055000    | 1.916667   | 2        | 69.0       |
| 3 | 4  | 28       | 0.083333    | 3.200000   | 3        | 89.6       |
| 4 | 5  | 41       | 0.257333    | 2.931707   | 3        | 120.2      |
| 5 | 6  | 37       | 0.136667    | 2.729730   | 3        | 101.0      |
| 6 | 7  | 37       | 0.136667    | 2.729730   | 3        | 101.0      |
| 7 | 8  | 11       | 0.038333    | 2.909091   | 3        | 32.0       |

```
In [4]: 1 #Order data per vegetation zone
2 df_per_zone = pd.DataFrame()
3 df_per_zone['zone'] = [1, 2, 3]
4 df_per_zone['Quantity'] = df_per_ID.groupby('veg_zone')['Quantity'].sum().values
5 df_per_zone['veg_density'] = df_per_ID.groupby('veg_zone')['veg_density'].mean().values
6 df_per_zone['avg_height'] = df_per_ID.groupby('veg_zone')['height_sum'].sum().values / df_per_zone['Quantity']
7
8 df_per_zone
```

```
Out[4]:
```

|   | zone | Quantity | veg_density | avg_height |
|---|------|----------|-------------|------------|
| 0 | 1    | 85       | 0.272917    | 6.252941   |
| 1 | 2    | 36       | 0.055000    | 1.916667   |
| 2 | 3    | 154      | 0.130467    | 2.881818   |

### Baptist roughness coefficient

```
In [5]: 1 #Calculate roughness coefficient by Baptist
2 baptist_manning = pd.DataFrame(columns=['h', 'Zone 1', 'Zone 2', 'Zone 3'])
3 baptist_chezy = pd.DataFrame(columns=['h', 'Zone 1', 'Zone 2', 'Zone 3'])
4
5 h = np.arange(0.1, 10.1, 0.1)
6 baptist_manning['h'] = h
7 baptist_chezy['h'] = h
8
9 manning = 0.045 #value from main channel
10 width = [50, 50, 200] #width of vegetation zones in the floodplain
11 cd = 1.65 #Constant from literature
12 karmen_constant = 0.4 #Constant from literature
13
14
15 for zone in [1, 2, 3]:
16     for H_id in range(len(h)):
17
18         cb = (((width[zone-1]*h[H_id])/width[zone-1])**1/6)/manning
19         n = df_per_zone['veg_density'].iloc[zone-1]
20         hv = df_per_zone['avg_height'].iloc[zone-1]
21
22
23         if (h[H_id]) < hv:
24
25             #Baptist equation non-submerged vegetation
26             baptist_chezy.iloc[H_id, zone] = 1/(np.sqrt((1/cb**2)+((cd*n*h[H_id])/(2*9.81))))
27
28         else:
29
30             #Baptist equation submerged vegetation
31             baptist_chezy.iloc[H_id, zone] = 1/(np.sqrt((1/cb**2)+
32                 ((cd*n*h[H_id])/(2*9.81))))+(np.sqrt(9.81)/karmen_constant) * np.log(h[H_id]/hv)
33
34
35             baptist_manning.iloc[H_id, zone] = (((width[zone-1]*
36                 h[H_id])/width[zone-1])**1/6)/baptist_chezy.iloc[H_id, zone]
37
38
39 baptist_manning.head()
```

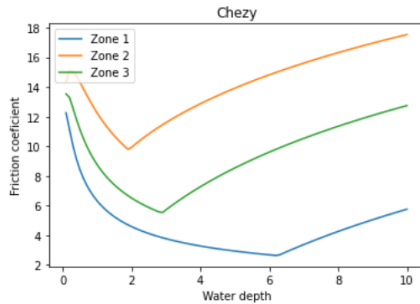
```
Out[5]:
```

|   | h   | Zone 1   | Zone 2   | Zone 3   |
|---|-----|----------|----------|----------|
| 0 | 0.1 | 0.055591 | 0.047325 | 0.050342 |
| 1 | 0.2 | 0.068625 | 0.050656 | 0.057518 |
| 2 | 0.3 | 0.081452 | 0.05435  | 0.065027 |
| 3 | 0.4 | 0.093752 | 0.058208 | 0.072517 |
| 4 | 0.5 | 0.105515 | 0.062134 | 0.07987  |

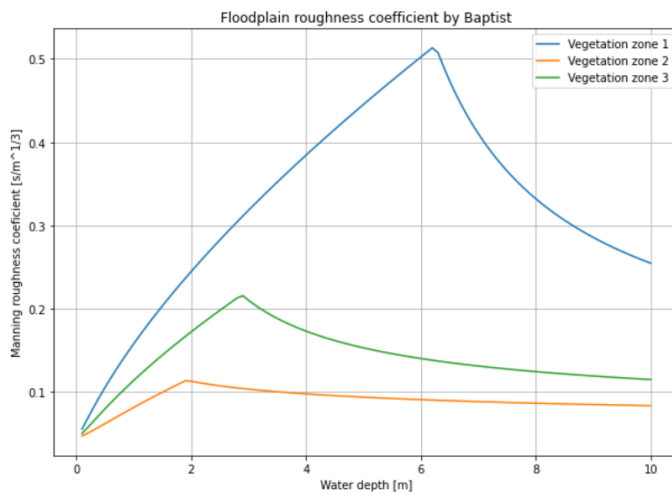
## Output

```
In [6]: 1 #Friction coefficient of Chezy
2 plt.plot(baptist_chezy['h'], baptist_chezy['Zone 1'], label='Zone 1')
3 plt.plot(baptist_chezy['h'], baptist_chezy['Zone 2'], label='Zone 2')
4 plt.plot(baptist_chezy['h'], baptist_chezy['Zone 3'], label='Zone 3')
5 plt.legend()
6 plt.xlabel('Water depth')
7 plt.ylabel('Friction coefficient')
8 plt.title('Chezy')
```

Out[6]: Text(0.5, 1.0, 'Chezy')



```
In [7]: 1 #Plot: friction coefficient of Manning
2 plt.figure(figsize=(10, 7))
3 plt.plot(baptist_manning['h'], baptist_manning['Zone 1'], label='Vegetation zone 1')
4 plt.plot(baptist_manning['h'], baptist_manning['Zone 2'], label='Vegetation zone 2')
5 plt.plot(baptist_manning['h'], baptist_manning['Zone 3'], label='Vegetation zone 3')
6 plt.legend()
7 plt.xlabel('Water depth [m]')
8 plt.ylabel('Manning roughness coefficient [s/m^1/3]')
9 plt.title('Floodplain roughness coefficient by Baptist')
10 plt.grid()
11
12 plt.savefig('Baptist.png')
```

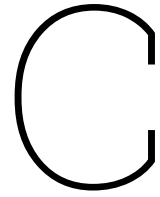


## Roughness coefficient for Delft3D

```
In [8]: 1 baptist_manning.iloc[np.arange(4, 45, 5)]
```

Out[8]:

|    | h   | Zone 1   | Zone 2   | Zone 3   |
|----|-----|----------|----------|----------|
| 4  | 0.5 | 0.105515 | 0.062134 | 0.07987  |
| 9  | 1.0 | 0.15804  | 0.08155  | 0.114004 |
| 14 | 1.5 | 0.203555 | 0.099835 | 0.144446 |
| 19 | 2.0 | 0.244662 | 0.113037 | 0.172257 |
| 24 | 2.5 | 0.282667 | 0.107547 | 0.198124 |
| 29 | 3.0 | 0.318326 | 0.103548 | 0.210225 |
| 34 | 3.5 | 0.352124 | 0.100426 | 0.188456 |
| 39 | 4.0 | 0.384395 | 0.097884 | 0.173237 |
| 44 | 4.5 | 0.41538  | 0.095754 | 0.161926 |



# Roughness coefficient input Delft3D scenario 2

**Table C.1:** Roughness coefficient with according water level at certain grid cell for a discharge of  $2000 \text{ m}^3/\text{s}$

| Vegetation zone | Grid number | Water level (m) | Roughness coefficient ( $s/m^{1/3}$ ) |
|-----------------|-------------|-----------------|---------------------------------------|
| 3               | 1           | -               | -                                     |
| 3               | 2           | -               | -                                     |
| 3               | 3           | 0.1             | 0.05                                  |
| 3               | 4           | 1.4             | 0.14                                  |
| 3               | 5           | 2.2             | 0.18                                  |
| 2               | 6           | 2.2             | 0.11                                  |
| 1               | 7           | 1.4             | 0.19                                  |
| Main channel    | 8           | -               | -                                     |
| Main channel    | 9           | -               | -                                     |
| Main channel    | 10          | -               | -                                     |
| 1               | 11          | 2.3             | 0.26                                  |
| 2               | 12          | 2.4             | 0.11                                  |
| 3               | 13          | 2.3             | 0.18                                  |
| 3               | 14          | 1.3             | 0.13                                  |
| 3               | 15          | 0.5             | 0.08                                  |
| 3               | 16          | 0.3             | 0.06                                  |
| 3               | 17          | 0.3             | 0.06                                  |
| 3               | 18          | 0.6             | 0.08                                  |
| 3               | 19          | 0.6             | 0.08                                  |
| 3               | 20          | 1.5             | 0.14                                  |
| 3               | 21          | 1.5             | 0.14                                  |

**Table C.2:** Roughness coefficient with according water level at certain grid cell for a discharge of  $1500 \text{ m}^3/\text{s}$ 

| Vegetation zone | Grid number | Water level (m) | Roughness coefficient ( $s/m^{1/3}$ ) |
|-----------------|-------------|-----------------|---------------------------------------|
| 3               | 1           | -               | -                                     |
| 3               | 2           | -               | -                                     |
| 3               | 3           | -               | -                                     |
| 3               | 4           | 0.3             | 0.06                                  |
| 3               | 5           | 0.6             | 0.08                                  |
| 2               | 6           | 0.6             | 0.06                                  |
| 1               | 7           | 0.4             | 0.09                                  |
| Main channel    | 8           | -               | -                                     |
| Main channel    | 9           | -               | -                                     |
| Main channel    | 10          | -               | -                                     |
| 1               | 11          | 0.7             | 0.12                                  |
| 2               | 12          | 0.7             | 0.06                                  |
| 3               | 13          | 0.6             | 0.08                                  |
| 3               | 14          | 0.2             | 0.06                                  |
| 3               | 15          | -               | -                                     |
| 3               | 16          | -               | -                                     |
| 3               | 17          | -               | -                                     |
| 3               | 18          | -               | -                                     |
| 3               | 19          | -               | -                                     |
| 3               | 20          | -               | -                                     |
| 3               | 21          | -               | -                                     |

**Table C.3:** Roughness coefficient with according water level at certain grid cell for a discharge of  $1000 \text{ m}^3/\text{s}$ 

| Vegetation zone | Grid number | Water level (m) | Roughness coefficient ( $s/m^{1/3}$ ) |
|-----------------|-------------|-----------------|---------------------------------------|
| 3               | 1           | -               | -                                     |
| 3               | 2           | -               | -                                     |
| 3               | 3           | -               | -                                     |
| 3               | 4           | -               | -                                     |
| 3               | 5           | 0.2             | 0.06                                  |
| 2               | 6           | 0.2             | 0.04                                  |
| 1               | 7           | -               | -                                     |
| Main channel    | 8           | -               | -                                     |
| Main channel    | 9           | -               | -                                     |
| Main channel    | 10          | -               | -                                     |
| 1               | 11          | 0.1             | 0.06                                  |
| 2               | 12          | 0.3             | 0.05                                  |
| 3               | 13          | 0.3             | 0.06                                  |
| 3               | 14          | -               | -                                     |
| 3               | 15          | -               | -                                     |
| 3               | 16          | -               | -                                     |
| 3               | 17          | -               | -                                     |
| 3               | 18          | -               | -                                     |
| 3               | 19          | -               | -                                     |
| 3               | 20          | -               | -                                     |
| 3               | 21          | -               | -                                     |

D

BASE station, offline test

#OFFLINE TEST

1. Charge the batteries

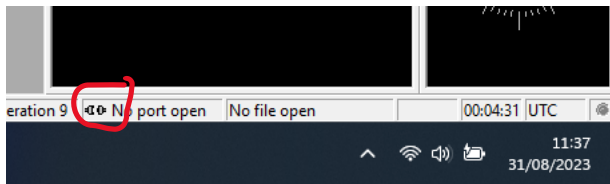
you can verify the charged status of the module by checking the led in the unit. the DONE light must be constantly on

2. Configure the GNSS unit

- I. Open U-Center 21 on your windows laptop.
- II. Connect the GNSS unit with your laptop via USB (watch out, there are 2 USB outputs on the GNSS unit, use the power+GPS one)
- III. Click on the icon below, and select the COM where the GNSS unit is.



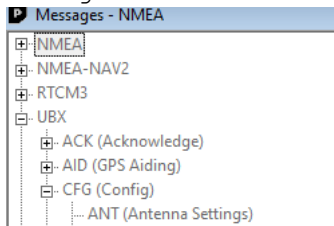
- IV. Verify a good connection by seeing a green blinking connection icon.



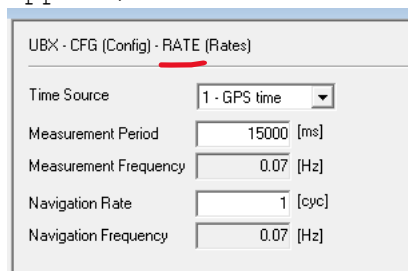
- V. Click on this icon



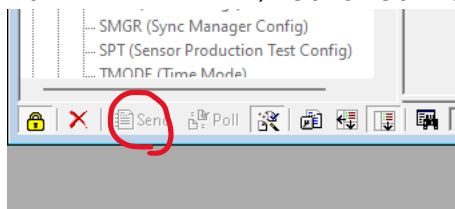
- VI. Navigate to the following directory



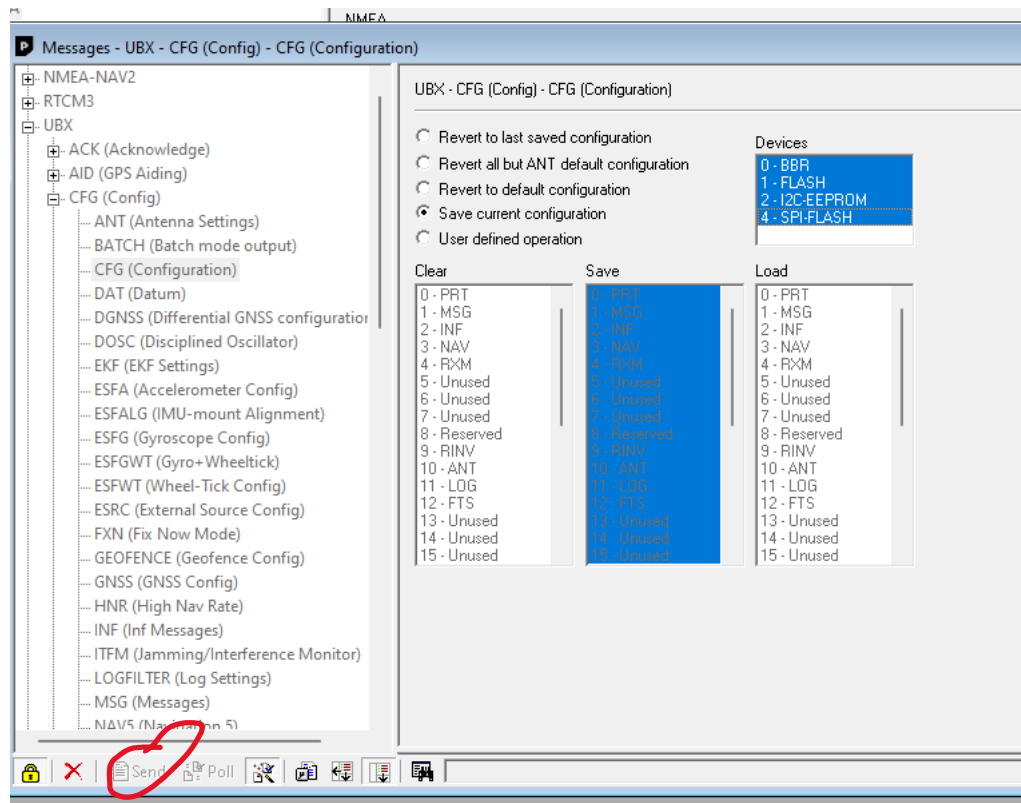
- VII. In this directory all the relevant settings can be edited.
  - a. Set the sample frequency to every 15000 msSelect the sub directory called RATE, then the below screen appear, set it accordingly



After doing this, click on **send** in the same window, DO THIS FOR EVERY EDIT, so also for step b,c,etc

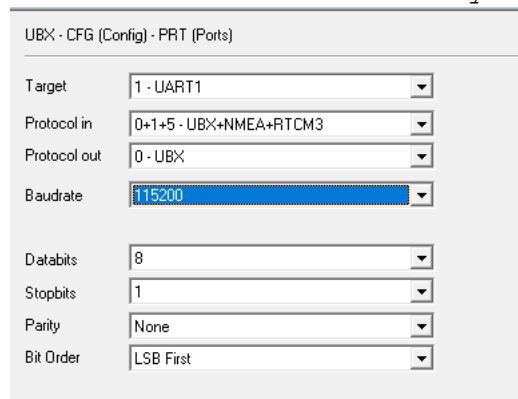


The edit is now on the GNSS unit, in order to save this edit, do the following

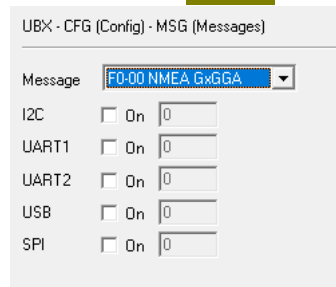


THIS SHOULD ALSO BE DONE FOR EVERY EDIT

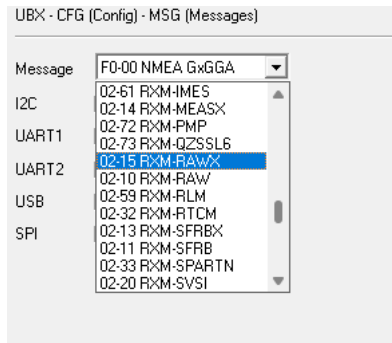
- b. Go to the PRT sub directory, and set it accordingly



- c. Go to the MSG sub directory and go to the Fxxx NMEA xxxxx messages, make sure non of these check boxes at UART1 are checked, you have to save each of them separately like I described **above**,



Then we need to go to



And check this box for UART1,

d.

### 3. Verify simcard connection

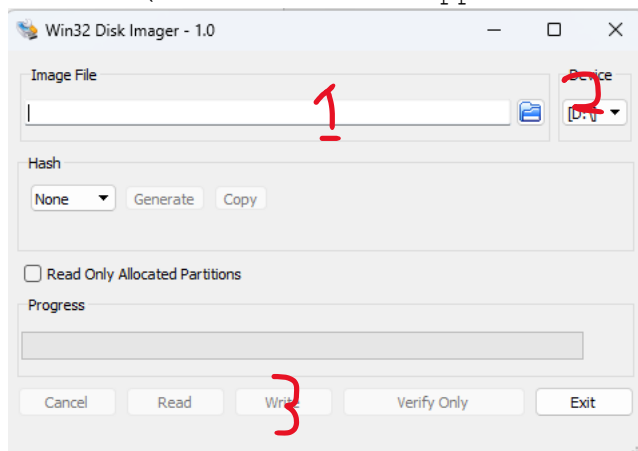
- I. Verify connecting with you sim card, by testing it in your own phone. Preferably dot this on a anadroid phone and check in the settings if 2G is possible. Try to do something on the internet on 2G. Now insert the simcard like this



- II. Make sure the PIN code is disabled, since the simmodule cannot insert a pincode.

### 4. Format SD card

- a. Format the Image of Andreas(copyright) to an empty sd card (16 GB), do this with the windows program win32.
- b. Firstly, erase everything on the sd card buy doing this:
  - i. Open "File Explorer."
  - ii. Right-click on the SD card drive and select "Format."
  - iii. Choose the appropriate file system (usually FAT32 for SD cards) and allocation unit size 2048.
  - iv. Ensure that "Quick Format" is checked.
  - v. Click "Start" to begin the formatting process.
- c. Now, the sd card is empty, verify this.
- d. Next, download the Image of Andreas
- e. Open Win32, insert the path of the image of andreas (copyright) at 1. Next, insert the terminal of the sd card at 2. At last, click Write aka 3. (this will cost approx 15 min)



- f. Now put the sd card in the raspberry zero w like this



**5. Let the GNSS reflectometry module run for 2 hours**

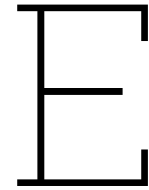
Switch on the main switch and also the gnss module switch, wait for 2 min and check if the SD write light is blinking (the most left indicator light)

**6. Verify the data**

For this step we will put the sd card of the GNSS module inside the raspberry pi 2. This symbols <> mean come up with something yourself, type it in without the weird <> signs.

- a. Login: pi, ww: basestation
- b. Create a new usb directory by typing in `*mkdir <usbdirectoryname>*` Next, type in `*pwd*` to get the correct path, note this path
- c. type in `*lsblk*` then search for your disk, when you found it use the part type as name an note this in the following format: `/dev/<name>`, usually it is something with sda
- d. merge the noted txt in the following format and put it in the terminal: `*sudo mount /dev/<name> /home/pi/<usbdirectoryname>*` Now all the data of the usb can be viewed in `this` path.
- e. Navigate to the sub directory: `home/pi/production/ubx_files/.` Then type `*ls*`. Now you should see one or two files beginning with AKTE0..... Note the whole name including .ubx at the end.
- f. Stay in this directory and type the following command: `*sudo cp AKTE02023_08_23_14_32.ubx /home/pi/<usbdirectoryname>*`
- g. Now the data is on the usb stick, to safely unmount the usb type in: `*sudo umount /dev/<name>*`

**7. Put the usb in the laptop, make sure it has some kb data on it and send it to jorrit**



## Post processing GNSS reflectometry

In order to obtain height data from the GNSS reflectometry module, the following steps need to be executed.

### Step 1: UBX to OBS

The raw data is delivered in .ubx file extension. UBX is a proprietary binary format created by the company u-blox. For RTKLIB the raw data needs to be converted to RINEX 3 format. This is done with the onboard CONVBIN application of RTKLIB. First navigate to the directory of the RTKLIB on your CMD, then insert the following command:

```
1 convbin -r C:\Users\x.ubx -o x.obs
```

Now your ubx file is copied and transformed to an obs file, the obs file should appear in the current working directory.

### Step 1a: UBX to clipped OBS

In many cases the ubx files containing some measurements that we do not want to take into considerations for our PPK measurements. In order to exclude them we will tweak the command of step 1 slightly with an time parameter:

```
1 convbin -os -od -f 5 -v 3.03 -ts 2023/09/24 00:35:30 -te 2023/09/24 00:40:30 -hm "GH00_P11" -  
  hn "GH00_P11" -hr "/UBLOX ZED-F9P/" -ha "/ANN-MB-00" -ho "Jorrit Okkerman/TU Delft" C:\  
  Users\x.ubx
```

Now your ubx file is copied, clipped and transformed to an obs file, the obs file should appear in the current working directory.

### Step 2: PPP the antenna

In order to use the reflection zones web application of Christine Larson, the precise position of the antenna is needed. This is done with the PPP web application of the Canadese government: <https://webapp.csrsc-scrs.nrcan-rncan.gc.ca/geod/tools-outils/ppp.php>.

Processing mode

Static  Kinematic

NAD83 ITRF

- The epoch will be the same as the GPS data.
- A UTM zone will be calculated from the longitude.

Vertical datum

CGVD2013

Contribute to passive control maintenance? ([What is this?](#))

Authorize the Canadian Geodetic Survey to archive and publish CSRS-PPP submission and solution

Official Canadian federal or provincial geodetic marker number

<station name>

► More options

RINEX observation file(s), 300 MB max (.zip, .gz, .Z, .tar, .?\*)

Note: You may submit multiple RINEX files in a single .zip or .tar archive

Bestand kiezen Geen bestand gekozen

Remove plots from CSRS-PPP solution PDF report ([Why?](#))

Submit to PPP

Figure E.1: NR CAN selection

Figure F.1 represents the selection menu with the correct options checked for PPP information. Submit to PPP, and check you email for the PPP estimates.

### Step 3: Reflection zones web application

Now we have to fill in the form on the following URL <https://gnss-reflections.org/rzones>. When this form is submitted a figure like figure x will appear. Check from which azimuth direction the reflection zones only cover the to be measured river. Note this direction range in degrees.

### Step 4: GNSS-IR web application

Go to the following website and fill in the form <https://gnss-reflections.org/api> (with the correct min and max azimuth, leave the rest as is. see figure E.2). Make sure that the rinex file (.obs) is zipped as an .gz extension before uploading. This can be done with 7-zip file manager.

API: Upload RINEX File

Bestand kiezen Geen bestand gekozen

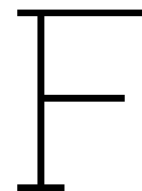
| Freq | MinRH | MaxRH | MinElAng | MaxElAng |
|------|-------|-------|----------|----------|
| L1   | 0.4   | 8.0   | 5.0      | 25.0     |

| ReqAmp | Pk2Noise | Output | MinAzim | MaxAzim | Rinex |
|--------|----------|--------|---------|---------|-------|
| 6      | 3.0      | txt    | 0       | 360     | 2.11  |

View

azim Submit

Figure E.2: GNSS-IR web application screenshot



# Post processing kinematics

This is a description of the workflow that we used to transform the raw GNSS data from our receivers to PPK results. This is done with the software package RTKLIB on a windows computer.

## Step 1: UBX to OBS

The raw data is delivered in .ubx file extension. UBX is a proprietary binary format created by the company u-blox. For RTKLIB the raw data needs to be converted to RINEX 3 format. This is done with the onboard CONVBIN application of RTKLIB. First navigate to the directory of the RTKLIB on your CMD, then insert the following command:

```
1 convbin -r C:\Users\x.ubx -o x.obs
```

Now your ubx file is copied and transformed to an obs file, the obs file should appear in the current working directory.

## Step 1a: UBX to clipped OBS

In many cases the ubx files containing some measurements that we do not want to take into considerations for our PPK measurements. In order to exclude them we will tweak the command of step 1 slightly with an time parameter:

```
1 convbin -os -od -f 5 -v 3.03 -ts 2023/09/24 00:35:30 -te 2023/09/24 00:40:30 -hm "GH00_P11" -  
  hn "GH00_P11" -hr "/UBLOX ZED-F9P/" -ha "/ANN-MB-00" -ho "Jorrit Okkerman/TU Delft" C:\  
  Users\x.ubx
```

Now your ubx file is copied, clipped and transformed to an obs file, the obs file should appear in the current working directory.

## Step 2: PPP the BASE station

In order to perform PPK, an estimate position coordinate of the BASE station must be obtained. This is done with the PPP web application of the Canadian government: <https://webapp.csrsc-scrs.nrcan-nrcan.gc.ca/geod/tools-outils/ppp.php>.

Processing mode

Static  Kinematic

NAD83 ITRF

- The epoch will be the same as the GPS data.
- A UTM zone will be calculated from the longitude.

Vertical datum

CGVD2013

Contribute to passive control maintenance? [\(What is this?\)](#)

Authorize the Canadian Geodetic Survey to archive and publish CSRS-PPP submission and solution

Official Canadian federal or provincial geodetic marker number

<station name>

► More options

RINEX observation file(s), 300 MB max (.zip, .gz, .Z, .tar, .7ZO)

Note: You may submit multiple RINEX files in a single .zip or .tar archive

Bestand kiezen Geen bestand gekozen

Remove plots from CSRS-PPP solution PDF report [\(Why?\)](#)

Submit to PPP

Figure F.1: NR CAN selection

Figure F.1 represents the selection menu with the correct options checked for PPP information. Submit to PPP, and check you email for the PPP estimates.

### Step 3: Obtain orbital information

In order to eliminate the satellite orbit position error, the PPK software needs the NAV file of the regarding constellation. In this way it knows the exact position of the satellite relative to the earth at any time during the measurements. For our application a single constellation is enough. Edit the following url with the specified year and day of the year. Search it, look for the brdc file, and download it. <https://tontos.jpl.nasa.gov/pub/pro/y2023/d288/>.

### Step 4: Preform the PPK

Firstly, see figure F.2, the obs file of the base and rover need to be inserted in the first two rows. Then the concerning brdc file need to be inserted in the third row.

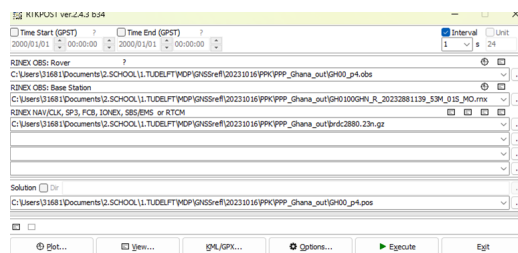


Figure F.2: Screenshot RTKPOST main

Then click on options and check if the 'settings1' and 'output' sub menu contain the same settings as figure F.3 and F.4.

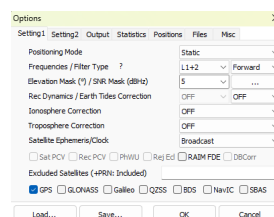
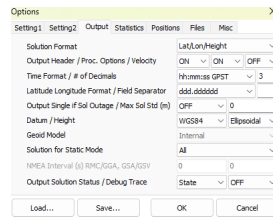
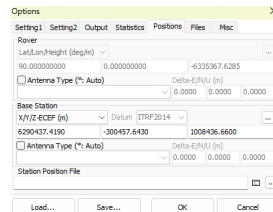


Figure F.3: Screenshot RTKPOST settings



**Figure F.4:** Screenshot RTKPOST output



**Figure F.5:** Screenshot RTKPOST position

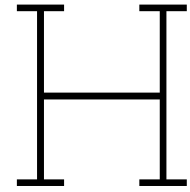
Now click on the 'position' sub menu and insert the XYZ base station position as reported in the PPP file. Then click on 'execute'. Now an .pos file is loaded in the current working directory. The last row of this file contains the most precise position estimation of the specific point (your PPK point).

# G

## Photos of study site



**Figure G.1:** Photos of the construction of the bridge at the Chache site, taken on 04-10-2023



# Floodplain data collection

**Table H.1:** Collected velocity measurements in two transects in the Chache floodplain. The upstream and downstream column coincide with the upstream and downstream velocity profiles in the floodplain given in figure 7.6.

| Distance to main channel [m] | v upstream [m/s] | v downstream [m/s] |
|------------------------------|------------------|--------------------|
| 0                            | 0.2              | 0.15               |
| 5                            | 0.01             | 0.07               |
| 10                           | 0.35             | 0.01               |
| 15                           | 0.26             | 0.01               |
| 20                           | 0.25             | -                  |
| 25                           | 0.28             | -                  |
| 30                           | 0.37             | -                  |
| 35                           | 0.38             | -                  |
| 40                           | 0.16             | -                  |
| 45                           | 0                | -                  |
| 50                           | 0.01             | -                  |
| 55                           | 0.3              | -                  |
| 60                           | 0.01             | -                  |

**Table H.2:** Vegetation survey data. As explained in chapter 7, vegetation occurrence was measured in 8 plots, indexed in the leftmost column. To quantify the stem density efficiently, stems were grouped into classes with mean structural properties. Stem density and total height (height + depth) are used to determine the roughness.

|   | Vegetation type | Stem thickness [m] | Bunch of stems | Amount of vegetation | Total amount of stems | Stem density [m stem/m <sup>2</sup> ] | Vegetation height [m] | Water depth (m) | Total veg. height (m) |
|---|-----------------|--------------------|----------------|----------------------|-----------------------|---------------------------------------|-----------------------|-----------------|-----------------------|
| 1 | shrub           | 0.025              | 1              | 40                   | 40                    | 0.166667                              | 2                     | 4.5             | 6.5                   |
| 1 | tree            | 0.2                | 1              | 2                    | 2                     | 0.066667                              | 3                     | 4.5             | 7.5                   |
| 2 | shrub           | 0.015              | 1              | 25                   | 25                    | 0.0625                                | 2                     | 3.5             | 5.5                   |
| 2 | tree            | 0.05               | 1              | 14                   | 14                    | 0.116667                              | 3                     | 3.5             | 6.5                   |
| 2 | tree            | 0.1                | 1              | 3                    | 3                     | 0.05                                  | 3.5                   | 3.5             | 7                     |
| 2 | tree            | 0.5                | 1              | 1                    | 1                     | 0.083333                              | 3.5                   | 3.5             | 7                     |
| 3 | shrub           | 0.005              | 10             | 6                    | 60                    | 0.05                                  | 0.5                   | 1               | 1.5                   |
| 3 | shrub           | 0.03               | 6              | 1                    | 6                     | 0.03                                  | 3                     | 1               | 4                     |
| 4 | shrub           | 0.005              | 10             | 2                    | 20                    | 0.016667                              | 2.5                   | 0.7             | 3.2                   |
| 4 | shrub           | 0.05               | 4              | 2                    | 8                     | 0.066667                              | 2.5                   | 0.7             | 3.2                   |
| 5 | shrub           | 0.002              | 1              | 17                   | 17                    | 0.005667                              | 0.4                   | 0.4             | 0.8                   |
| 5 | shrub           | 0.03               | 1              | 17                   | 17                    | 0.085                                 | 4                     | 0.4             | 4.4                   |
| 5 | tree            | 0.1                | 1              | 6                    | 6                     | 0.1                                   | 4                     | 0.4             | 4.4                   |
| 5 | tree            | 0.4                | 1              | 1                    | 1                     | 0.066667                              | 5                     | 0.4             | 5.4                   |
| 6 | shrub           | 0.01               | 1              | 32                   | 32                    | 0.053333                              | 2.5                   | 0               | 2.5                   |
| 6 | tree            | 0.05               | 1              | 4                    | 4                     | 0.033333                              | 4                     | 0               | 4                     |
| 6 | tree            | 0.3                | 1              | 1                    | 1                     | 0.05                                  | 5                     | 0               | 5                     |
| 7 | shrub           | 0.01               | 1              | 32                   | 32                    | 0.053333                              | 2.5                   | 0               | 2.5                   |
| 7 | tree            | 0.05               | 1              | 4                    | 4                     | 0.033333                              | 4                     | 0               | 4                     |
| 7 | tree            | 0.3                | 1              | 1                    | 1                     | 0.05                                  | 5                     | 0               | 5                     |
| 8 | shrub           | 0.005              | 3              | 2                    | 6                     | 0.005                                 | 2                     | 0               | 2                     |
| 8 | tree            | 0.04               | 1              | 5                    | 5                     | 0.033333                              | 4                     | 0               | 4                     |